COMPENSATION TOPOLOGIES IN WIRELESS POWER TRANSFER CONVERTERS

YING LIU

PhD

The Hong Kong Polytechnic University

This programme is jointly offered by The Hong Kong Polytechnic University and Harbin Institute of Technology

2021

The Hong Kong Polytechnic University

Department of Electronic and Information Engineering

Harbin Institute of Technology

School of Electrical Engineering and Automation

Compensation Topologies in Wireless Power Transfer Converters

Ying Liu

A thesis submitted in partial fulfillment of

the requirements for the degree of

Doctor of Philosophy

June 2021

CERTIFICATE OF ORIGINALITY

I hereby declare that this thesis is my own work and that, to the best of my knowledge and belief, it reproduces no material previously published or written, nor material that has been accepted for the award of any other degree or diploma, except where due acknowledgment has been made in the text.

________________(Signed)

Ying Liu (Name of student)

Abstract

This thesis aims to study second and higher order compensation topologies for wireless power transfer (WPT) covering inductive power transfer (IPT) and capacitive power transfer (CPT) systems, and to provide design guidelines for various types of compensation circuits for addressing the common and inevitable issues arising from wide variations of coupling and compensation parameters.

This thesis first presents a unified T-type two-port network model for IPT and CPT converters, contributing to offer direct insights into the choice of appropriate compensation topologies and their relationship with performance. General transfer characteristics and corresponding operating conditions of the presented T-model IPT and CPT converters are summarized. On this basis, all possible second-order compensation topologies are systematically analyzed in depth.

A systematic extension of the basic second-order compensated IPT and CPT converters is then presented for achieving load-independent current (LIC) or load-independent voltage (LIV) output, to higher order compensated converters through adding an inductor or capacitor at the input or output side. Conditions on the parameters to achieve the required output performance are given. Then, the system's sensitivity to various parameters' fluctuation is analyzed. Results from sensitivity analysis provide a convenient design guide for selecting parameters and compensation topologies to achieve the required LIV and LIC operation for IPT and CPT systems with fewer design constraints. Moreover, the analysis effectively reveals the roles of extra input-side or output-side inductors and

capacitors in making the whole system less sensitive, and hence provides a fast understanding of the choice of various compensation circuits for applications addressing wide ranges of coupling and compensation parameter values.

Finally, to highlight the advantages of different compensation topologies for WPT systems, specific configurations of IPT systems for multi-load applications are further developed. Since the versatility of the coupling structure and the choice of parameter values are crucial due to the diversity of load appliance types and operating conditions, the features of four coupling structures, namely single-input single-output (SISO), single-input multiple-output (SIMO), multiple-input single-output (MISO) and multiple-input multiple-output (MIMO), are analyzed in depth, from which general transfer characteristics are obtained. Based on the series-series compensation topology, a set of design principles for IPT circuits satisfying various output requirements in a multi-load environment is presented. Control strategies to address the impedance matching issue are also proposed. Moreover, a third-order compensation scheme is presented to improve the performance of IPT systems with multiple outputs and to facilitate the control process.

List of Publications

Journal papers

- **Y. C. Liu**, J. Zhang, C. K. Tse, C. Zhu, and S. C. Wong, "General Pathways to Higher Order Compensation Circuits for IPT Converters via Sensitivity Analysis," *IEEE Transactions on Power Electronics*, vol. 36, no. 9, pp. 9897–9906, September 2021.
- **Y. C. Liu**, X. L. Li, J. Zhang, C. K. Tse, C. Zhu, and S. C. Wong, "Systematic Analysis of Capacitive Power Transfer Converters: From Second Order to Higher Order Compensation," *IEEE Transactions on Power Electronics.* (Submitted)
- **Y. C. Liu**, C. K. Tse, C. Zhu, and S. C. Wong, "Unified Design Principles of Inductive Power Transfer Systems for Multi-Load Applications," *IEEE Transactions on Industry Applications.* (Submitted)

Conference papers

- **Y. Liu**, C. K. Tse, C. Zhu, and S. C. Wong, "Comparison of Second-Order and Third-Order Compensation of Inductive Power Transfer Converters Based on Sensitivity Analysis," in *Proc. IEEE International Symposium on Circuits and Systems*, Seville, Spain, 2020, pp. 1–5.

Acknowledgments

I am truly grateful for the opportunity to pursue a joint PhD program at the Hong Kong Polytechnic University and Harbin Institute of Technology. The continuous support by both universities, and later also by City University of Hong Kong, are gratefully acknowledged. My three-year stay in Hong Kong has been one of the most memorable experiences of my life.

First and foremost, I would like to express my immense gratitude to my supervisors Prof. Michael Tse and Dr. S. C. Wong in Hong Kong, and Prof. Chunbo Zhu and Prof. C. C. Chan in Harbin, for their intellectual inspiration, patient guidance and wholehearted support throughout my study. Their professionalism, expertise and rich knowledge have deeply impressed me and will continue to influence my perspective on academic research and life.

I wish to thank all my colleagues and friends at the Hong Kong Polytechnic University for their kind help and company during these three years. They made my stay in Hong Kong very enjoyable. I shall always treasure the memory.

Finally, my deepest thanks go to my family for their selfless love and continuous support. Their sustained encouragement gives me the confidence and strength to overcome difficulties.

Contents

List of Figures

List of Tables

Chapter 1

Introduction

1.1 Background

The last few decades have witnessed a rapid development of wireless power transfer (WPT) technologies in a variety of fields. As the name implies, a WPT system transfers energy from the power source to the load without the use of conductive wires or physical contacts. With the increasing maturity of the development of IPT technologies, various applications have been materialized in the market, including wireless charging for electric vehicles [6–11], implant medical devices [12–14], autonomous underwater vehicles [15–18], consumer electronics [19–22], etc., as exemplified in Figs. 1.1, 1.2 and 1.3.

The concept of WPT was first presented in the late 19th century by Nikola Tesla [23–25], who carried out a variety of WPT experiments and made attempts to realize large-scale and high-power wireless power transfer. The series of studies conducted by Tesla laid the foundation for the development of modern WPT systems. Since then, many researchers have been inspired to contribute to the practical realization of WPT systems. Applications of wireless charging for implant medical devices, electric brushes, and electric vehicles have been proposed in quick succession. In 2007, a research group led by Prof. Marin Soljačić from

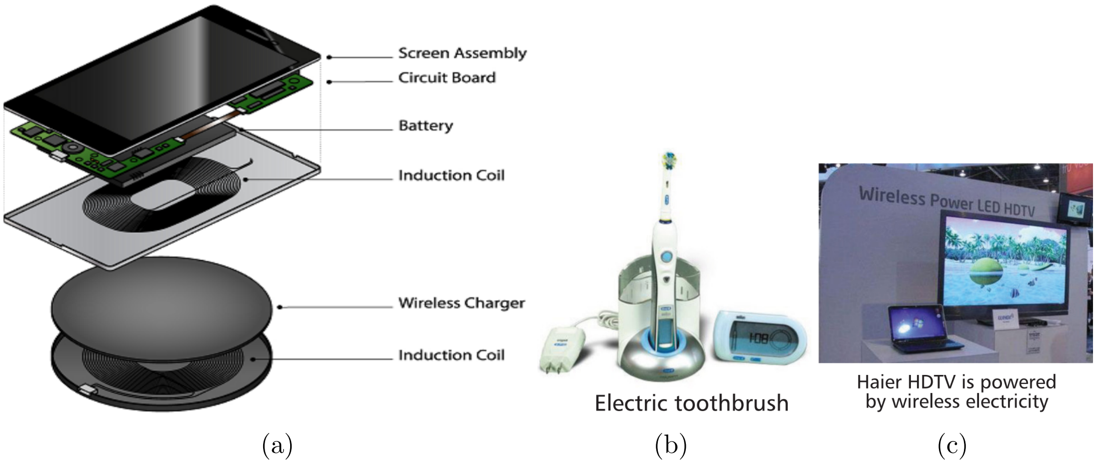

Figure 1.1: Examples of wireless power transfer applied for consumer electronics: (a) Smart phone [1]; (b) electric toothbrush [2]; (c) HDTV [2].

(a) Copyright 2018, with permission from F. H. Sumi; (b)(c) copyright 2013, with permission from IEEE.

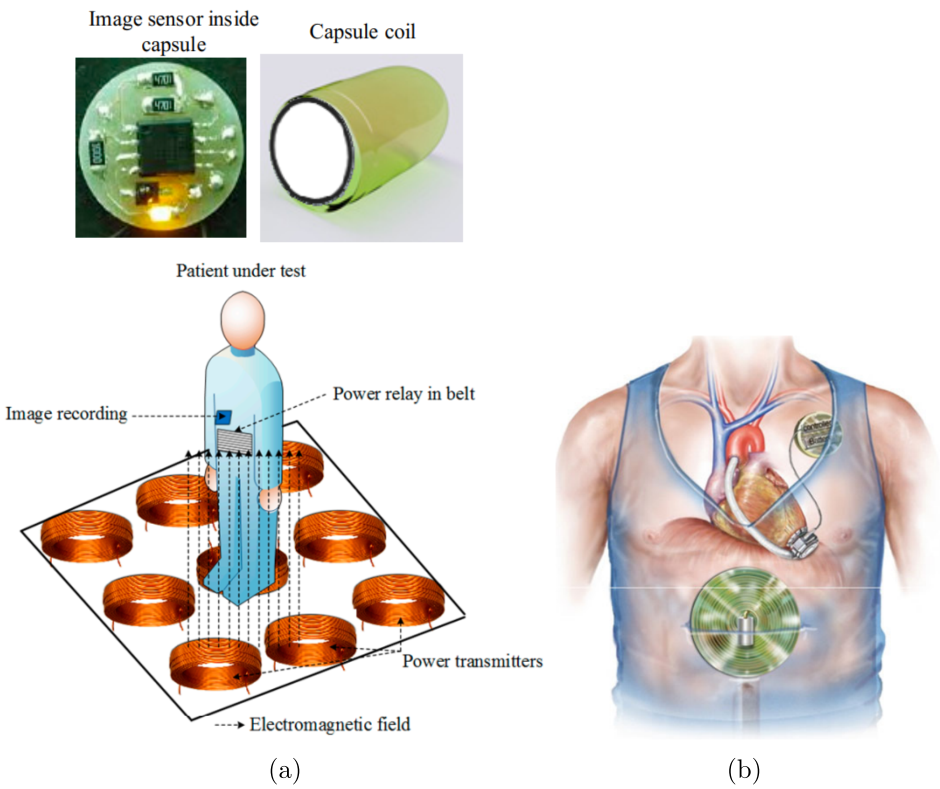

Figure 1.2: Examples of wireless power transfer applied for implant medical devices: (a) Capsule endoscopy inspection [3]; (b) portable charger for ventricular assist devices [4].

(a) Copyright 2018, with permission from A. M. Jawad; (b)(c) copyright 2013, with permission from IEEE.

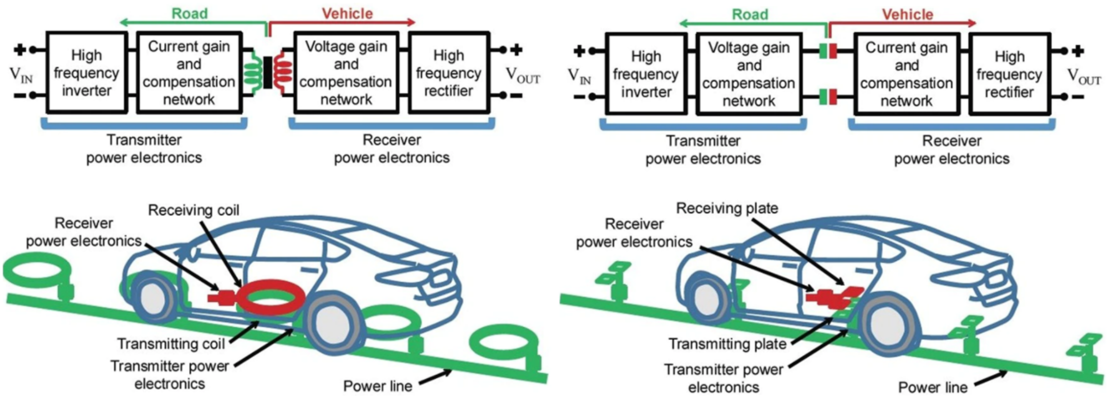

(a) (b)

Figure 1.3: Applications of wireless charging including two approaches of (a) inductive power transfer (IPT) and (b) capacitive power transfer (CPT) for electric vehicles [5].

Massachusetts Institute of Technology (MIT) "caught" the emitted electromagnetic waves by making the transmitter and receiver of a WPT system resonate at the same frequency, and successfully lit a 60 W light bulb two metres away, further validating Tesla's conception of using resonance to transfer energy over a long distance [26]. The research findings published in *Science* brought the research on WPT to a wide spectrum of scientific audience, although the subject of IPT and related circuit technologies have been studied long before the MIT experiment were published [19, 27, 28].

According to the transfer distance, the current common WPT approaches can be classified into far-field and near-field WPT, as shown in Fig. 1.4. The far-field WPT is generally in the form of microwaves or lasers [29], with transmitting and receiving antennas, to achieve long-range power transfer [30–32]. Although this approach enables power transfer over a long distance, the transmission of electromagnetic waves through space limits the transfer efficiency, and the application of antennas also requires extreme directionality for power transmission and reception and cannot cross obstacles.

Near-field WPT can be divided into inductive power transfer (IPT) and ca-

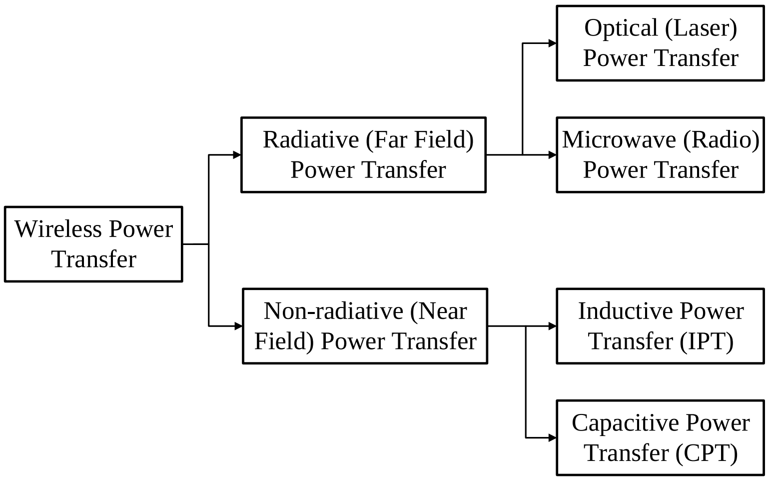

Figure 1.4: Classification of wireless power transfer systems.

pacitive power transfer (CPT), the former using magnetic fields and the latter using electric fields. The non-radiative magnetic or electric fields are generated by virtue of mutually coupled transformers or parallel capacitor plates to achieve the transmission of energy over medium distances. This approach is characterized by a non-sensitive directionality and the ability to transfer power through non-magnetic substances. By operating at resonant frequencies and using compensation topologies to reduce the processing of reactive power, the approaches of IPT and CPT have the advantage of high efficiency in power transmission. In this thesis, we mainly focus on the study of characteristics and performance of IPT and CPT systems.

1.2 Motivation

The emerging technology of WPT offers a viable solution for facilitating sustainable and efficient power supply in a wide range of applications. Compared to the conventional technology of conductive charging, WPT has the following merits.

1. Safety and longevity. In traditional power supply systems, the fraying and aging of the wires may cause electric shock. This safety hazard can be

eliminated by using WPT due to the absence of conducting contact in WPT systems. Moreover, WPT significantly reduces surface abrasion of the devices during operation, hence extending the service life of the devices significantly.

2. Resource conservation. Compared to fixed-location charging posts, WPT chargers can be laid below ground, saving public resources in the city and reducing land occupation. Moreover, the charging process can be completely unmanned, i.e., charging and billing in public places can be handled automatically. In this case, a significant amount of human and material resources can be saved.

3. Convenience and neatness. Charging with WPT eliminates the need for plugging and unplugging connectors, making the charging process more convenient. In addition, the charging environment such as the desktop and the ground, especially when multiple devices are charged simultaneously, becomes simpler and cleaner by getting rid of the shackles of wires.

4. Availability for specific environments. In addition to providing convenience for daily life, WPT is indispensable in some specific situations such as charging for mining equipment, which requires extremely high explosion-proof. In this scenario, traditional plug-in approach may generate sparks, thus causing gas explosions. WPT contributes to guarantee the safety during operation. In space applications, mechanical slip rings are adopted as the traditional power supply unit for the solar wing. The employment of WPT can effectively address the abrasion and extend the life of satellites in orbit. Meanwhile, the bi-directional WPT between space stations enables distribution of power flows, and improves energy utilization and reliability. For the scenario of charging for unmanned underwater vehicles (UUV), the underwater wet plugging method suffers from low alignment accuracy. WPT

allows for effective underwater power supply over a wide range of transfer distance, increasing the efficiency of underwater operations.

Despite its popular use in the design of various products, WPT is still far from being optimal, and some fundamental analytical issues remain unresolved, as detailed below.

In the design of IPT converters, a variety of compensation topologies, including second order and higher order circuits, have been proposed and adopted to address specific issues in practical applications. However, connections between IPT circuits of different orders have not been established systematically to facilitate design. Moreover, the use of higher order compensation circuits for combating various parameters' variations is still not clearly understood and systematically applied to achieve specific performance requirements.

In the design of CPT converters, the study of compensation topologies is still in an early stage. Firstly, for second-order compensation topologies, there is no complete and systematic analysis of the features of second-order compensated CPT converters. A convenient practical model to facilitate the analysis of transfer features is still not available. In addition, although some of the higher order compensation topologies have been proposed for specific applications, no systematic analysis is available to provide a fast understanding of the connections between various compensation topologies that enables design choices to be made conveniently for design compensation topologies in IPT and CPT converters with single or multiple input/output terminals.

1.3 Literature Review

In this section, equivalent circuit models that are widely used for analysis of IPT and CPT systems are reviewed, the purpose being to lay the foundation for exploring the various design choices in the following chapters. Here, to obtain a comprehensive understanding of the role of compensation in a WPT system, various compensation topologies adopted for inductive and capacitive power transfer are reviewed.

1.3.1 Equivalent Circuit Models

To explore the topological properties of wireless power transfer systems, some important equivalent circuit models that are most widely used are reviewed.

IPT Circuit Model

The most well-known equivalent circuit model for IPT converters is the mutual-inductance model [33, 34], where two series equivalent inductors are connected with two induced voltage sources at the primary and secondary sides, respectively, as illustrated in Fig. 1.5(a). Here, L_p and L_s are the self-inductance of the primary (transmitting) and secondary (receiving) windings of the transformer, respectively. The coupling between the windings at the two sides is represented by mutual inductance M, and $M = k\sqrt{L_\mathrm{p}L_\mathrm{s}}$, where k denotes the coupling coefficient. This mutual-inductance model has been adopted as a general equivalent circuit model for the study of IPT systems in the literature [35–42].

To facilitate the analysis of IPT topologies, and hence to observe transfer properties of IPT converters with various compensation topologies more clearly, a T-type two-port network model has been employed [43–45]. In this model, the two self-inductors L_p and L_s together with the induced voltage source are simplified as a T-type inductor structure, as illustrated in Fig. 1.5(b).

CPT Circuit Model

As the research on IPT gradually matures, a number of issues have emerged that cannot be ignored. In addition to the high cost of the Litz wires and cores required in the design of transformers, the presence of metal objects around the system becomes a safety hazard due to the eddy current losses generated by

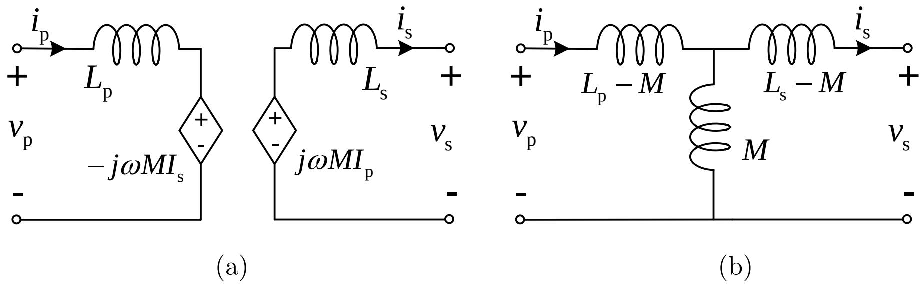

Figure 1.5: Equivalent (a) mutual-inductance model and (b) T-type model of the coupled IPT transformer.

magnetic fields [46]. To address the root causes of these issues, capacitive power transfer (CPT) technology has gradually gained research interest in recent years [47–49]. By transferring energy via the electric field generated by a coupled capacitor pair, the issues of high cost and safety hazard caused by the presence of metal objects can be effectively solved [47, 50, 51].

A typical CPT coupler is usually composed of two symmetrically positioned coupled pairs, and the coupled pairs are constructed by four parallel metal (usually aluminium or copper) plates, as shown in Fig. 1.6(a). Here, P_1 and P_2 are coupling plates at the primary (transmitting) side, and P_3 and P_4 are coupling plates at the secondary (receiving) side. According to the definition of parallel plate capacitors, there usually exist six mutual capacitors generated by the coupling electric field between any two of the plates [9].

Due to the complexity of the six-capacitor model, a variety of equivalent circuit models are adopted. The two-capacitor model is the most widely used equivalent circuit model of the CPT coupler, as shown in Fig. 1.6(b), where the coupler is simplified as two series capacitors connecting each two coupled pairs, i.e., C_{s1} and C_{s2}. In the early stages of study on CPT, the four mutual capacitors except C_{13} and C_{24} in Fig. 1.6(a) were ignored [52], i.e., C_{13} being represented by C_{s1} in Fig. 1.6(b), and C_{24} being represented by C_{s2}. In some of the recent works [8, 53], the CPT coupler comprised of two capacitor plates are used to

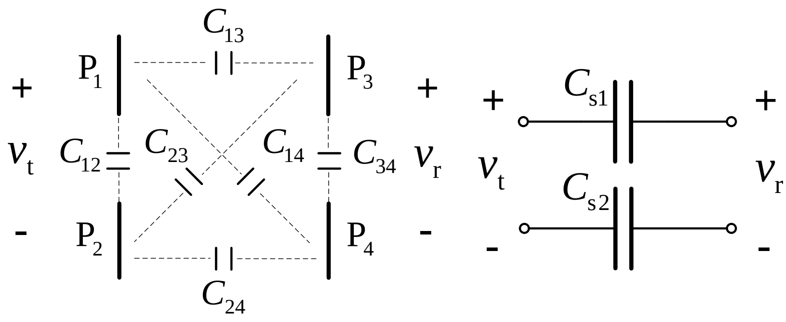

Figure 1.6: Equivalent (a) six-capacitor model and (b) equivalent two-capacitor model of the CPT coupler.

simplify the coupling structure. In Lu *et al.*'s work [10], by setting the relative positions of the coupling plates so that a certain gap is maintained between them, the coupling capacitance can be ignored.

The establishment of equivalent circuit models with high accuracy has gradually been attracting attention. In the literature [54], four mutual capacitors are considered while the two cross ones are ignored. Zhang *et al.* [9] proposed an induced current source (ICS) model for describing CPT converters, taking all six capacitors into account. In this model, the six mutual capacitors are equivalent to two shunt capacitors connected with an induced current source at the primary and secondary sides, respectively. To observe the transfer characteristics of CPT converters more clearly, a Π-type network model has been proposed based on the ICS model. This Π network model is much less computationally demanding, and is increasingly being used. Unfortunately, both the ICS model and the Π model have the common disadvantage that any change in capacitance value of the six mutual capacitors will have an impact on the calculated results of the two equivalent capacitors. This means that any change in the position of coupling plates may lead to significated discrepancies in describing the operation of the CPT system. To address this issue, Wang *et al.* [55] proposed an induced voltage source (IVS) model. In this model, the concept of self-capacitance is introduced from the physical viewpoint so that the equivalent capacitance is not affected by the coupling distance.

In summary, although the analysis on the common equivalent circuit models of IPT converters has reached a mature stage, there is still a lack of simplified circuit models for CPT converters which can accurately describe the circuit features when the coupling capacitance generated by the CPT coupled pairs changes and facilitate the analysis of various topologies of CPT converters.

1.3.2 Compensation Topologies for Inductive Power Transfer

In many practical applications, the power supply terminals are required to provide either constant voltage (CV) or constant current (CC), and in some applications, such as battery charging, the power supply is required to provide both CV and CC depending on the operating phase of the charging process [56, 57], as the equivalent resistance of the battery varies significantly during the charging process. In order to operate in a wide load range, various compensation topologies have been applied in IPT systems to achieve load-independent current (LIC) and load-independent voltage (LIV) output. Research on basic second-order compensation has already entered a mature stage. It is well known that four basic compensation topologies, namely, series/series (S/S), series/parallel (S/P), parallel/series (P/S), and parallel/parallel (P/P) configurations, can achieve LIC or LIV output at specific operating frequencies [27, 28, 39, 58–60]. Further study of the basic compensation networks for both LIC and LIV output has been conducted [61–63], and a series of optimization design based on the second-order compensation schemes have been proposed [64–68].

Moreover, to enhance the operating range and to combat parameter variations, higher order compensation schemes are developed. Recently, a family of higher order compensation topologies have been studied [45]. While achieving LIC or LIV output, these topologies, interpreted in terms of transformer model (T-model) or mutual inductance model (M-model), show good performance in combating the transformer parameter constraints. Specifically, an LCL compensated IPT system has been proposed to provide constant primary current, which is particularly suitable for multi-pickup applications [69–73]. Furthermore, an LCC compensation network has been utilized to enhance the tolerance for lateral misalignment and permits reduction of the system size [38, 74].

However, despite the many individual reports focusing on the use of higher order compensation in combating parameter variations [40, 45, 75], there is still a lack of systematic analysis with clear physical meanings that can guide engineers to design compensation circuits more effectively. In the work of Lu *et al.* [76], sensitivity analysis of voltage gain and efficiency to variation in system parameters has been carried out for various topologies operating in CV mode, aiming at simplifying the control algorithm and minimizing additional converters. The essential connection between second-order and higher order compensation circuits remains unattended. Recently, the transformation between second-order and third-order compensation circuits at the input side, based on sensitivity analysis of selected topologies, has been briefly discussed [77]. Up to now, no systematic analysis on the connection between basic second-order and higher order compensation networks that can provide clear physical interpretations of the roles of extra components in higher order circuits has been reported. Different from the specific inductors and capacitors added for filtering or achieving soft switching of inverters in the many converters, the components of inductors and capacitors in this study serve as part of the compensation to clearly demonstrate the impact of compensation components on the system performance.

1.3.3 Compensation Topologies for Capacitive Power Transfer

Similar to the design of IPT converters, compensation topologies are necessary in CPT converters to enhance power transfer capacity. In much of the reported works, compensation topologies are proposed and designed for certain performance requirements and specific applications concerned. To compensate for the high leakage capacitance, basic series-series (S/S) compensation topology is introduced, where two inductors are connected to the coupler in series at the primary and secondary sides, respectively [47, 78]. To improve the output power level, and reduce the value of the compensated inductance, higher order compensation schemes of double-sided LC (a series inductor connected with a shunt capacitor adjacent to the coupler) [79–81], double-sided LCL (one inductor in parallel with a capacitor, then in series with an inductor next to the coupler) [82, 83] and double-sided LCLC (add a shunt capacitor between LCL and the coupler) [10] have been proposed. In Mai *et al.*'s work [81], the double-sided CL compensation is able to simplify the compensation topology while permitting the capability of long-distance and high-power transmission. Huang *et al.* [52] introduced the Z impedance compensation network for CPT converters, addressing the issue of voltage spikes produced by the branch circuit where the series compensated inductance is located due to the sudden removal of the secondary side. In Sinha *et al.*'s work [84], the effect of parasitic capacitance has been mitigated through dividing the compensated inductors, at the cost of increased complexity of the circuit design. Li *et al.* [85] presented a family of compensation topologies for CPT converters cater for high-power energy transmission. However, the essential connection and transformation between circuits of different orders still receives little attention.

In a recent work [86], systematic analysis from multiple aspects of connection between basic second-order and higher order compensation networks applied for IPT converters are discussed. A similar interpretation for CPT converters will be greatly helpful for designing the compensation topology and selecting parameter sets. Although the CPT circuit performs as a duality of the IPT circuit, there are still fundamental differences between a CPT coupler and an IPT transformer due to the difference in coupling principles. Moreover, there is still a lack of systematic analysis of the basic compensation topologies for CPT converters based on an equivalent circuit model where system parameters are coupling-independent.

1.4 Objectives of the Thesis

The objectives of this thesis are to analyze inductive power transfer (IPT) and capacitive power transfer (CPT) converters with various compensation topologies by establishing connections between basic and higher order compensation networks from a circuit theoretic point of view. All possible extensions from the input side and the output side of basic second-order compensation topologies in IPT and CPT converters will be derived on the basis of a simplified generic circuit model. To identify suitable topologies combating changes of system parameters in the converter, comparisons using sensitivity analysis of various compensation networks will be investigated. In addition, IPT converters with multiple input and output terminals will be illustrated and analyzed in detail to offer unified design principles for multi-load applications. The study offers a convenient interpretation of the mechanisms that contribute to various desirable performance aspects. Analytical studies and experimental verifications will be reported.

1.5 Outline of the Thesis

This thesis is organized as follows.

Chapter 1 introduces the development of wireless power transfer converters, covering equivalent models and compensation topologies of IPT and CPT circuits. The objectives of this research work and the outline of the thesis are provided.

Chapter 2 reviews the fundamental IPT and CPT systems including basic second-order compensation circuits and equivalent models. A new circuit model for CPT systems is presented, which facilitates the calculation of operating conditions for stable and parameter-insensitive power transfer. Transfer characteristics of IPT and CPT circuits with second-order compensation are calculated and analyzed in detail.

Chapter 3 explores the systematic extension of second-order compensation to higher order compensation through current source and voltage source interchange, together with load-independent current and load-independent voltage output conversion, for both IPT circuits. Furthermore, we examine the sensitivity of the basic second-order compensation circuits against system parameters' variation in comparison to higher order compensation circuits. Based on the comparison results of the performance of various compensation topologies, general design pathways to higher order compensated IPT converters are given, which can conveniently provide design guidelines for appropriate compensation topologies that meet specific desired functions. Experimental results are presented to verify the analysis of the various compensation topologies of IPT converters.

Chapter 4 presents connections between second-order and higher order compensated CPT converters in a similar approach to Chapter 3. Systematic extensions to higher order compensation are explored from input, output, and double sides. In addition to third-order compensation, fourth and higher compensations are also exemplified in this chapter. Comparisons and detailed analysis on sensitivity to system parameters of both second-order and higher order compensation are examined, the aim being to offer a fast understanding on merits and defects of various compensation scheme in CPT converters, thus serving to determine a proper compensation topology with expected characteristics. Experimental results are presented to verify the analysis of the various compensation topologies of CPT converters.

Chapter 5 studies an application of multi-input multi-output IPT systems. Based on the appropriate compensation and operating conditions that achieve the required load-independent output, various input and output terminations with desired output power can be realized. General expressions for optimal load values of IPT systems with various inputs and outputs are given. Various control strategies for power regulation are presented. On this basis, a set of design principles for IPT systems in a multi-load environment is proposed. Moreover, improvement with a higher order compensation is derived to facilitate the parameter design.

Finally, Chapter 6 concludes the thesis with a summary of contributions and discussions of some future directions.

Chapter 2

Overview of Basic Compensation Topologies

As mentioned in the previous chapter, the mutual-inductance model is most commonly used as the equivalent circuit model for analysis of inductive power transfer (IPT) converters. In some recent works, an equivalent model based on two-port networks has been established to directly observe the transfer features, especially the operating conditions of IPT converters with various compensation circuits. However, for capacitive power transfer (CPT) converters, which can be viewed as the dual version of IPT converters, general equivalent models for directly analysing the fundamental features are not available. Moreover, systematic analysis of second and higher order compensation topologies in CPT converters is still lacking.

In this chapter, the transfer characteristics of second order compensated IPT circuits based on the two-port network model are reviewed in terms of load-independent (LI) output conditions and corresponding transfer ratios. In addition, two-port based models for CPT circuits are established and analyzed in detail. On this basis, the operating properties of four second-order compensation topologies of CPT circuits are investigated in depth to provide a theoretical basis

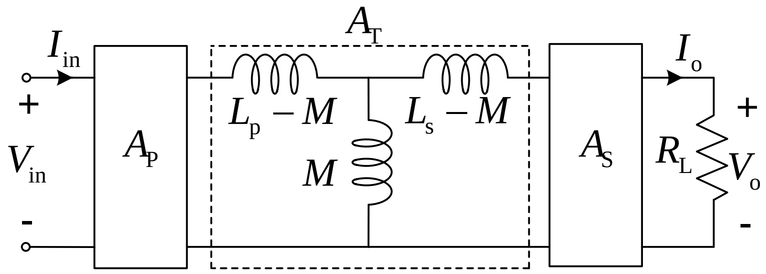

Figure 2.1: Equivalent two-port network model of IPT converter. A_P is the primary-side compensation circuit, A_T the coupled inductor pair, and A_S the secondary-side compensation circuit.

for further analysis of various compensation topologies.

2.1 Equivalent Circuit Models

2.1.1 Two-Port Network Model for IPT

Fig. 2.1 shows an equivalent two-port network of the IPT converter with the T-type transformer derived from a mutual-inductance model. The converter can be driven by an AC voltage or current source, and loaded with an equivalent resistance R_L. Also, V_{in}, I_{in}, V_o and I_o are the input voltage, input current, output voltage and output current, respectively. Practically, the voltage source can be realized by an inverter connected with a rectifier. The current source can be achieved by adding a buck-boost converter between the rectifier and the inverter and tracking the current flowing through the inverter to maintain a constant current. Here, we assume that the input voltage and current sources are both theoretically pure sinusoidal AC sources. Then, the transfer characteristic of the network [87, 88] can be expressed in matrix form as

$$\begin{bmatrix} V_{in} \\ I_{in} \end{bmatrix} = A \begin{bmatrix} V_o \\ I_o \end{bmatrix} \tag{2.1}$$

where A denotes the transmission matrix of the two-port network for IPT converters, and consists of three subnetworks, which are the primary compensation circuit A_{P}, the transformer A_{T}, and the secondary compensation circuit A_{S}. Here, the transformer is represented by a T-type model, as illustrated in Fig. 2.1, where L_{p} and L_{s} denote self-inductance of the transformer at primary and secondary sides, respectively, and M is the mutual inductance between L_{p} and L_{s}. A definition of coupling coefficient k is usually adopted in the analysis of IPT converters, which is given by

$$k = \frac{M}{\sqrt{L_{\mathrm{p}} L_{\mathrm{s}}}} \tag{2.2}$$

All diagonal elements A_{P}, A_{T} and A_{S} are found to be real numbers and all elements off the diagonal are imaginary numbers [89]. Thus, the second-order square matrix A can be obtained by

$$A = A_{\mathrm{P}} A_{\mathrm{T}} A_{\mathrm{S}} = \begin{bmatrix} a_{11} & ja_{12} \\ ja_{21} & a_{22} \end{bmatrix} \tag{2.3}$$

where a_{11}, a_{12}, a_{21} and a_{22} are all real. Using $I_{\mathrm{o}} = V_{\mathrm{o}}/R_{\mathrm{L}}$, $Z_{\mathrm{in}} = V_{\mathrm{in}}/I_{\mathrm{in}}$, and putting (2.3) in (2.1), the voltage gain G_v and trans-conductance G_i for circuits terminated by a voltage source, the current gain H_i and trans-impedance H_i for circuits terminated by a current source, and the input impedance Z_{in} of the IPT circuit can be expressed by the following equations

$$G_v = \frac{V_{\mathrm{o}}}{V_{\mathrm{in}}} = \frac{R_{\mathrm{L}}}{a_{11}R_{\mathrm{L}} + ja_{12}} \tag{2.4}$$

$$G_i = \frac{I_{\mathrm{o}}}{V_{\mathrm{in}}} = \frac{1}{a_{11}R_{\mathrm{L}} + ja_{12}} \tag{2.5}$$

$$H_v = \frac{V_{\mathrm{o}}}{I_{\mathrm{in}}} = \frac{R_{\mathrm{L}}}{ja_{21}R_{\mathrm{L}} + a_{22}} \tag{2.6}$$

$$H_i = \frac{I_{\mathrm{o}}}{I_{\mathrm{in}}} = \frac{1}{ja_{21}R_{\mathrm{L}} + a_{22}} \tag{2.7}$$

$$Z_{\mathrm{in}} = \frac{V_{\mathrm{in}}}{I_{\mathrm{in}}} = \frac{a_{11}R_{\mathrm{L}} + ja_{12}}{ja_{21}R_{\mathrm{L}} + a_{22}} \tag{2.8}$$

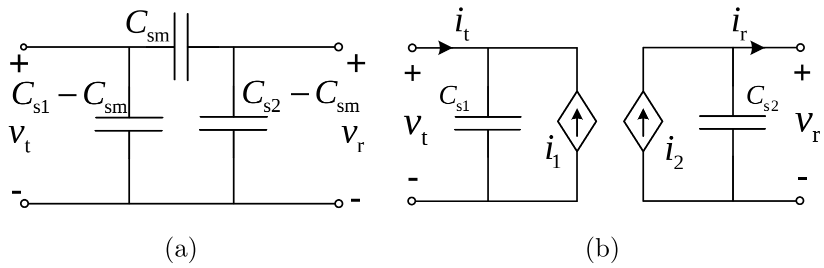

Figure 2.2: (a) Equivalent Π-type two-port network model and (b) equivalent induced-current source model of the coupled CPT pairs.

2.1.2 Two-Port Network Model for CPT

Fig. 2.2(a) shows an equivalent Π-type based two-port network of the CPT coupler. The network can be derived from an induced-current source model, as shown in Fig. 2.2(b), which is commonly adopted as the simplified equivalent circuit model of a CPT converter. It has been shown [61] that C_{s1}, C_{s2} and C_{sm} are given by

$$C_{s1} = \frac{C_{12} + (C_{13} + C_{14})(C_{23} + C_{24})}{C_{13} + C_{14} + C_{23} + C_{24}} \tag{2.9}$$

$$C_{s2} = \frac{C_{34} + (C_{13} + C_{23})(C_{14} + C_{24})}{C_{13} + C_{14} + C_{23} + C_{24}} \tag{2.10}$$

$$C_{sm} = \frac{C_{24}C_{13} - C_{23}C_{14}}{C_{13} + C_{14} + C_{23} + C_{24}} \tag{2.11}$$

where $C_{12}, C_{13}, C_{14}, C_{23}, C_{24}, C_{34}$ are equivalent capacitors among the four plates illustrated in Figs.1.6(a) of Chapter 1.

Then, the coupling coefficient k_{sm} can be defined as

$$k_{sm} = \frac{C_{sm}}{\sqrt{C_{s1}C_{s2}}} \tag{2.12}$$

From the above expressions, we can see that the values of C_{s1} and C_{s2} vary with the equivalent capacitor of the coupler. This imposes strict requirements on the capacitor plates, with the relative positions of the four plates being absolutely

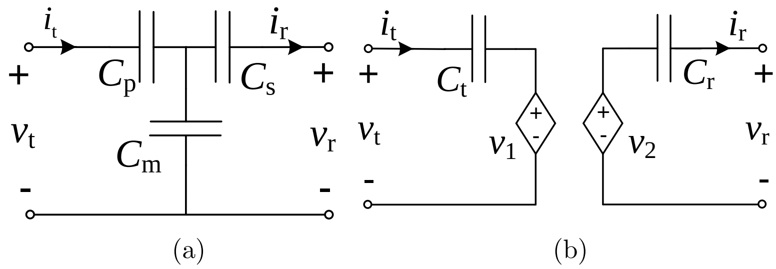

Figure 2.3: (a) Equivalent T-type two-port network model and (b) equivalent induced-voltage source model of the coupled CPT pair.

fixed to maintain the resonance state. In addition, resonance conditions of the compensation parameters are relatively complex and are all coupling-dependent, which would make the subsequent analysis of parameter sensitivity complicated. These limitations will be theoretically analyzed in detail in Section 2.3.

To address the above issues, we present a T-type based two-port network model as shown in Fig. 2.3(a). The network can be derived from an induced-voltage source model [55], as shown in Fig. 2.3(b). It should be noted that capacitor C_{m} is not equal to C_{sm}, and capacitors C_{t} and C_{r} are not C_1 and C_2 in the Π-type model. Here, C_{t} (C_{r}) has a clear physical meaning of the transmitting (receiving) capacitance when secondary (primary) plates P_3 and P_4 (P_1 and P_2) are removed. Thus, similar to the concept of self-inductance in IPT converters, C_{t} and C_{r} can be regarded as self-capacitance of a CPT converter, and only depend on the distance between the primary and secondary plates. Furthermore, C_{t} and C_{r} can also be expressed with regard to equivalent capacitors illustrated in Fig. 1.6(a) as [55]

$$\begin{aligned} C_{\mathrm{t}} = {} & C_{12} + \\ & \frac{C_{13}C_{14}(C_{23}+C_{24})+C_{23}C_{24}(C_{13}+C_{14})+C_{34}(C_{13}+C_{14})(C_{23}+C_{24})}{(C_{13}+C_{23})(C_{14}+C_{24})+C_{34}(C_{13}+C_{14}+C_{23}+C_{24})} \end{aligned} \tag{2.13}$$

$$\begin{aligned} C_{\mathrm{r}} = {} & C_{34} + \\ & \frac{C_{23}C_{14}(C_{13}+C_{24})+C_{13}C_{24}(C_{23}+C_{14})+C_{12}(C_{13}+C_{14})(C_{23}+C_{24})}{(C_{13}+C_{23})(C_{14}+C_{24})+C_{34}(C_{13}+C_{14}+C_{23}+C_{24})} \end{aligned} \tag{2.14}$$

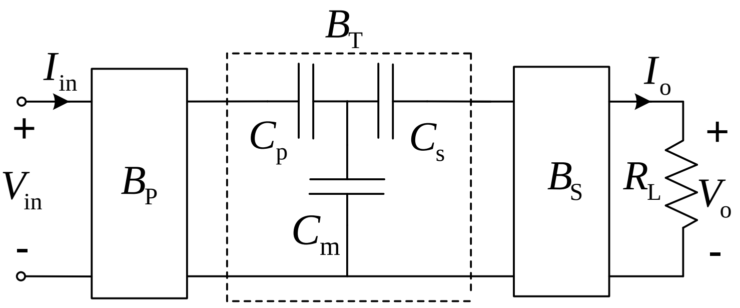

Figure 2.4: Equivalent T-type two-port network model of CPT converter. B_{P} is the primary-side compensation circuit, B_{T} the coupled capacitor pairs, and B_{S} the secondary-side compensation circuit.

Then, the parameters in the T-type model can be defined by the following equations:

$$C_{\mathrm{p}} = \frac{C_{\mathrm{m}}C_{\mathrm{t}}}{C_{\mathrm{m}} - C_{\mathrm{t}}} \tag{2.15}$$

$$C_{\mathrm{s}} = \frac{C_{\mathrm{m}}C_{\mathrm{r}}}{C_{\mathrm{m}} - C_{\mathrm{r}}} \tag{2.16}$$

$$k_{\mathrm{c}} = \frac{\sqrt{C_{\mathrm{t}}C_{\mathrm{r}}}}{C_{\mathrm{m}}} \tag{2.17}$$

Fig. 2.4 illustrates the complete T-type based two-port network of a CPT converter, which can be driven by an AC voltage or current source, and loaded with an equivalent resistance R_{L}. Here, V_{in}, I_{in}, V_{o} and I_{o} are the input voltage, input current, output voltage and output current, respectively. Similar to the analysis in the previous section, the transfer characteristic of the CPT network can be expressed in matrix form as

$$\begin{bmatrix} V_{\mathrm{in}} \\ I_{\mathrm{in}} \end{bmatrix} = B \begin{bmatrix} V_{\mathrm{o}} \\ I_{\mathrm{o}} \end{bmatrix} \tag{2.18}$$

where B denotes the transmission matrix of the two-port network for CPT converters, and consists of the primary compensation B_{P}, the coupler B_{T}, and the

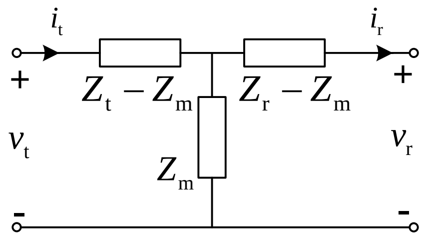

Figure 2.5: An unified two-port network model for IPT and CPT converters.

secondary compensation B_S, and the second-order square matrix B can be obtained by

$$B = B_P B_T B_S = \begin{bmatrix} b_{11} & jb_{12} \\ jb_{21} & b_{22} \end{bmatrix} \tag{2.19}$$

where b_{11}, b_{12}, b_{21} and b_{22} are all real [75]. Using $I_o = V_o/R_L$, $Z_{in} = V_{in}/I_{in}$, and substituting (2.19) into (2.18), the transfer ratios G_v and G_i for circuits terminated by a voltage source, H_v and H_i for circuits terminated by a current source, and the input impedance Z_{in} of the CPT circuit can be derived as follows:

$$G_v = \frac{R_L}{b_{11}R_L + jb_{12}} \tag{2.20}$$

$$G_i = \frac{1}{b_{11}R_L + jb_{12}} \tag{2.21}$$

$$H_v = \frac{R_L}{jb_{21}R_L + b_{22}} \tag{2.22}$$

$$H_i = \frac{1}{jb_{21}R_L + b_{22}} \tag{2.23}$$

$$Z_{in} = \frac{b_{11}R_L + jb_{12}}{jb_{21}R_L + b_{22}} \tag{2.24}$$

2.1.3 Unified Two-Port Network Model

Based on the aforementioned modeling process for IPT and CPT converters, a unified two-port network model can be developed for the transformer of IPT converters and the coupler of CPT converters, using the principle of duality, as shown in Fig. 2.5. Here the coupling coefficient K is defined as

$$K = \frac{Z_\mathrm{m}}{\sqrt{Z_\mathrm{t} Z_\mathrm{r}}} \tag{2.25}$$

where Z_t and Z_r are the self-impedances at the primary and secondary sides, respectively, and Z_m is the mutual impedance between Z_t and Z_r. Specifically, for IPT converters, we have

$$Z_\mathrm{t,r,m} = j\omega L_\mathrm{t,r,m} \tag{2.26}$$

$$K = \frac{L_\mathrm{m}}{\sqrt{L_\mathrm{t} L_\mathrm{r}}} \tag{2.27}$$

where K represents k in (2.2), and the symbols of L_t, L_r and L_m are the same as the L_p, L_s and M in Section 2.1.1, respectively. For CPT converters, we have

$$Z_\mathrm{t,r,m} = \frac{1}{j\omega C_\mathrm{t,r,m}} \tag{2.28}$$

$$K = \frac{\sqrt{C_\mathrm{t} C_\mathrm{r}}}{C_\mathrm{m}} \tag{2.29}$$

where K represents k_c in (2.17). Thus, we have established the equivalent model to provide a theoretical basis for analysis of various compensation topologies in IPT and CPT converters.

2.2 Second-order Compensated IPT Circuits

Four basic second-order compensation topologies of an IPT converter [39, 90], based on the most commonly used mutual-inductance model, are shown in Fig. 2.6. As dictated by Kirchhoff's laws, the input must be terminated by a voltage (current) source when series (parallel) compensation is applied at the primary side. Thus, from the circuit theoretic point of view, the series/series (S/S) and se-

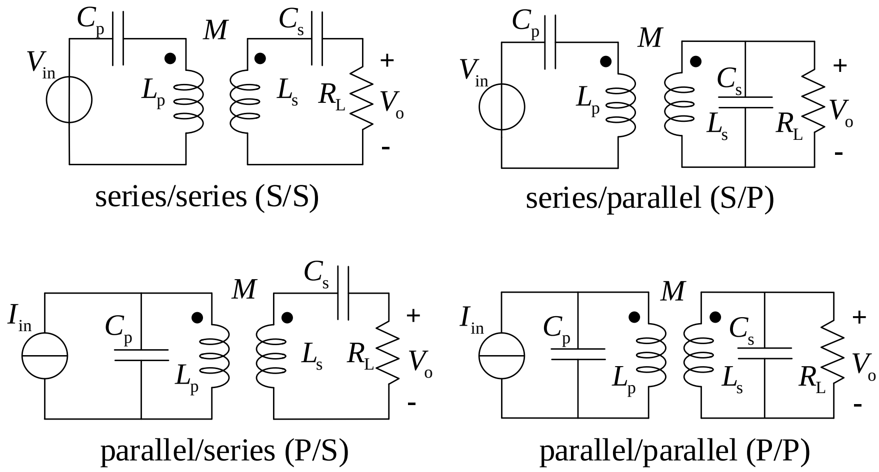

Figure 2.6: Equivalent circuits of IPT converters with basic second-order compensation circuits.

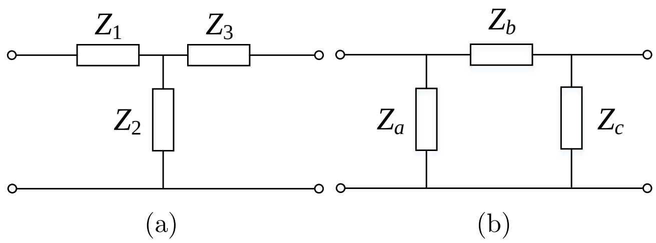

Figure 2.7: Equivalent (a) T-type and (b) Π-type impedance models.

ries/parallel (S/P) compensation circuits require an input voltage source, whereas the parallel/series (P/S) and parallel/parallel (P/P) compensation circuits require a current source feeding the input.

Using the theory of two-port networks [91], the T-network and Π-network illustrated in Fig. 2.7 can be expressed in matrix form as

$$Z_{\mathrm{T}} = \begin{bmatrix} \dfrac{Z_1+Z_2}{Z_2} & \dfrac{Z_1Z_2+Z_1Z_3+Z_2Z_3}{Z_2} \\ \dfrac{1}{Z_2} & \dfrac{Z_2+Z_3}{Z_2} \end{bmatrix} \tag{2.30}$$

$$Z_{\Pi} = \begin{bmatrix} \dfrac{Z_b+Z_c}{Z_c} & Z_b \\ \dfrac{Z_a+Z_b+Z_c}{Z_aZ_c} & \dfrac{Z_a+Z_b}{Z_a} \end{bmatrix} \tag{2.31}$$

where Z's are impedances.

Table 2.1: Properties of IPT Converters with Various Conditions Based on the Two-Port Network Model.

Requirement		Condition	Ratio
VS	LIV	$a_{12}=0$	$G_v=\frac{1}{a_{11}}$
	LIV & ZPA	$a_{12}=a_{21}=0$	$Z_{\mathrm{in}}=\frac{a_{11}}{a_{22}}R_{\mathrm{L}}$
	LIC	$a_{11}=0$	$G_i=\frac{1}{a_{12}}$
	LIC & ZPA	$a_{11}=a_{22}=0$	$Z_{\mathrm{in}}=\frac{a_{12}}{a_{21}R_{\mathrm{L}}}$
CS	LIV	$a_{22}=0$	$H_v=\frac{1}{ja_{21}}$
	LIV & ZPA	$a_{11}=a_{22}=0$	$Z_{\mathrm{in}}=\frac{a_{12}}{a_{21}R_{\mathrm{L}}}$
	LIC	$a_{21}=0$	$H_i=\frac{1}{a_{22}}$
	LIC & ZPA	$a_{12}=a_{21}=0$	$Z_{\mathrm{in}}=\frac{a_{11}}{a_{22}}R_{\mathrm{L}}$

LIV(C): load-independent voltage (current); ZPA: zero phase angle.

Thus, according to (2.30), the primary (secondary) matrix $A_{\mathrm{P(S)}}$ with series and parallel compensation can be expressed as

$$A_{\mathrm{P(S)-series}}=\begin{bmatrix}1 & \dfrac{1}{j\omega C_{\mathrm{p}}}\\ 0 & 1\end{bmatrix} \tag{2.32}$$

$$A_{\mathrm{P(S)-parallel}}=\begin{bmatrix}1 & 0\\ j\omega C_{\mathrm{p}} & 1\end{bmatrix} \tag{2.33}$$

where C_{p} and C_{s} are compensation capacitors at the primary and secondary sides. ω is the operating frequency. Then, the T-type transformer A_{T} is given by

$$A_{\mathrm{T}}=\begin{bmatrix}\dfrac{L_{\mathrm{p}}}{M} & j\omega M(k^{-2}-1)\\ \dfrac{1}{j\omega M} & \dfrac{L_{\mathrm{s}}}{M}\end{bmatrix} \tag{2.34}$$

On this basis, the transfer matrices of the four IPT circuits can be obtained. According to equations (2.4) $\sim$ (2.7), to achieve a constant load-independent (LI)

Table 2.2: Basic Properties of Second-order Compensated IPT Circuits Under Load-Independent Output Conditions. $k = M/\sqrt{L_\mathrm{p}L_\mathrm{s}}$.

Type	Operating frequency	Transfer ratio	LI feature	ZPA
S/S	$\omega = \frac{1}{\sqrt{L_\mathrm{p}C_\mathrm{p}}} = \frac{1}{\sqrt{L_\mathrm{s}C_\mathrm{s}}}$	$G_i = \frac{1}{\omega M}$	LIC	Yes
S/S	$\omega = \frac{1}{\sqrt{(L_\mathrm{p}-M)C_\mathrm{p}}} = \frac{1}{\sqrt{(L_\mathrm{s}-M)C_\mathrm{s}}}$	$G_v = 1$	LIV	No
S/P	$\omega = \frac{1}{\sqrt{(1-k^2)L_\mathrm{p}C_\mathrm{p}}} = \frac{1}{\sqrt{L_\mathrm{s}C_\mathrm{s}}}$	$G_v = \frac{L_\mathrm{s}}{M}$	LIV	Yes
S/P	$\omega = \frac{1}{\sqrt{(L_\mathrm{p}-M)C_\mathrm{p}}} = \frac{1}{\sqrt{(L_\mathrm{s}-M)C_\mathrm{s}}}$	$G_i = \frac{1}{\omega(L_\mathrm{s}-M)}$	LIC	No
P/S	$\omega = \frac{1}{\sqrt{L_\mathrm{p}C_\mathrm{p}}} = \frac{1}{\sqrt{(1-k^2)L_\mathrm{s}C_\mathrm{s}}}$	$H_i = \frac{L_\mathrm{p}}{M}$	LIC	Yes
P/S	$\omega = \frac{1}{\sqrt{L_\mathrm{s}C_\mathrm{s}}}$	$H_v = j\omega M$	LIV	No
P/P	$\omega = \frac{1}{\sqrt{(1-k^2)L_\mathrm{p}C_\mathrm{p}}} = \frac{1}{\sqrt{(1-k^2)L_\mathrm{s}C_\mathrm{s}}}$	$H_v = j\omega M(1-k^{-2})$	LIV	Yes
P/P	$\omega = \frac{1}{\sqrt{L_\mathrm{s}C_\mathrm{s}}}$	$H_i = \frac{M}{L_\mathrm{s}}$	LIC	No

LI: load independent; LIV(C): load-independent voltage (current); ZPA: zero phase angle.

output, including load-independent voltage (LIV) and load-independent current (LIC), various operating conditions are required to be satisfied. Here, we take an IPT converter driven by a voltage source with LIV output as an example, from (2.4), the transfer matrix need to satisfy

$$a_{12} = 0. \tag{2.35}$$

Then, the voltage gain and input impedance are given by

$$G_v = \frac{1}{a_{11}} \tag{2.36}$$

$$Z_\mathrm{in} = \frac{a_{11}R_\mathrm{L}}{ja_{21}R_\mathrm{L} + a_{22}} \tag{2.37}$$

In some specific applications, to improve the power transfer capacity of an IPT converter, zero reactive power input is always required, i.e., zero phase angle (ZPA) input. This means that the input impedance is purely resistive. Thus, a_{21}

in (2.37) should be zero, and Z_{in} can be simplified as

$$Z_{\text{in}} = \frac{a_{11}}{a_{22}} R_{\text{L}} \tag{2.38}$$

Likewise, conditions of the IPT converters with other output and input requirements can be theoretically obtained, as summarized in Table 2.1. The expressions listed in this table are also applicable to CPT converters when parameter a_{ij} is replaced by parameter b_{ij} in the CPT transfer matrix, where $i, j = 1$, 2.

Combining the expressions in Table 2.1 and transfer matrices (2.32) $\sim$ (2.34), we can obtain the transfer properties of basic second-order compensated IPT converters, as listed in Table 2.2.

2.3 Second-order Compensated CPT Circuits

2.3.1 Properties based on Π-type model

As introduced in Section 2.1.2, a CPT converter can be represented by a Π-type or T-type two-port network model, derived from the induced-current source or induced-voltage source model, respectively. We assess the transfer features based on the Π-type model first.

Fig. 2.8 shows four second-order compensated CPT circuits. As a dual version of the IPT converter, the CPT converter is compensated with inductors in series or in parallel at the primary and secondary sides. Specifically, L_{p} denotes the primary compensated inductor, and L_{s} denotes the secondary compensated inductor. Similarly as in the IPT circuit, in a CPT circuit, the S/S and S/P compensated topologies are usually driven by an input voltage source, whereas the P/S and P/P compensation circuits are driven by an input current source according to Kirchhoff's law. Using the theory of two-port networks, the series

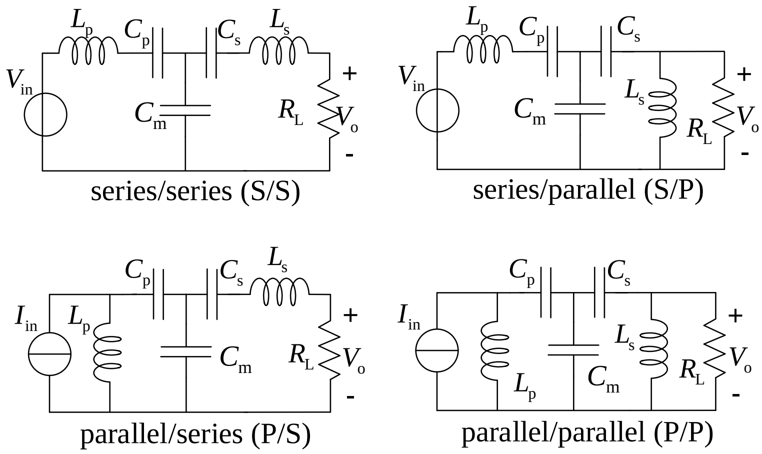

Figure 2.8: Equivalent circuits of CPT converters with basic second-order compensation circuits.

and parallel compensation can be expressed in matrix form as

$$B_{\mathrm{P(S)-series}} = \begin{bmatrix} 1 & j\omega L_{\mathrm{p}} \\ 0 & 1 \end{bmatrix} \tag{2.39}$$

$$B_{\mathrm{P(S)-parallel}} = \begin{bmatrix} 1 & 0 \\ \dfrac{1}{j\omega L_{\mathrm{p}}} & 1 \end{bmatrix} \tag{2.40}$$

where ω is the operating frequency. According to (2.31), the Π-type transformer B_Π is given by

$$B_\Pi = \begin{bmatrix} \dfrac{C_{\mathrm{s2}}}{C_{\mathrm{sm}}} & \dfrac{1}{j\omega C_{\mathrm{sm}}} \\ j\omega\dfrac{C_{\mathrm{s1}}C_{\mathrm{s2}}(1-{k_{\mathrm{sm}}}^2)}{C_{\mathrm{sm}}} & \dfrac{C_{\mathrm{s1}}}{C_{\mathrm{sm}}} \end{bmatrix} \tag{2.41}$$

The analysis of operating conditions for IPT converters in the previous section also applies to the CPT converters here. On the basis of conditions summarized in Table 2.1 and the above equations, the transfer characteristics of Π-type two-port model based CPT converters with second-order compensations can be obtained, as listed in Table 2.3.

It can be observed from the calculation results that to achieve the required LI

Table 2.3: Basic Properties of Second-order Compensated Π-model CPT Circuits Under Load-Independent Output Conditions. $k_{\mathrm{sm}} = \frac{C_{\mathrm{sm}}}{\sqrt{C_{\mathrm{s1}}C_{\mathrm{s2}}}}$.

Type	Operating frequency	Transfer ratio	Feature
S/S	$\omega = \frac{1}{\sqrt{L_{\mathrm{p}}C_{\mathrm{s1}}(1-k_{\mathrm{sm}}^2)}} = \frac{1}{\sqrt{L_{\mathrm{s}}C_{\mathrm{s2}}(1-k_{\mathrm{sm}}^2)}}$	$G_i = j\omega C_{\mathrm{sm}}(1-k_{\mathrm{sm}}^{-2})$	LIC & ZPA
S/P	$\omega = \frac{1}{\sqrt{L_{\mathrm{p}}C_{\mathrm{s1}}}} = \frac{1}{\sqrt{L_{\mathrm{s}}C_{\mathrm{s2}}(1-k_{\mathrm{sm}}^2)}}$	$G_v = \frac{C_{\mathrm{s1}}}{C_{\mathrm{sm}}}$	LIV & ZPA
P/S	$\omega = \frac{1}{\sqrt{L_{\mathrm{p}}C_{\mathrm{s1}}(1-k_{\mathrm{sm}}^2)}} = \frac{1}{\sqrt{L_{\mathrm{s}}C_{\mathrm{s2}}}}$	$H_i = \frac{C_{\mathrm{s2}}}{C_{\mathrm{sm}}}$	LIC & ZPA
P/P	$\omega = \frac{1}{\sqrt{L_{\mathrm{p}}C_{\mathrm{s1}}}} = \frac{1}{\sqrt{L_{\mathrm{s}}C_{\mathrm{s2}}}}$	$H_v = j\frac{1}{\omega C_{\mathrm{sm}}}$	LIV & ZPA

LIV(C): load-independent voltage (current); ZPA: zero phase angle.

output, the operating frequency of each compensation topology depends on the mutual capacitance because C_{s1} and C_{s1} are both related to coupling parameters, i.e., ω is always coupling-dependent. This indicates that, although capacitance C_{s1} and C_{s2} can be regarded as fixed values by minimizing the other capacitances among the coupling plates (via increasing the distance between the plates on the same side), the resonance conditions are still quite complicated and the resonance frequency is sensitive to the environment during practical operations.

2.3.2 Properties based on T-type model

Similar to the expression in equation (2.34), the CPT coupler represented by a T-type model in matrix form is given by

$$B_{\mathrm{T}} = \begin{bmatrix} \dfrac{C_{\mathrm{m}}}{C_{\mathrm{t}}} & \dfrac{k_{\mathrm{c}}^{-2}-1}{j\omega C_{\mathrm{m}}} \\ j\omega C_{\mathrm{m}} & \dfrac{C_{\mathrm{m}}}{C_{\mathrm{r}}} \end{bmatrix} \tag{2.42}$$

Using the S/S compensated CPT converter as an example, the detailed derivation process for transfer features with various operating requirements is given as follows.

According to (2.42) and (2.39), the transfer function of the S/S compensated CPT converter can be expressed as

$$B_{\text{series/series}} = \begin{bmatrix} \dfrac{C_{\mathrm{m}}}{C_t} - \omega^2 C_{\mathrm{m}} L_{\mathrm{p}} & \dfrac{j(k_{\mathrm{c}}^2 - 1)}{k_{\mathrm{c}}^2 \omega C_{\mathrm{m}}} + j\omega C_{\mathrm{m}} \left(\dfrac{L_{\mathrm{p}}}{C_{\mathrm{r}}} + \dfrac{L_{\mathrm{s}}}{C_{\mathrm{t}}} - \omega^2 L_{\mathrm{p}} L_{\mathrm{s}} \right) \\ j\omega C_{\mathrm{m}} & \dfrac{C_{\mathrm{m}}}{C_r} - \omega^2 C_{\mathrm{m}} L_{\mathrm{s}} \end{bmatrix} \tag{2.43}$$

On the basis of the properties and conditions in Table 2.1 in Section 2.2, we put $b_{11} = b_{22} = 0$ into (2.43), the resonance conditions for achieving LIC output and ZPA input simultaneously can be obtained as

$$\omega = \frac{1}{\sqrt{L_{\mathrm{p}} C_{\mathrm{t}}}} = \frac{1}{\sqrt{L_{\mathrm{s}} C_{\mathrm{r}}}} \tag{2.44}$$

The corresponding trans-conductance G_i can be found as

$$G_i = \frac{1}{b_{12}} = -j\omega C_{\mathrm{m}} \tag{2.45}$$

For requirements with LIV output and ZPA input, it can be readily obtained from (2.43) that b_{21} is not zero, because coupling should exist for power to be transferred from the primary side to the secondary side. This implies that ZPA input cannot be achieved in S/S compensated CPT converters. Then, substituting $b_{12} = 0$ by (2.43), we get the LIV output conditions as

$$\omega = \frac{1}{\sqrt{L_{\mathrm{p}} C_{\mathrm{p}}}} = \frac{1}{\sqrt{L_{\mathrm{p}} C_{\mathrm{p}}}} \tag{2.46}$$

where $C_{\mathrm{p}} = \frac{C_{\mathrm{m}} C_{\mathrm{t}}}{C_{\mathrm{m}} - C_{\mathrm{t}}}$, $C_{\mathrm{s}} = \frac{C_{\mathrm{m}} C_{\mathrm{r}}}{C_{\mathrm{m}} - C_{\mathrm{r}}}$.

Then, the corresponding trans-conductance G_v can be derived as

$$G_i = \frac{1}{b_{11}} = 1 \tag{2.47}$$

Table 2.4: Basic Properties of Second-order Compensated T-model CPT Circuits Under Load-Independent Output Conditions. $k_\mathrm{c} = \frac{\sqrt{C_\mathrm{t}C_\mathrm{r}}}{C_\mathrm{m}}$.

Type	Operating frequency	Transfer ratio	LI feature	ZPA
S/S	$\omega = \frac{1}{\sqrt{L_\mathrm{p}C_\mathrm{t}}} = \frac{1}{\sqrt{L_\mathrm{s}C_\mathrm{r}}}$	$G_i = -j\omega C_\mathrm{m}$	LIC	Yes
S/S	$\omega = \frac{1}{\sqrt{L_\mathrm{p}C_\mathrm{p}}} = \frac{1}{\sqrt{L_\mathrm{s}C_\mathrm{s}}}$	$G_v = 1$	LIV	No
S/P	$\omega = \frac{1}{\sqrt{L_\mathrm{p}C_\mathrm{t}(1-{k_\mathrm{c}}^2)^{-1}}} = \frac{1}{\sqrt{L_\mathrm{s}C_\mathrm{r}}}$	$G_v = \frac{C_\mathrm{m}}{C_\mathrm{r}}$	LIV	Yes
S/P	$\omega = \frac{1}{\sqrt{L_\mathrm{p}C_\mathrm{p}}} = \frac{1}{\sqrt{L_\mathrm{s}C_\mathrm{s}}}$	$G_i = j\omega C_\mathrm{s}$	LIC	No
P/S	$\omega = \frac{1}{\sqrt{L_\mathrm{p}C_\mathrm{t}}} = \frac{1}{\sqrt{L_\mathrm{s}C_\mathrm{r}(1-{k_\mathrm{c}}^2)^{-1}}}$	$H_i = \frac{C_\mathrm{m}}{C_\mathrm{t}}$	LIC	Yes
P/S	$\omega = \frac{1}{\sqrt{L_\mathrm{p}C_\mathrm{t}}} = \frac{1}{\sqrt{L_\mathrm{s}C_\mathrm{r}}}$	$H_v = j\frac{1}{\omega C_\mathrm{p}}$	LIV	No
P/P	$\omega = \frac{1}{\sqrt{L_\mathrm{p}C_t(1-{k_\mathrm{c}}^2)^{-1}}} = \frac{1}{\sqrt{L_\mathrm{s}C_\mathrm{r}(1-{k_\mathrm{c}}^2)^{-1}}}$	$H_v = j\frac{1-{k_\mathrm{c}}^2}{\omega C_\mathrm{m}{k_\mathrm{c}}^2}$	LIV	Yes
P/P	$\omega = \frac{1}{\sqrt{L_\mathrm{p}C_\mathrm{p}}} = \frac{1}{\sqrt{L_\mathrm{s}C_\mathrm{s}}}$	$H_i = -\frac{C_\mathrm{s}}{C_\mathrm{p}}$	LIC	No

LI: load independent; LIV(C): load-independent voltage (current); ZPA: zero phase angle.

The basic transfer properties of CPT converters with other compensations can be obtained in a similar way to the above derivation process. The calculation results of second-order compensated CPT converters are listed in Table 2.4.

2.4 Summary

In this chapter, we first review the equivalent models and basic properties of inductive power transfer (IPT) converters with four second-order compensation circuits. Based on the circuit duality principle, we present a T-type two-port network model applied for capacitive power transfer (CPT) converters. A unified two-port network model for both IPT and CPT converters is summarized. Then, four basic second-order series/series, series/parallel, parallel/series and parallel/parallel compensated CPT converters are presented and analyzed in depth. The limitations of the commonly used Π-type model are investigated in terms of the requirements of coupled capacitor pairs and complexity of the operating conditions.

Furthermore, the transfer features of the second-order compensated CPT converters based on Π and the presented T models are theoretically analyzed to highlight the advantages of the presented model in coupling independence and simplicity for circuit analysis. This chapter provides a theoretical basis for the detailed study presented in the subsequent chapters.

Chapter 3

Pathways to Higher Order Compensated IPT Circuits

In this chapter, we attempt to make a clear connection of higher order compensation circuits with the basic well-known second-order compensation circuits, thereby offering a convenient interpretation of the mechanism that contributes to the widened operating range and enhanced performance. Specifically, based on the properties of basic second-order compensation IPT topologies analyzed in the previous chapter, we first explore the transformation of second-order compensation to third-order compensation through current source and voltage source interchange, together with LIC and LIV output conversion, which can be accomplished by adding an extra inductor or capacitor to the input or output of the original basic second-order compensation circuit. After that, we examine the sensitivity of the basic second-order compensation circuits against input voltage and system parameters' variation in comparison to third-order compensation circuits. In this chapter, we focus our attention on practical applications where the input is fed by a voltage source. For instance, we consider the input voltage variation in the original basic second-order compensation circuit being translated to input *current* variation in the new third-order compensation circuit. Under this interpretation, we easily see that the extra inductor serves to convert the voltage source (which may be varying over a wide range) to a near constant current source. Thus, the widening in operating range can be systematically analyzed in terms of sensitivity of the circuits against input voltage variation.

3.1 Connecting Second and Higher Order Compensation Circuits

Shown in Fig. 3.1 are equivalent circuits of the second-order and the extended third-order compensation circuits for inductive power transfer. As mentioned in Chapter 2, the S/S and S/P compensation circuits require an input voltage source, whereas the P/S and P/P compensation circuits require a current source feeding the input. Moreover, input voltage source is strictly prohibited for the P/S and P/P circuits unless an inductor is connected in series with it, as given in the LC/S and LC/P circuits. Here,"LC" stands for the compensation topology composed of a series inductor and a shunt capacitor. These extended circuits are third-order compensation circuits and are rooted from the P/S and P/P circuits, though they can now be fed by an input voltage source, like the S/S and S/P circuits. Likewise, we can extend the S/S and S/P circuits at the load (secondary) side, resulting in third-order compensation circuits with voltage and current interchanged termination. As extra circuit parameters are available in the third-order compensation circuits, the possible operating ranges are expected to be widened, leading to improved design flexibility. In the following, we will evaluate these third-order circuits as extensions of the standard second-order compensation circuits in terms of their sensitivity to input voltage variation and parameter fluctuations. To keep our discussion practical, we will focus our attention on compensation circuits that are designed for input voltage termination.

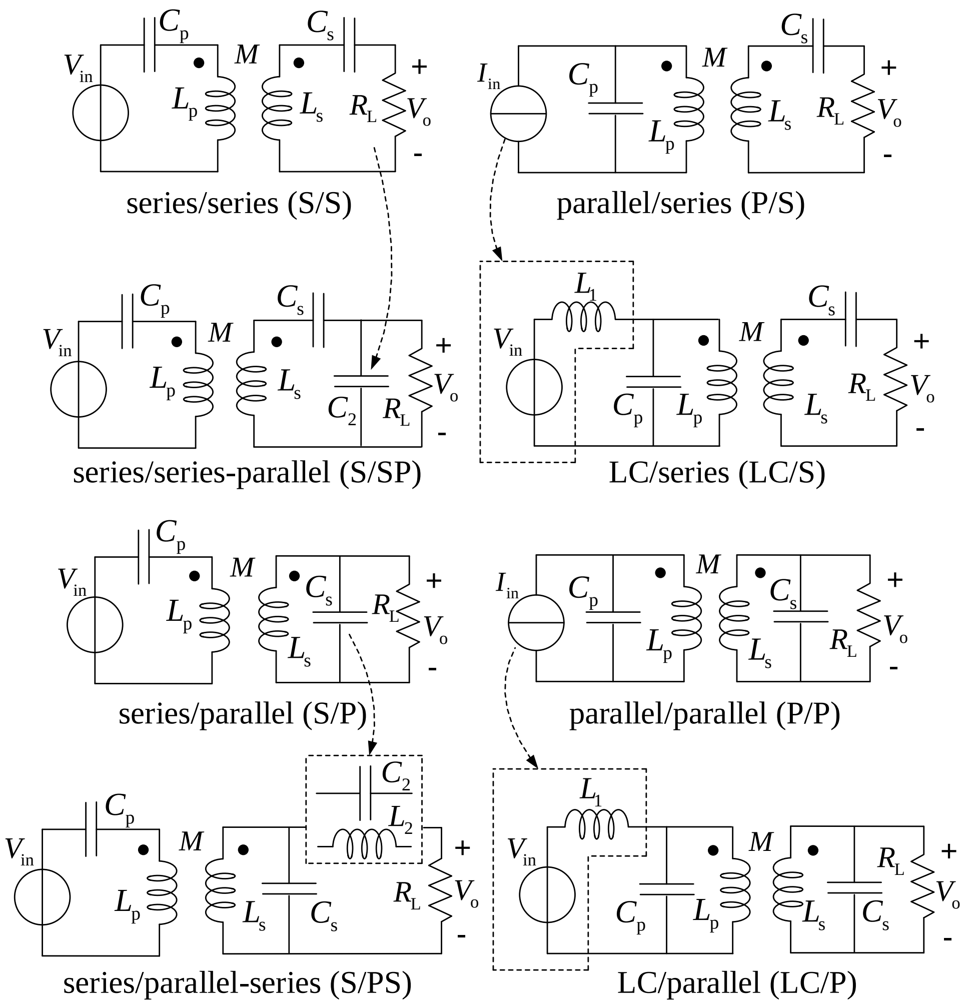

Figure 3.1: Equivalent circuits of IPT converters with basic second-order and extended third-order compensation circuits.

3.1.1 Input-side Extension

Voltage sources are commonly utilized as the input sources at the primary side of IPT converters. With an additional inductor in series with the input voltage source, a near constant input current can be realized, which is equivalent to a current source, as shown in Fig. 3.4(a). Specifically, the equivalent current source reduces the order of compensation network from third-order to second-order. In this case, the input-side series inductor L_1 serves a unique role in maintaining a near constant or less fluctuated current, as well as in reducing the sensitivity to input variation. Thus, the design of the matching compensation circuits in primary and secondary sides can be based on the current source compensation.

Application of routine circuit analysis gives the input impedance of LC/S and LC/P compensation circuits shown in Fig. 3.1 as

$$Z_{\mathrm{in}} = j\omega L_1 + \frac{1}{j\omega C_{\mathrm{p}}} \parallel \left(j\omega L_{\mathrm{p}} + \frac{\omega^2 M^2}{Z_{\mathrm{S}}} \right) \tag{3.1}$$

where $Z_{\mathrm{S-S}} = j\omega L_{\mathrm{S}} + \frac{1}{j\omega C_{\mathrm{s}}} + R_{\mathrm{L}}$ for the LC/S compensated circuit, and $Z_{\mathrm{S-P}} = j\omega L_{\mathrm{S}} + \frac{1}{j\omega C_{\mathrm{s}}} \parallel R_{\mathrm{L}}$ for the LC/P compensated circuit. Then, the input current of the LC/S compensated circuit can be calculated as

$$I_{\mathrm{in-LC/S}} = \frac{V_{\mathrm{in}}}{j\omega \left(L_1 - L_{\mathrm{p}} \right) + R_{\mathrm{L}} {L_{\mathrm{p}}}^2 / M^2} \tag{3.2}$$

According to the properties listed in Table 3.1, since the system operates at the resonance frequency, we can obtain the condition of L_1 of the LC/S compensated circuit for achieving near constant input current as follows:

$$k^2 \left(\frac{L_1}{L_{\mathrm{p}}} - 1 \right) Q_{\mathrm{L-S}} \gg 1 \tag{3.3}$$

Likewise, the input current and the condition of L_1 in the LC/P compensated circuit are given by

$$I_{\mathrm{in-LC/P}} = \frac{jk^2 R_{\mathrm{L}} V_{\mathrm{in}}}{j\omega^2 L_{\mathrm{p}} L_{\mathrm{s}} (1-k^2)^2 - \omega k^2 R_{\mathrm{L}} \left(L_1 - (1-k^2) L_{\mathrm{p}} \right)} \tag{3.4}$$

$$\frac{k^2}{1-k^2} \left(\frac{L_1}{(1-k^2) L_{\mathrm{p}}} - 1 \right) Q_{\mathrm{L-P}} \gg 1 \tag{3.5}$$

where k is the coupling coefficient, and $k = \frac{M}{L_{\mathrm{p}} L_{\mathrm{s}}}$. Also, $Q_{\mathrm{L-S}} = \frac{\omega L_{\mathrm{s}}}{R_{\mathrm{L}}}$ and $Q_{\mathrm{L-P}} = \frac{R_{\mathrm{L}}}{\omega L_{\mathrm{s}}}$.

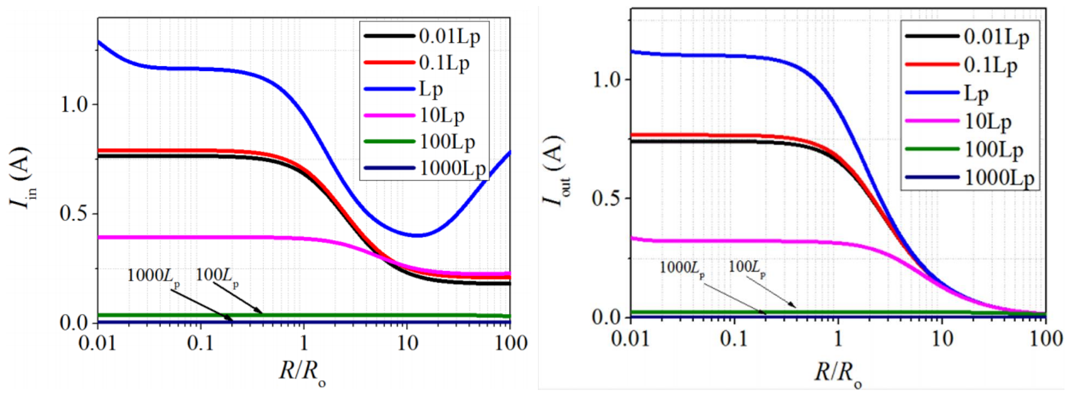

(a) (b)

Figure 3.2: (a) Input current and (b) output current versus load resistance for LC/S compensation topologies at different values of L_1 ($R_0 = 100\ \Omega$).

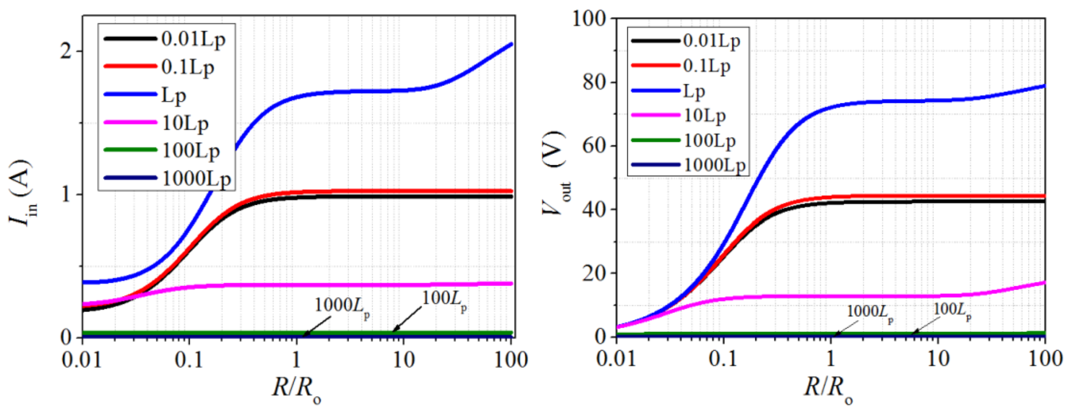

(a) (b)

Figure 3.3: (a) Input current and (b) output voltage versus load resistance for LC/P compensation topologies at different values of L_1 ($R_0 = 100\ \Omega$).

Fig. 3.5 illustrates the basic compensation topologies according to the type of input source. The topologies for voltage source input include S/S and S/P compensation circuits, and those for current source input include P/P and P/S compensation circuits. Interchanging Thévenin and Norton representations, S/S circuits can be converted to P/S circuits when $L_1 > \beta L_{\mathrm{p}}$, via LC/S circuit. Likewise, S/P circuits can be converted to P/P circuits when $L_1 > \alpha L_{\mathrm{p}}$, via LC/P circuit. Here, α and β denote the ratio of L_1 to L_{p}.

To illustrate clearly, simulation models of LC/S and LC/P compensated IPT converters are established based on the properties in Table 3.1. The parameters listed in Table 4.3 are used in the simulations. Since inductor L_1 serves as part of compensation components, connecting the basic S/S and LC/S circuits (S/P and LC/P circuits), the impact of the inductance of L_1 on the input current would be evaluated from an analytical viewpoint to assess the performance of higher order compensation topologies in combating the variation of system parameters. Figs. 3.2 and 3.3 illustrate the input and output characteristics versus L_1 value. It can be readily observed from Fig. 3.2(a) that the LC/P compensated IPT converter can achieve constant input current under all load conditions when $\alpha \geq 100$, i.e., the voltage source is converted to a constant current source within the full load range. However, in this case, the output current level is limited, as shown in Fig. 3.2(b). Furthermore, from Fig. 3.2, when α >10 and within a certain load range, both the input and output current can be regarded as approximately constant. Likewise, from Fig. 3.3(a), when $\beta \geq 100$, the voltage source of an LC/P compensated IPT converter is converted to a constant current source within the full load range. The resulting output voltage level is limited, as shown in Fig. 3.3(b). When β >10 and the load resistance exceeds a certain value, both the input current and output voltage are maintained approximately constant.

Both analytical and simulated results reveal that a near constant input current can be achieved when α or β exceeds 10, i.e., the LC-compensated primary side with voltage source can exhibit the same transfer characteristics as the P-compensated primary side. Moreover, the main function of L_1 is to realize a near constant current input, and hence to ensure that the compensation network works well over wider input and load variation ranges.

3.1.2 Load-side Extension

The principle of voltage-current interchange can be applied at the load side in a likewise manner. For the LIC output scenario, with an additional capacitor in parallel with the load R_L, as shown in Fig. 3.4(b), the output voltage can be kept nearly constant. Similarly, in a third-order compensation network, with C_2 connected in parallel with R_L, the combined $C_2 \| R_\mathrm{L}$ load serves as an equivalent capacitive load Z_L, which reduces the order of compensation circuit to second-order. In this case, the secondary-side parallel capacitor C_2 converts the LIC output to an LIV output by extending the second-order compensation to third-order compensation.

In order to achieve a constant output, basic operating conditions listed in Table 3.1 should be satisfied. For the S/SP circuit extended from an S/S circuit, using equations (2.3), (2.4) and (2.34), the voltage gain can be expressed as

$$G_{v-\mathrm{S/SP}} = \frac{1}{\omega^2 M C_2 \left(1 - \frac{j}{\omega C_2 R_\mathrm{L}}\right)} \tag{3.6}$$

It can be readily obtained that the S/SP compensated circuit can achieve LIV output when

$$\omega C_2 R_\mathrm{L} \gg 1 \tag{3.7}$$

Likewise, for the S/PS circuit extended from the S/P circuit, the transconductance can be calculated as

$$G_{i-\mathrm{S/PS}} = \frac{L_\mathrm{s}}{R_\mathrm{L} M \left(1 + \frac{j\omega L_2}{R_\mathrm{L}}\right)} \tag{3.8}$$

To achieve LIC output, the system parameters need to satisfy

$$\frac{\omega L_2}{R_\mathrm{L}} \gg 1. \tag{3.9}$$

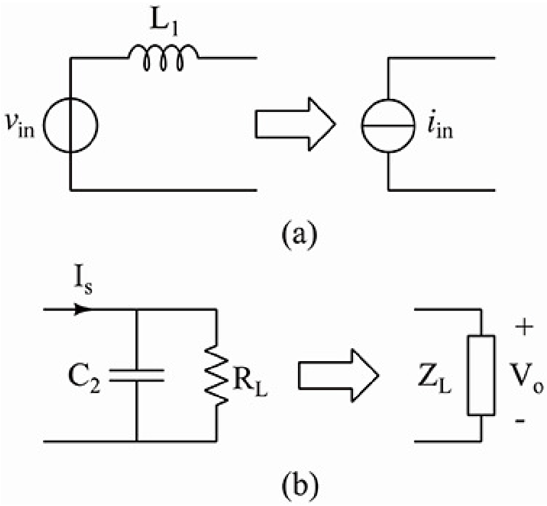

Figure 3.4: Transformation of (a) input voltage source to input current source and (b) LIC output to LIV output between second-order and third-order compensations.

Based on the above extension at both the input side and the output side, a fourth-order LC/CL compensation can be obtained, with operating conditions and transfer characteristics shown in Table 3.1. The above theoretical analysis shows that when operating at a fixed frequency, a larger capacitor (inductor) in parallel (series) at the load side helps maintain a constant output voltage (current).

3.2 Sensitivity Analysis

In this section, we compare basic second-order compensation circuits with the extended compensation circuits in terms of the sensitivity against system parameters' fluctuation, the aim being to establish the performance difference between higher order and second-order compensation circuits.

From Table 2.1, we see that the circuit can achieve load-independent voltage (LIV) output when $a_{12} = 0$, and load-independent current (LIC) output when $a_{11} = 0$. Thus, the transfer characteristics that satisfy load-independent (LI) output conditions can be obtained, as shown in Table 3.1, where LC/S (LC/P)

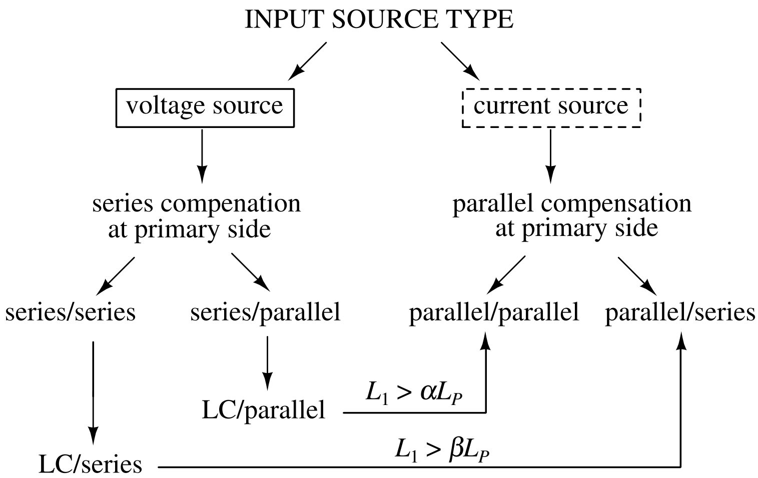

Figure 3.5: Transformation from second-order to third-order compensation at primary side.

denotes compensation with inductor-capacitor on the primary side and a capacitor in series (parallel) on the secondary side, S/CL denotes compensation with a capacitor in series on the primary side and capacitor-inductor on the secondary side.

To compare the differences of the extended higher order compensations with basic second-order compensations in terms of the influence to output when system parameters fluctuate, here we define the sensitivity of topology A's output against variation of parameter x as $S(x)_A$, i.e., for voltage output cases, we have

$$S_v(x)_{\mathrm{A}} = \left| \frac{\Delta V_{\mathrm{o}}(x)_{\mathrm{A}}}{\Delta x} \right|. \tag{3.10}$$

Then, the sensitivity ratio of topology A to topology B with LIV output against variation of x can be expressed as

$$\lambda_v(x)_{\mathrm{A-B}} = \frac{S_v(x)_{\mathrm{A}}}{S_v(x)_{\mathrm{B}}} = \left| \frac{\Delta V_{\mathrm{o}}/\Delta x|_{\mathrm{A}}}{\Delta V_{\mathrm{o}}/\Delta x|_{\mathrm{B}}} \right|. \tag{3.11}$$

3.2.1 Sensitivity to Input Voltage

According to (3.10) and (3.11), the sensitivity ratio λ of LC/P compensation circuits to S/P compensation circuits against input voltage variation can be expressed as

$$\lambda_v(V_{\mathrm{in}})_{\mathrm{LCP-SP}} = \frac{\left.\dfrac{\Delta V_{\mathrm{o}}}{\Delta V_{\mathrm{in}}}\right|_{\mathrm{LC/P}}}{\left.\dfrac{\Delta V_{\mathrm{o}}}{\Delta V_{\mathrm{in}}}\right|_{\mathrm{S/P}}} = \frac{G_{v-\mathrm{LC/P}}}{G_{v-\mathrm{S/P}}}. \tag{3.12}$$

Thus, for input voltage variation, the LC/P circuit is less sensitive than the S/P circuit when $\lambda_i(V_{\mathrm{in}})_{\mathrm{LC/P-S/P}} < 1$. Likewise, the LC/S circuit is less sensitive than the S/S circuit when $\lambda_v(V_{\mathrm{in}})_{\mathrm{LC/S-S/S}} < 1$. According to the expressions of transfer ratios listed in Table 3.1, the above conditions can be further expressed as

$$\begin{aligned}
&L_1 > 2L_{\mathrm{p}} && \Rightarrow \text{LC/S less sensitive than S/S for LIC}\\
&L_1 > kL_{\mathrm{p}} && \Rightarrow \text{LC/S less sensitive than S/S for LIV}\\
&L_1 > M && \Rightarrow \text{LC/P less sensitive than S/P for LIC}\\
&L_1 > (1-k^2)L_{\mathrm{p}} && \Rightarrow \text{LC/P less sensitive than S/P for LIV}
\end{aligned} \tag{3.13}$$

The connection between third-order compensation and second-order compensation can be conveniently established in terms of the sensitivity ratios. Here, we clearly see that compared with the second-order S/S circuit, the extended third-order LC/S and LC/P circuits have a widened input voltage range, by virtue of their input current source characteristic.

3.2.2 Sensitivity to Transformer and Compensation Parameters

Based on the above analytical results of LI output expressions and corresponding conditions, the impacts of variations of system parameters L_{p}, C_{s} and k are considered in this section.

Table 3.1: Basic Properties of Voltage-Input Compensation Circuits Under Load-Independent Output Conditions (LIV or LIC) and higher order Extensions at Input and Load Sides. $k = M/\sqrt{L_\mathrm{p}L_\mathrm{s}}$.

Type	Extension	Operating frequency	G_v at LIV or G_i at LIC
S/S	basic	$\omega_\mathrm{o} = \frac{1}{\sqrt{L_\mathrm{p}C_\mathrm{p}}} = \frac{1}{\sqrt{L_\mathrm{s}C_\mathrm{s}}}$	$G_i = \frac{1}{\omega_\mathrm{o}M}$
S/S	basic	$\omega_\mathrm{o}' = \frac{\omega_\mathrm{o}}{\sqrt{1\pm k}}$	$G_v = \sqrt{\frac{L_\mathrm{s}}{L_\mathrm{p}}}$
LC/S	L + P/S	$\omega_\mathrm{o} = \frac{1}{\sqrt{L_\mathrm{p}C_\mathrm{p}}} = \frac{1}{\sqrt{L_\mathrm{s}C_\mathrm{s}}}$	$G_i \approx \frac{1}{j\omega_\mathrm{o}M(\frac{L_1}{L_\mathrm{p}}-1)}$
LC/S	L + P/S	$\omega_\mathrm{o}' = \frac{1}{\sqrt{L_1C_\mathrm{p}}} = \frac{1}{\sqrt{L_\mathrm{s}C_\mathrm{s}}}$	$G_v \approx \frac{M}{L_1}$
SP/S	C + P/S	$\omega_\mathrm{o} = \frac{1}{\sqrt{L_\mathrm{p}(C_1+C_\mathrm{p})}} = \frac{1}{\sqrt{L_\mathrm{s}C_\mathrm{s}}}$	$G_v = j\frac{\omega_o L_\mathrm{p}C_1}{M}$
S/SP	S/S + C	$\omega_\mathrm{o} = \frac{1}{\sqrt{L_\mathrm{p}C_\mathrm{p}}} = \frac{1}{\sqrt{L_\mathrm{s}C_\mathrm{s}}}$	$G_v \approx \frac{1}{\omega_\mathrm{o}^2 MC_2}$
S/P	basic	$\omega_\mathrm{o} = \frac{1}{\sqrt{L_\mathrm{p}C_\mathrm{p}(1-k^2)}} = \frac{1}{\sqrt{L_\mathrm{s}C_\mathrm{s}}}$	$G_v = \frac{L_\mathrm{s}}{M}$
S/P	basic	$\omega_\mathrm{o}' = \frac{\omega_o}{\sqrt{1\pm k}}$	$G_i = \frac{1}{\omega_\mathrm{o}' L_\mathrm{s}}$
LC/P	L + P/P	$\omega_\mathrm{o} = \frac{1}{\sqrt{L_\mathrm{p}C_\mathrm{p}(1-k^2)}} = \frac{1}{\sqrt{L_\mathrm{s}C_\mathrm{s}}}$	$G_v \approx \frac{(1-k^2)M}{k^2L_1}$
LC/P	L + P/P	$\omega_\mathrm{o}' = \frac{1}{\sqrt{L_1C_\mathrm{p}}} = \frac{1}{\sqrt{L_\mathrm{s}C_\mathrm{s}}}$	$G_i = \frac{M}{j\omega_\mathrm{o}' L_1 L_\mathrm{s}}$
SP/P	C + P/P	$\omega_\mathrm{o} = \frac{1}{\sqrt{L_\mathrm{p}(C_1+C_\mathrm{p})}} = \frac{1}{\sqrt{L_\mathrm{s}C_\mathrm{s}}}$	$G_v = j\frac{\omega_o L_\mathrm{p}C_1}{M}$
S/PS	S/P + C	$\omega_\mathrm{o} = \frac{1}{\sqrt{L_\mathrm{p}C_\mathrm{p}(1-k^2)}} = \frac{1}{\sqrt{L_\mathrm{s}C_\mathrm{s}}}$	$G_i \approx \frac{\omega_o L_S C_2}{jM}$
S/CL	S/P + L	$\omega_\mathrm{o} = \frac{1}{\sqrt{L_\mathrm{p}C_\mathrm{p}(1-k^2)}} = \frac{1}{\sqrt{L_\mathrm{s}C_\mathrm{s}}}$	$G_i \approx \frac{L_\mathrm{s}}{j\omega_o ML_2}$
LC/CL	L+P/P+L	$\omega_\mathrm{o} = \frac{1}{\sqrt{L_\mathrm{p}C_\mathrm{p}}} = \frac{1}{\sqrt{L_\mathrm{s}C_\mathrm{s}}}$	$G_i \approx \frac{M}{j\omega_o L_\mathrm{s}L_1}$

Table 3.2: Basic Properties of Voltage-Input Compensation Circuits Under Load-Independent Output Conditions (LIV or LIC) and higher order Extensions at Input and Load Sides. $k = M/\sqrt{L_\mathrm{p}L_\mathrm{s}}$.

Type	Output feature	Input range	Tolerance of L_p variation	Tolerance of C_s variation	Coupling range (e.g., gap width, alignment)
S/S	LIC	narrow	–	high	narrow
S/S	LIV	narrow	low	low	narrow
LC/S	LIC	extended	–	high	narrow
LC/S	LIV	extended	high	low	wide
SP/S	LIV	narrow	–	high	narrow
S/SP	LIV	narrow	medium	high	wide
S/P	LIV	narrow	–	high	narrow
S/P	LIC	narrow	low	low	narrow
LC/P	LIV	extended	–	low	narrow
LC/P	LIC	extended	high	low	wide
SP/P	LIV	narrow	–	high	narrow
S/PS	LIC	narrow	medium	high	wide
S/CL	LIC	narrow	low	high	wide
LC/CL	LIC	extended	high	medium	wide

Based on the definition given in (3.10) and (3.11), the sensitivity with respect to specific parameters for the topologies listed in Table 3.1 can be obtained. For parameters at the primary side, C_{p} is a designed parameter (value) determined by the operating condition as listed in Table 3.1. We will assess the variation of L_{p} (transformer parameter) which is considered as system parameter here. Taking LC/S and S/S circuits with LIV output as examples, we substitute the G_v expressions of LC/S and S/S in Table 3.1 by (3.10) and (3.11), the sensitivity ratio with respect to L_{p} fluctuation is given by

$$\lambda_v(L_{\mathrm{p}})_{\mathrm{LC/S-S/S}} = \frac{kL_{\mathrm{p}}}{L_1} \tag{3.14}$$

According to the analysis given in Section 3.1, the inductance of L_1 should be larger than L_{p} to achieve the desired constant input current. Thus, it can be readily observed that $\lambda_v(L_{\mathrm{p}})_{\mathrm{LC/S-S/S}}$ is always less than one, meaning that an IPT converter compensated with LC/S performs better in tolerance and robustness than the S/S counterpart when L_{p} fluctuates. Similarly, S/P circuits with input-side extension, and other output-side extension can also be analyzed and compared in terms of the sensitivity to L_{p}, as shown in Table 3.1. Figs. 3.6(a) and 3.6(b) illustrate the effects on the transfer ratio of various compensation networks when L_{p} changes, using the data listed in Table 4.3. Normalization of data is applied here to clearly see the differences of sensitivity among the topologies. Both analytical and simulated results show that for the LIV output situation, the LC/S compensated circuit presents a higher tolerance to L_{p} variation compared to the S/S counterpart under the same operating condition. Likewise, for the LIC output situation, the LC/P and LC/CL compensated circuits perform better than the S/P circuit in terms of the tolerance to L_{p} variation under the same operating condition. This reveals that the input-side extension can be applied to widen the tolerance range of parameters and thus improve the robustness of the system during operation.

For parameters at the secondary side, assuming that the priority of achieving load-independent (LI) output is higher than that of zero phase angle (ZPA) input, the effects of capacitor C_{s}'s fluctuation are discussed as follows.

Take the S/S and the extended S/SP compensation circuits as examples. For the S/S compensated circuit with LIC output, according to the transfer matrix given in Section 3.1 and equation (2.4), LIC can be achieved by satisfying

$$a_{11} = \frac{L_{\mathrm{p}}}{M} - \frac{1}{\omega^2 M C_{\mathrm{p}}} = 0. \tag{3.15}$$

Now, putting (3.15) in (2.5), the transfer ratio G_i can be found as

$$G_{i-\mathrm{S/S}} = j\frac{1}{\omega M} \tag{3.16}$$

which is also given in Table 3.1. It can be readily observed from the above calculation that secondary compensated capacitor C_{s} has almost no effect on the S/S compensation with LIC output. However, in the LIV output scenario, substituting the primary compensation condition and the operating frequency into (2.4), we get the LIV condition as

$$a_{12} = \frac{jkL_{\mathrm{p}}({\omega_{\mathrm{o}}}^2 L_{\mathrm{s}} C_{\mathrm{s}} - 1)}{\omega M C_{\mathrm{s}}} \tag{3.17}$$

which means that the transfer ratio of S/S compensation with LIV output varies with the variation of C_{s}.

For the S/SP compensated circuit, since LIV output can be achieved with operating parameters of the basic S/S circuit with LIC output, the corresponding LIV condition is the same as given in (3.15). Combining with G_v expression in (3.6), it can be observed that the output of the S/SP compensated circuit is theoretically independent of the C_{s} value.

Likewise, the S/P compensated circuit with output-side extension and with other input-side extension can also be analyzed in terms of the sensitivity to C_s, as shown in Table 3.1. To illustrate the theoretical results more clearly, numerical simulations are performed, as given in Figs. 3.6(c) and 3.6(d). The parameters listed in Table 4.3 are used in the calculations. From Fig. 3.6(c), the results reveal that by adding a capacitor in parallel at the output side, the S/S compensated circuit can convert LIC to LIV output, still maintaining a high tolerance to C_s fluctuation. Similarly, Fig. 3.6(d) shows that with an additional capacitor or inductor in series at the output side, the conversion of LIV to LIC preserves the high tolerance to C_s variation of the S/P compensated circuit.

Based on the above analysis, it can be observed that various compensation networks possess different sensitivities to transformer parameter changes. In practice, apart from the fluctuation in circuit components, the gap width and lateral misalignment between the primary coil and the secondary coil may also vary during the operation. Such changes can be considered as variation in coupling coefficient k. According to Table 3.1 and equation (2.4), the S/SP compensated circuit can achieve higher voltage gain than the S/S compensated circuit when the system parameters satisfy

$$\omega^2 M C_2 < 1 \tag{3.18}$$

Considering that the operating frequency ω and capacitor C_2 need to meet the LIV condition, as per (3.7), requiring a relatively large value of C_2 when ω is fixed, the above condition can be further expressed as

$$M < \frac{1}{\omega^2 C_2} \tag{3.19}$$

Likewise, for the S/PS compensated circuit, comparing the output expressions

Table 3.3: Parameters of IPT Circuits for Simulation

Parameter	S/S	LC/S	S/SP	S/P	LC/P	S/PS	S/CL	LC/CL
L_p [μH]	76	76	76	76	76	76	76	76
L_s [μH]	76	76	76	76	76	76	76	76
L_1 [μH]	-	76	-	-	52.8	-	-	76
L_2 [μH]	-	-	-	-	-	-	76	76
C_p [nF]	33.3	33.3	33.3	47.9	47.9	47.9	47.9	33.3
C_s [nF]	33.3	33.3	33.3	33.3	33.3	33.3	33.3	33.3
C_2 [nF]	-	-	300	-	-	33.3	-	-
k	0.55	0.55	0.55	0.55	0.55	0.55	0.55	0.55
f [kHz]	100	100	100	100	100	100	100	100
$V_{\mathrm{in-pp}}$ [V]	50	50	50	50	50	50	50	50
r_p, r_s [Ω]	1	1	1	1	1	1	1	1
R_L [Ω]	10	10	10	10	10	10	10	10

listed in Table 3.1, a higher output current can be obtained if

$$\frac{{L_\mathrm{s}}^2}{ML_2} > 1 \tag{3.20}$$

Analytical results are shown graphically in Figs. 3.6(e) and 3.6(f), which show explicitly that the S/SP compensated circuit performs better in transferring higher voltage than the S/S compensated circuit with same system parameters and loosely coupled transformers. Moreover, the S/PS compensated circuit possesses a higher transconductance than the S/P circuit under the same operating condition.

3.3 General Pathways to Higher-Order Compensation Circuits

From the foregoing discussions, we can readily connect systematically the basic second-order compensation circuits and the higher order compensation circuits according to the extensions and the expected characteristics. First, we recognize

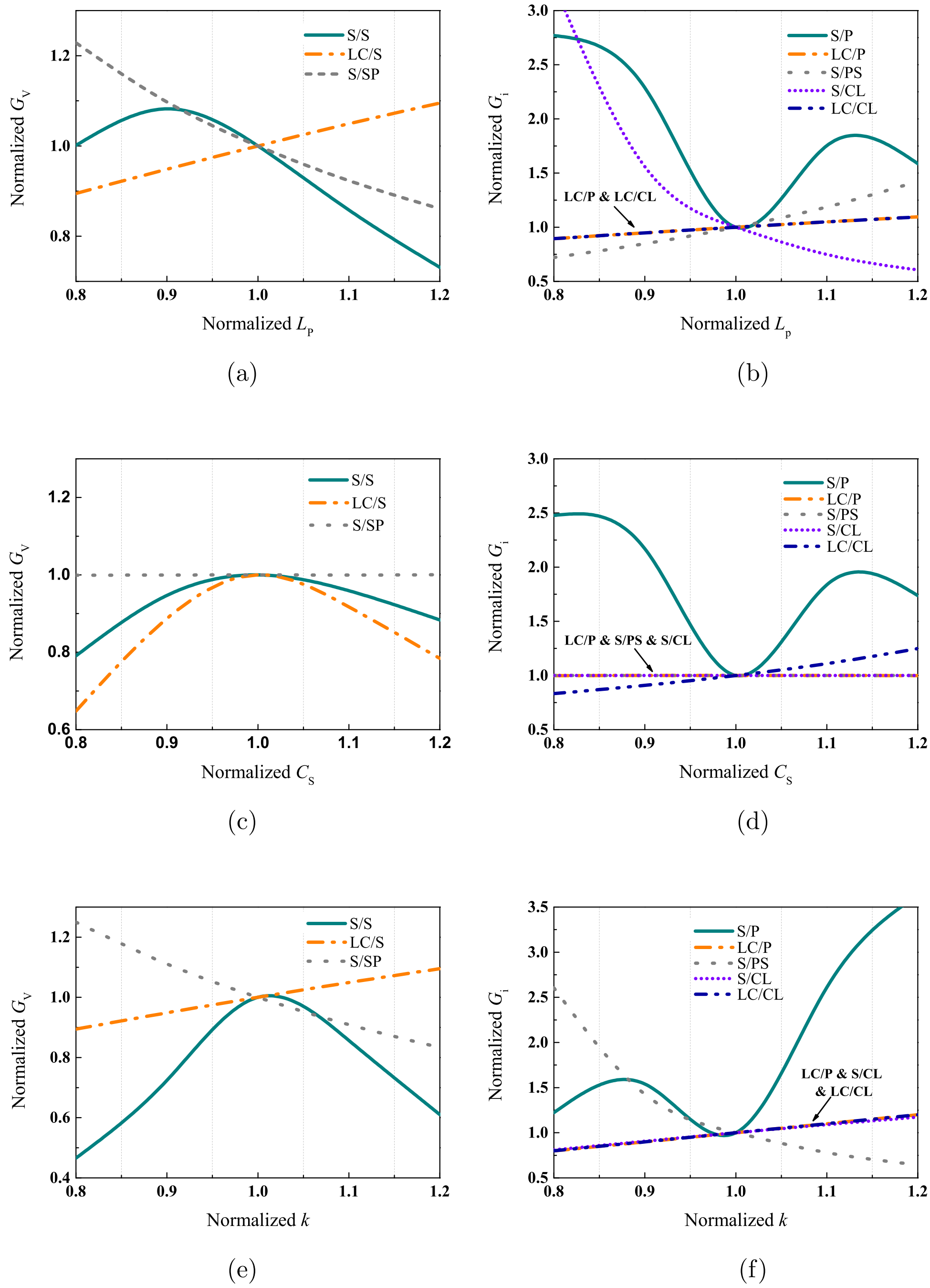

Figure 3.6: (a) Normalized voltage gain versus normalized primary inductor L_p for S/S, LC/S and S/SP compensated IPT circuits with LIV output; (b) normalized transconductance versus normalized primary inductor L_p for S/P, LC/P, S/PS, S/CL and LC/CL compensated IPT circuits with LIC output; (c) normalized voltage gain versus normalized secondary capacitor C_s for S/S, LC/S and S/SP compensated IPT circuits with LIV output; (d) normalized transconductance versus normalized secondary capacitor C_s for S/P, LC/P, S/PS, S/CL and LC/CL compensated IPT circuits with LIC output; (e) normalized voltage gain versus normalized coupling coefficient k for S/S, LC/S and S/SP compensated IPT circuits with LIV output; (f) normalized transconductance versus normalized coupling coefficient k for S/P, LC/P, S/PS, S/CL, and LC/CL compensated IPT circuits with LIC output.

that a higher order circuit allows more flexibility in design due to the extended parameter set, and if appropriate values of parameters and topologies are chosen, desirable characteristics can be achieved, as summarized below for the input voltage terminated IPT circuits:

1. The S/S and S/P compensation circuits are the two basic types of compensation circuits that cater for input voltage termination.

2. Sensitivity to variation in the input voltage and primary inductance improves significantly if the input is converted to a current source by connecting upfront an inductor in series. The resulting circuits are LC/S and LC/P configurations, which are effectively current-fed P/S and P/P circuits. The range of input voltage is widened due to the near constant input current. The extended circuits become more tolerant to inductance L_p fluctuation because of the change of compensation conditions at the primary side.

3. The output-side LIC-LIV and LIV-LIC conversions contribute to maintaining the high tolerance to fluctuation of the compensation component C_s. Specifically, the S/S topology achieves LIC with optimized low sensitivity to C_s fluctuation. To preserve the simple advantage but serve an LIV application, one may extend the secondary side to S/SP to achieve LIV, which preserves the near zero sensitivity to C_s variation.

4. The input-side and output-side extensions based on the basic second-order compensation topologies can be systematically applied to widen the coupling range, and hence to provide a higher degree of freedom for choosing parameter values. Specifically, output-side extensions perform well with loosely coupled transformers. This means that in situations where high capacity is needed to address varying misalignment and transfer gap, the output-side extension topologies can be considered.

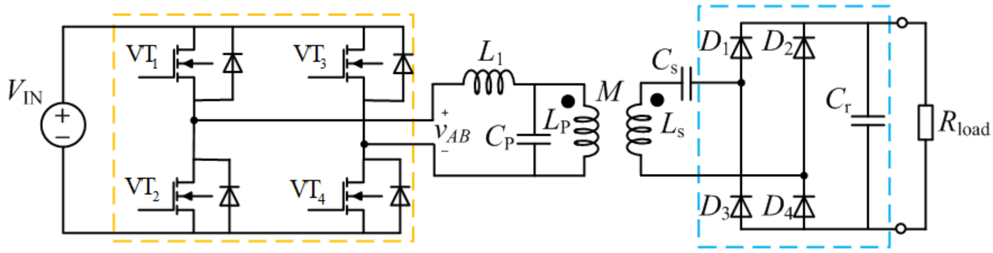

Figure 3.7: Experimental LC/S compensated IPT converters.

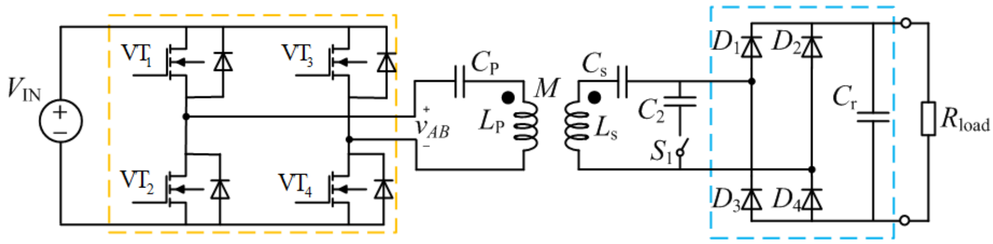

Figure 3.8: Experimental S/S and extended S/SP compensated IPT converters.

3.4 Experimental Validation

To validate the analysis presented above, S/S, LC/S and S/SP compensated IPT configurations are constructed, as shown in Figs. 3.7 and 3.8. The inverter, shown in the yellow dashed box, consists of MOSFET VT_1 to VT_4, using C2M0080120. The rectifier, shown in the blue dashed box, consists of diodes D_1 to D_4 which are implemented by IDH08G65C6XKSA. The filter capacitor C_{r} is 5 μF. A photo of the experimental setup is shown in Fig. 3.9. The specific parameters listed in Table 4.4 are used in our experiments.

Fig. 3.10 shows the analytical and measured sensitivity ratio of LC/S circuit to S/S circuit against input voltage variation under LIV output condition. Compared with the analytical results of $\lambda_v(V_{\mathrm{in}})_{\mathrm{LC/S-S/S}}$, the measured results show a higher sensitivity when L_1 is small. The reason is that a small series inductor does not guarantee near constant input current, and the sensitivity of the circuit with an input-side inductor will change dramatically when the inductance value is small. When the value of $\lambda_v(V_{\mathrm{in}})_{\mathrm{LC/S-S/S}}$ equals 1, the sensitivity of the output to input voltage variation of the LC/S topology is the same as that of

Table 3.4: Parameters of IPT Circuits for Experiments under LIV Output Condition

Parameters	S/S-LIV	S/S-LIC	LC/S	S/SP
L_{p} [μH]	75.76	75.76	75.76	75.76
L_{s} [μH]	76.85	76.85	76.85	76.85
C_{p} [nF]	33.43	33.43	33.43	33.43
C_{s} [nF]	32.96	32.96	32.96	32.96
L_1 [μH]	NA	NA	76.20	NA
C_2 [nF]	NA	NA	NA	320.6
k	0.552	0.552	0.552	0.552
f [kHz]	149.4	100	100	100
$V_{\text{in-pp}}$ [V]	50	50	50	50

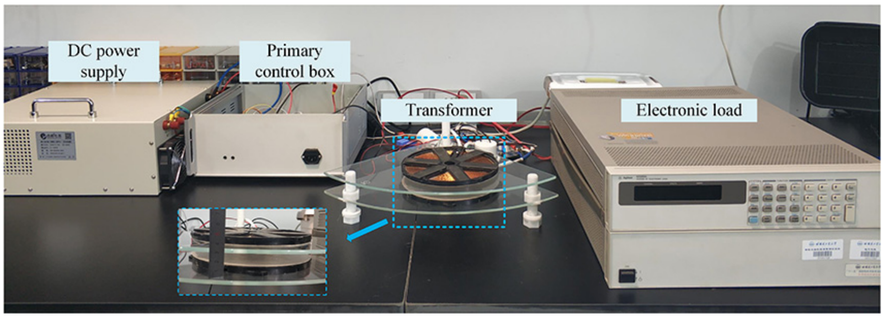

Figure 3.9: Experimental setup of IPT converters.

the S/S topology. The measured results of input current versus load variation of S/S and LC/S compensated IPT converters are shown in Fig. 3.11. The normalized input current of the S/S converter varies dramatically as load resistance increases, whereas the LC/S converter permits a near constant input current as load changes. This indicates that the external series inductor at a certain value connected with the voltage source allows for a near constant current at the input side.

Figs. 3.12(a) and 3.12(b) show the transient waveforms when the load resistance is stepped from 10 Ω to 50 Ω in the S/S compensated converter, and the S/SP compensated converter is extended by S/S compensation, respectively. It is found that the output current of the S/S converter and the output voltage of the

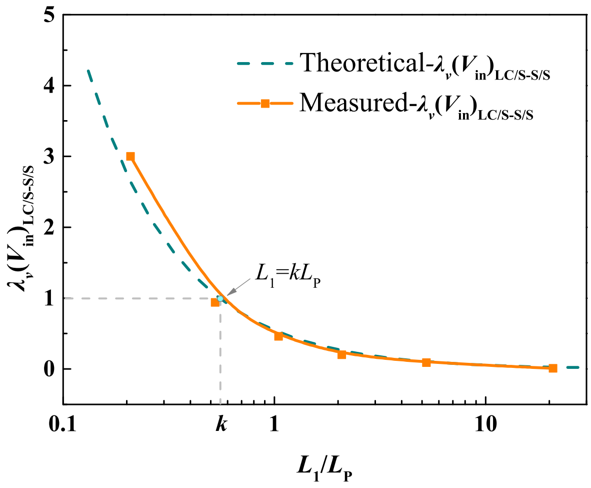

Figure 3.10: Ratio of input-voltage-to-output-voltage sensitivity of LC/S to that of S/S compensation circuits.

S/SP converter are almost unchanged as the load resistance varies. This matches well with the analytical results. Fig. 3.13 shows the measured output current of the S/S compensated converter and the output voltage of the S/SP compensated converter versus the load resistance. The results show that by adding a capacitor in parallel at the output side, a constant current output can be converted to a constant voltage output.

To facilitate comparison of different topologies, normalized values are used. In particular, we normalize values of inductance, capacitance and coupling coefficient with respect to the resonant point, with the corresponding voltage gain and transconductance being set to 1. Thus, the universal range from 0.8 to 1.2 can be used for comparison instead of the actual values. Figs. 3.14(a), 3.14(b) and 3.14(c) demonstrate the measured normalized voltage gain versus the normalized value of L_{p}, C_{s} and k of the experimental S/S, LC/S and S/SP compensated converters with LIV output, respectively. Here, the variation of the value of k is achieved by changing the gap of the transformer in the IPT converter. It can be readily observed from Fig. 3.14(a) that the LC/S topology is capable of maintaining a relatively constant output for a larger L_{p} variation. This means that the

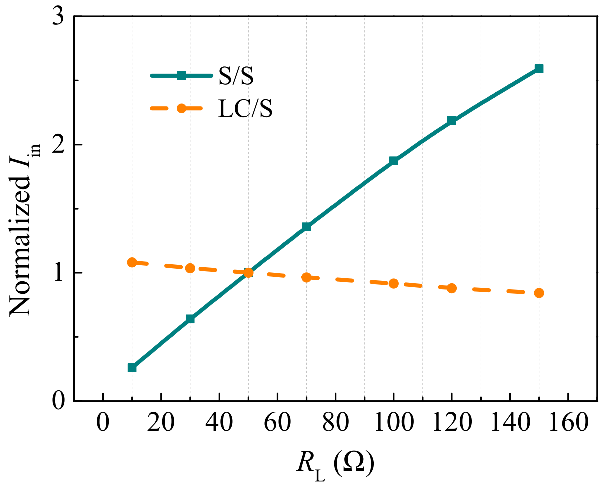

Figure 3.11: Input current versus load resistance for S/S and LC/S compensated IPT converters.

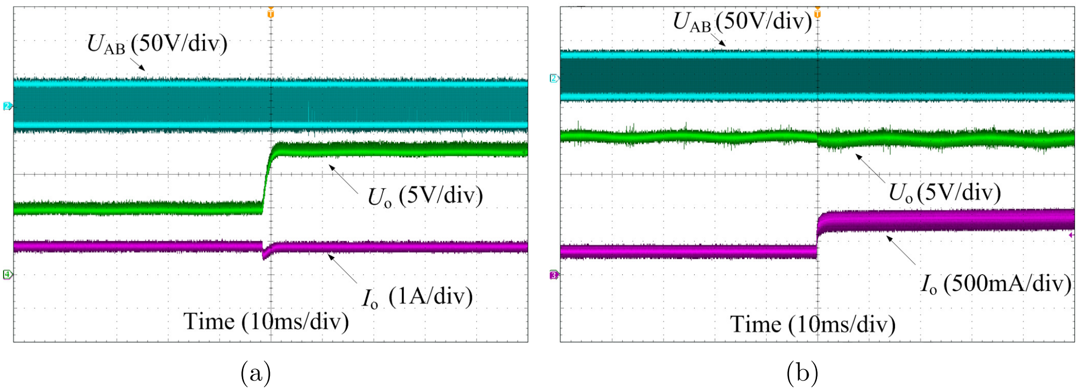

Figure 3.12: Experimental waveforms of (a) S/S compensated and (b) S/SP compensated IPT converters when load resistance varies from 10 Ω to 50Ω.

input-side extension helps to make the IPT converter less sensitive against variation of L_p at the primary side. Likewise, in Fig. 3.14(b), when the normalized value of C_s changes from 0.8 to 1.2, the normalized voltage gain of the S/SP compensated converter changes very little compared with the other two converters, verifying that the output-side extension serves to reduce the system sensitivity to variation of C_s at the secondary side. Fig. 3.14(c) illustrates that when k decreases, the voltage gain of the S/SP topology increases, while the other two topologies show different rates of decline in voltage gain. Thus, compared with second-order compensated circuits and their input-side extensions, the output-

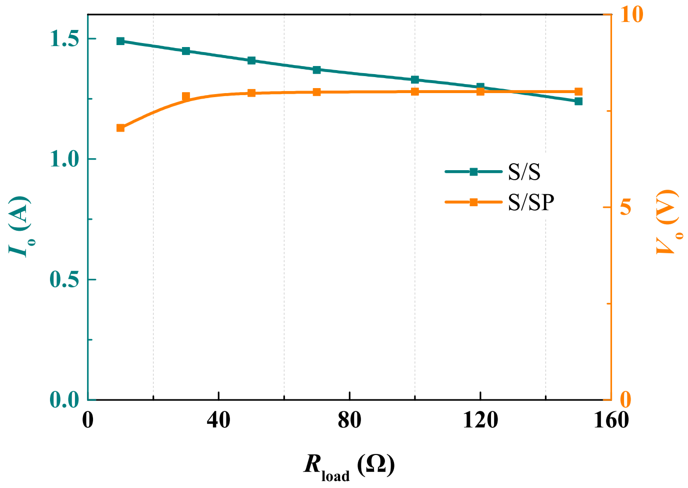

Figure 3.13: Output current or voltage versus load resistance for S/S and S/SP compensated IPT converters showing sensitivity to load change.

side extensions perform better in maintaining constant output voltage when the transformer has a loose coupling or large misalignment. The above experimental results agree with the analytical results.

Thus, we have clearly seen the connection from second-order to third-order compensation circuits, and the parameter conditions under which both widening the range of input voltage and converting LIC output to LIV output can be achieved. In addition, the system sensitivity of output to parameter fluctuations are shown to be improved by extending second-order to higher order compensations.

3.5 Summary

The literature abounds with numerous design examples of higher order compensation circuits for inductive power transfer converters that address the variation of parameters and improve the operating range for the applications concerned. It is generally accepted that higher order circuits offer better flexibility and higher degree of design freedom by expanding the parameter space. Specific applications

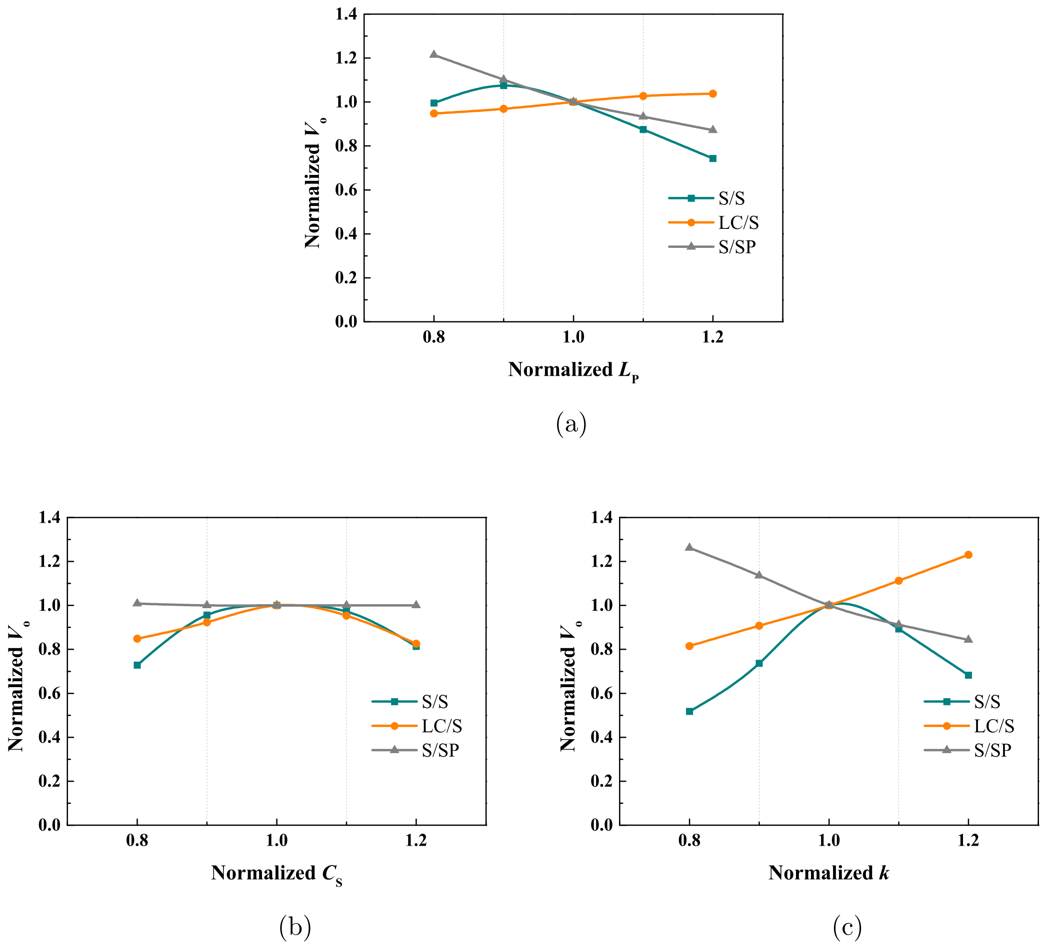

Figure 3.14: Measured normalized voltage gain versus (a) normalized L_p; (b) normalized C_s; (c) normalized coupling coefficient k of S/S, LC/S and S/SP compensated IPT converters.

require combating variation of specific variables or parameters such as input voltage variation, load variation and transformer's coupling variation. In much of the reported work, specific topologies were proposed with detailed analytical equations derived corresponding to the specific topologies. However, a general circuit theoretic pathway leading to a suitable design for specific application is neither available nor well understood.

This chapter presents a new perspective of higher order compensation circuits based on sensitivity analysis, and compares the sensitivities of various compensation topologies with the basic second-order compensation circuits in terms of input voltage change, design parameter change and coupling range. The analysis presented here provides a convenient connecting pathway from second-order circuits to higher order circuits, mapping each type of topological extension with the specific performance outcome. In practice, the presented analysis offers a quick design guideline for deriving higher order compensation circuits capable of enhancing specific performance areas such as widening of input and load ranges. Specifically, the results show that adding an inductor or capacitor at input side and output side of a second-order circuit in specific fashions can effectively reduce the sensitivity of the system to parameter variation, provided the added inductor or capacitor exceeds a certain value. In addition, with higher order compensation at the output side, the system can achieve a higher voltage gain. Furthermore, with a certain range of the inductance in series (or capacitance in parallel), a voltage source (constant current output) can be made equivalent to a constant current source (constant voltage output). The proposed perspective of topological extension from second-order compensated circuits offers a simple and effective basis for understanding how higher order compensation circuits combat parameter variation.

Chapter 4

Pathways to Higher Order Compensated CPT Circuits

In this chapter, we examine the compensation topologies of CPT converters from the circuit viewpoint, and connect basic second-order and higher order compensated CPT circuits systematically, thereby providing a comprehensible interpretation on design pathways from second-order to higher order compensated CPT converters. Similar to the IPT analysis, we first establish the connection between second-order and higher order compensated CPT circuits through the transformation between a voltage source and a current source, and the conversion between load-independent current (LIC) and load-independent voltage (LIV) outputs. Moreover, we compare compensation schemes of different orders in terms of sensitivity to coupling and compensation parameters, and provide a methodology for extending to higher order compensated converters at the input and output sides, achieving better performance in tolerance of parameter variations while retaining the original merits.

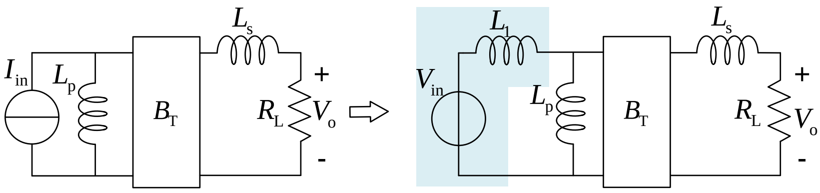

Figure 4.1: Transformation from P/S to SP/S compensation circuits

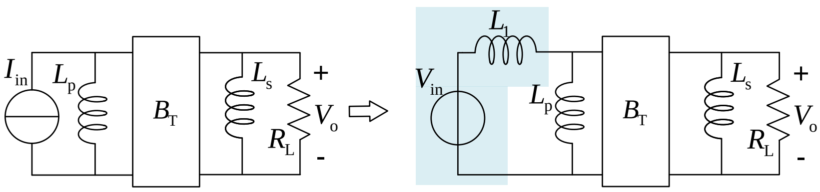

Figure 4.2: Transformation from P/P to SP/P compensation circuits

4.1 Connecting Second and Higher Order Compensations

4.1.1 Input-side Extension

For the basic compensation circuits discussed in the last section, an input current source is required when parallel compensation is adopted at the primary side. In practice, this requirement is usually achieved by connecting a voltage source in series with an inductor at the input side. As exemplified in Fig. 4.1, by adding a series inductor L_1 to the voltage source, a third-order series-parallel/series (SP/S) compensation circuit is obtained, which is rooted from the P/S compensation circuit. To permit the characteristic of constant input current as in P/S circuits, the value of L_1 in the SP/S circuit should satisfy some specific conditions. With the requirement of LIC output, we put the operating conditions as (2.24), and the input current of the SP/S circuit can be obtained as

$$I_{\mathrm{in}} = \frac{k_{\mathrm{c}}^2 L_{\mathrm{s}} V_{\mathrm{in}}}{L_{\mathrm{p}} R_{\mathrm{L}} + j k_{\mathrm{c}}^2 \omega L_{\mathrm{s}} (L_1 + L_{\mathrm{p}})}. \tag{4.1}$$

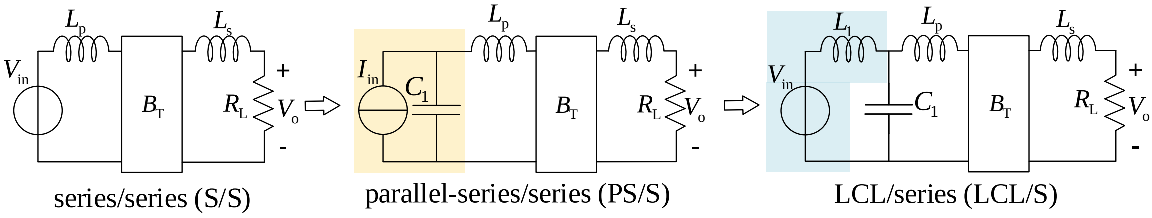

Figure 4.3: Transformation from S/S to LCL/S compensation circuits.

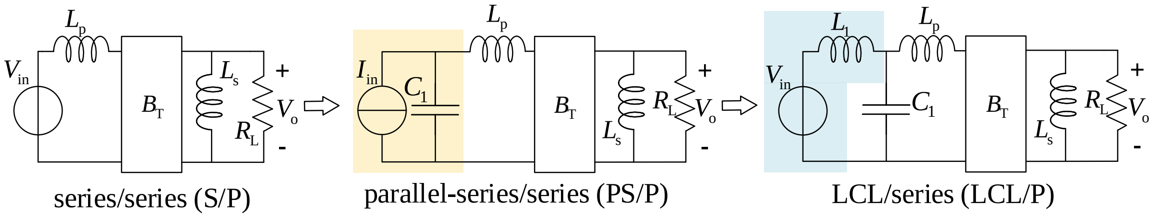

Figure 4.4: Transformation from S/P to LCL/P compensation circuits.

Thus, the condition of L_1 of the SP/S circuit for achieving near constant input current can be expressed as follows:

$$\frac{L_1}{L_\mathrm{p}} \gg \frac{R_\mathrm{L}}{\omega k_\mathrm{c}^2 L_\mathrm{s}} - 1. \tag{4.2}$$

Likewise, a third-order series-parallel/parallel (SP/P) compensated circuit can be extended from the basic P/P compensated circuit by adding a series inductor at the input side, as shown in Fig. 4.2. To maintain a near constant input current, the value of L_1 in the SP/P circuit should satisfy

$$\frac{L_1}{L_\mathrm{p}} \gg k_\mathrm{c}^{-2}(\omega^{-2}{L_\mathrm{s}}^{-2}{R_\mathrm{L}}^2 + 1)^{-\frac{1}{2}} - 1. \tag{4.3}$$

For primary series compensation terminated by an input voltage source, higher order compensation can also be obtained via transformation from a voltage source to a current source. For example, as illustrated in Fig. 4.3, the S/S compensated circuit can be theoretically extended to a parallel-series/series (PS/S) compensated circuit, by replacing the input voltage source with a current source connected in parallel with a capacitor C_1. Then, the third-order PS/S compensation

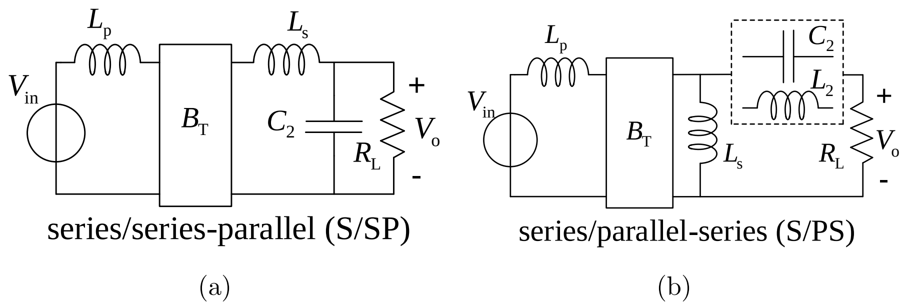

Figure 4.5: Equivalent circuits of third-order CPT converters with extensions at the output side of (a) S/SP circuits derived from S/S circuits and (b) S/PS circuits derived from S/P circuits.

can be further extended to a fourth-order LCL/S compensation, using a voltage source in series with an inductor L_1 serving as an equivalent current source. In this case, the value of L_1 should satisfy

$$|L_1 - L_\mathrm{p}| \gg \left| \frac{k_\mathrm{c}^2 \omega L_\mathrm{s} {R_\mathrm{L}}^{-1} - 1}{\omega^2 C_\mathrm{t}} \right|. \tag{4.4}$$

Similarly, in order to maintain a constant input current, the condition of L_1 in an LCL/P compensated circuit, which is extended from the basic S/P circuit (explicated in Fig. 4.4), can be found as

$$L_1 \gg \frac{k_\mathrm{c}^2 C_\mathrm{r} R_\mathrm{L}}{\omega C_\mathrm{t}}. \tag{4.5}$$

The transfer properties of the above extended compensated circuits can be obtained using (2.20) to (2.24), as listed in Table 4.1.

4.1.2 Output-side Extension

The principle of transformation between voltage source and current source can be applied to the output side. As discussed in Section 2.3, an S/S compensated circuit can achieve LIC output when operating at the resonant frequency. In order to convert the LIC output to an LIV output without changing the operating condition, an external shunt capacitor is connected with the load, as shown in Fig. 4.5(a), hence extending the second-order S/S compensation to a third-order S/SP compensation. Likewise, Fig. 4.5(b) shows that an LIV output can be converted to an LIC output by adding a series inductor or capacitor at the load side of the S/P compensation. Then, a third-order S/PS compensated circuit is obtained. Since these extended circuits operate under the same conditions as listed in Table 2.4, the value of b_{12} or b_{21} would be non-zero when using (2.20) and (2.21) to describe the output characteristics. In this case, the LIV(C) output conditions of S/SP and S/PS compensated circuits can be calculated as follows:

$$\omega C_2 R_{\mathrm{L}} \gg 1 \quad \text{for S/SP circuits} \tag{4.6}$$

$$|Z_2|\, {R_{\mathrm{L}}}^{-1} \gg 1 \quad \text{for S/PS circuits} \tag{4.7}$$

where Z_2 denotes the impedance of the external component L_2 (C_2) in the S/PS circuit, i.e., $Z_2 = j\omega L_2$ or $Z_2 = (j\omega C_2)^{-1}$.

Thus, the basic second-order compensation circuits, and the third-order compensation circuits which are extended from the output side, can be connected by performing conversion between CC and CV outputs.

Furthermore, in order to achieve a ZPA input while realizing the conversion of output characteristics, higher order compensation is needed and can be obtained via adding more components at the output side. Taking the fourth-order S/LCL compensated circuit as an example, we substitute the G_v and Z_{in} expressions in (2.20) and (2.24) by elements of the transfer matrix of S/LCL circuits. Then, the transfer properties can be obtained, as listed in Table 4.1.

Since both S/SP and S/LCL compensated circuits can be derived from the basic S/S circuits at the load side, we compare these three circuits together. According to the features listed in Tables 2.4 and 4.1, it can be observed that both S/SP and S/LCL compensated circuits are capable of realizing the conversion

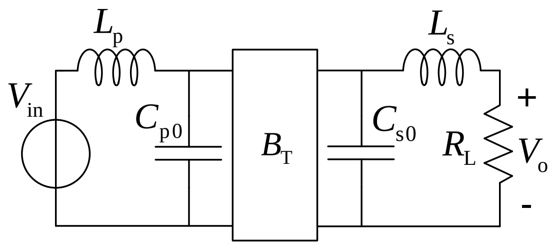

Figure 4.6: Equivalent circuit of double-sided LC compensated CPT converters.

from CC to CV output at a k_c-independent frequency. Moreover, S/SP circuits maintain the original operating conditions at the expense of losing the feature of ZPA input, whereas S/LCL circuits permit the feature of ZPA input by changing the resonant condition of L_s at the secondary side. On this basis, we can determine appropriate compensation topologies with various desired features.

4.1.3 Double-side Extension

In practice, the capacitance values of C_t and C_r are generally quite small, and relatively large inductors are required for compensation [47,92]. In order to reduce the required inductance, external capacitors are usually connected in parallel with the coupling capacitors at both sides of the CPT converter [9,10,80]. Considering the shunt capacitors C_{p0} and C_{s0} as components of the compensation topology, the S/S compensation circuit can be derived into a double-sided LC compensation circuit, as depicted in Fig. 4.6. In this case, the operating conditions of LC/CL circuits for LIC output can be derived, i.e.,

$$\omega = \frac{1}{\sqrt{L_p(C_{p0} + \frac{C_t C_2}{C_2 - k_c^2 C_{s0}})}} = \frac{1}{\sqrt{L_s(C_{s0} + \frac{C_r C_1}{C_1 - k_c^2 C_{p0}})}} \tag{4.8}$$

It should be noted that in many of the existing studies on CPT topologies, the external shunt capacitors C_{p0} and C_{s0} are always considered as components of the capacitor coupler. In this case, capacitance of C_t, C_r and C_m in Fig. 2.5 in Chapter 2 are changed to C_t', C_r' and C_m'. According to Kirchhoff's voltage

Table 4.1: Basic Properties of Higher order Compensated CPT Circuits Under Load-Independent Output Conditions. $k_\mathrm{c} = \frac{\sqrt{C_\mathrm{t}C_\mathrm{r}}}{C_\mathrm{m}}$.

Type	Operating frequency	Transfer ratio
SP/S	$\omega = \frac{1}{\sqrt{(L_\mathrm{p}\Vert L_1)C_\mathrm{t}}} = \frac{1}{\sqrt{\frac{L_\mathrm{p}L_\mathrm{s}}{L_\mathrm{p}+k_\mathrm{c}^2L_1}C_r}}$	$G_i = -j\frac{\omega C_\mathrm{m}L_\mathrm{p}}{L_1+L_\mathrm{p}}$
SP/P	$\omega = \frac{1}{\sqrt{(L_\mathrm{p}\Vert L_1)C_\mathrm{t}(1-k_\mathrm{c}^2)^{-1}}} = \frac{1}{\sqrt{L_\mathrm{s}C_r}}$	$G_v = \frac{C_p}{C_\mathrm{m}}$
LCL/S	$\omega = \frac{1}{\sqrt{L_1C_1}} = \frac{1}{\sqrt{L_\mathrm{s}C_\mathrm{r}}} = \frac{1}{\sqrt{L_\mathrm{p}(C_1\Vert C_\mathrm{t})}}$	$G_v = -\frac{C_1}{C_\mathrm{m}}$
LCL/P	$\omega = \frac{1}{\sqrt{L_1C_1}} = \frac{1}{\sqrt{L_\mathrm{s}C_\mathrm{r}}} = \frac{1}{\sqrt{(L_\mathrm{p}-L_1)C_\mathrm{t}(1-k_\mathrm{c}^2)^{-1}}}$	$G_i = -j\frac{\omega C_1C_s}{C_\mathrm{m}}$
S/SP	$\omega = \frac{1}{\sqrt{L_\mathrm{p}C_\mathrm{t}}} = \frac{1}{\sqrt{L_\mathrm{s}C_r}}$	$G_v \approx -\frac{C_\mathrm{m}}{C_2}$
S/PS	$\omega = \frac{1}{\sqrt{L_\mathrm{p}C_\mathrm{t}(1-k_\mathrm{c}^2)^{-1}}} = \frac{1}{\sqrt{L_\mathrm{s}C_r}}$	$G_i \approx \frac{C_\mathrm{m}}{C_\mathrm{r}Z_2}$
S/LCL	$\omega = \frac{1}{\sqrt{L_\mathrm{p}C_\mathrm{t}}} = \frac{1}{\sqrt{L_2C_2}} = \frac{1}{\sqrt{L_\mathrm{s}(C_2\Vert C_\mathrm{r})}}$	$G_v = -\frac{C_\mathrm{m}}{C_2}$

and current equations, the changed parameters of the coupler can be expressed as follows [55]:

$$C'_\mathrm{t} = C'_{12} + \frac{C_\mathrm{t}(C'_{34} + C'_\mathrm{r})}{C_\mathrm{r} + C'_{34}(1 - {k_\mathrm{c}}^2)} \tag{4.9}$$

$$C'_\mathrm{r} = C'_{34} + \frac{C_\mathrm{r}(C'_{12} + C'_\mathrm{t})}{C_\mathrm{t} + C'_{12}(1 - {k_\mathrm{c}}^2)} \tag{4.10}$$

$$C'_\mathrm{m} = \frac{C_\mathrm{m}(C'_{12} + C_\mathrm{t})(C'_{34} + C_\mathrm{r})}{C_\mathrm{t}C_\mathrm{r}} - \frac{C'_{12}C'_{34}}{C_\mathrm{m}} \tag{4.11}$$

From the expressions of the new parameters in the coupler, it can be noticed that the coupling parameter k_c is involved in determining the value of new self-capacitors C'_t and C'_r. This means that these equivalent self-capacitances are not fixed anymore when the coupling parameters change, i.e., C'_t and C'_r are both coupling-dependent. This property would complicate the further analysis on system's sensitivity. Thus, to analyse the sensitivity against coupling parameters precisely and coveniently, the afore-mentioned calculation method of taking the external shunt capacitors as part of the compensation is adopted in this chapter.

Table 4.2: Basic Properties of Higher order Compensated CPT Circuits Under Load-Independent Output Conditions. $k_{\mathrm{c}} = \frac{\sqrt{C_{\mathrm{t}} C_{\mathrm{r}}}}{C_{\mathrm{m}}}$.

Type	Extension	Output property	ZPA input
SP/S	L + P/S	LIC	Yes
SP/P	L + P/P	LIV	No
LCL/S	LC + S/S	LIV	Yes
LCL/P	LC + S/P	LIC	Yes
S/SP	S/S + C	LIV	No
S/PS	S/P + L(C)	LIC	No
S/LCL	S/S + CL	LIV	Yes

LIV(C): load-independent voltage (current); ZPA: zero phase angle.

4.2 Sensitivity Analysis

In this section, the basic second-order and the extended higher order compensated CPT circuits are compared in terms of their sensitivity against fluctuations of system parameters, with the purpose of establishing the performance difference between higher order and second-order compensations of CPT converters. According to the above analytical results of LIV(C) output expressions and corresponding conditions, the impacts of variations in coupling and compensated parameters are considered in this section. Before detailed analysis, we define the sensitivity of CPT topology A's transfer ratio (i.e., the voltage gain G_v or the trans-conductance G_i) against the variation of parameter x as $S(x)_A$. For example, for current output cases, we have

$$S_i(x)_A = \left| \frac{\Delta G_i(x)}{\Delta x} \right|_A . \tag{4.12}$$

4.2.1 Sensitivity to Coupling Parameters

As mentioned in Section 2.3, with requirements of specific output characteristics, the operating frequencies of some of the basic second-order compensated CPT circuits are related to mutual capacitance C_m. The effect of fluctuation in the coupling parameter on the circuit output can be expressed in terms of the sensitivity to C_m. Taking S/S and the corresponding extended compensation circuits as examples, we substitute the G_v expressions of S/S with LIV output in Table 2.4 by (4.12), the sensitivity against C_m when C_m fluctuates to λC_m can be calculated as

$$\begin{aligned} S_v(C_\mathrm{m})_\mathrm{S/S} &= \left|\tfrac{G_v(\lambda C_\mathrm{m})-G_v(C_\mathrm{m})}{(\lambda-1)C_\mathrm{m}}\right| \\ &= \left|\tfrac{-\lambda\omega R_\mathrm{L}+j(\lambda+1){C_\mathrm{m}}^{-1}}{\lambda^2\omega C_\mathrm{m}R_\mathrm{L}+j(1-\lambda^2)}\right|. \end{aligned} \tag{4.13}$$

where λ is the variation factor, and $\lambda > 0$.

Similarly, the sensitivity of LCL/S and S/LCL circuits with LIV output against C_m fluctuation can be expressed as

$$S_v(C_\mathrm{m})_\mathrm{LCL/S} = \frac{C_1}{\lambda C_\mathrm{m}^2} \tag{4.14}$$

$$S_v(C_\mathrm{m})_\mathrm{S/LCL} = \frac{1}{C_2}. \tag{4.15}$$

To illustrate the theoretical results more clearly, numerical simulations are performed as shown in Figs. 4.7(a) and 4.7(b). The parameters listed in Table 4.3 are used in our simulations. Normalization of data is applied here to provide a clear view of differences in sensitivity among the topologies.

In LIV output cases, from Fig. 4.7(a), it can be observed that for S/S, S/P, and SP/P circuits (formed by extending the input side of P/P circuits), the voltage gain decreases rapidly when mutual capacitance C_m changes. In contrast, the voltage gain of S/S-based output-side extension of S/SP and S/LCL circuits increases proportionally with the increase of C_m, whereas the voltage gain of input-side extension of LCL/S circuits is approximately inversely proportional to C_m. This means that fourth-order compensated circuits perform better in permitting both ZPA input and LIV output, with the same sensitivity to coupling parameter as third-order compensated circuits. Moreover, the tolerance of S/S

Table 4.3: Parameters of CPT Circuits for Simulation

Parameter	Value	Parameter	Value
C_{t} [pF]	19.73	C_{r} [pF]	19.73
C_{m} [pF]	24.86	f [MHz]	1.2
$V_{\mathrm{in-pp}}$ [V]	50	R_{L} [Ω]	10

based compensated circuits with LIV output against coupling parameters can be substantially enhanced, by adding a capacitor at the load side of the S/S circuit meeting the LIC output requirement, i.e, the S/SP circuit are much less sensitive to C_{m} than the S/S circuit when achieving an LIV output.

Likewise, for LIC output cases shown in Fig. 4.7(b), S/P and LCL/P compensated circuits show the worst performance in maintaining the output current when C_{m} fluctuates. In comparison, the S/LC (one type of the S/PS) circuit is less sensitive to C_{m} fluctuation, whereas the S/LL (the other type of the S/PS) circuit presents a quite high maximum output point within the fluctuation range of C_{m}. Also, S/S and SP/S circuits (rooted from P/S circuits) show the same sensitivity to C_{m} fluctuation with LIC output. The results reveal that when LIC output is required by extending the load side of a basic S/P compensated circuit to a proper third-order S/LC compensated circuit, a higher tolerance of the output current to fluctuation in coupling parameters can be achieved.

Based on the above analysis, it can be observed that the output voltage or current of some specific compensated circuits drops dramatically when coupling parameters fluctuate. This implies that in practice, when the coupling distance or transfer media changes between any two plates of the capacitor coupler, the system performance will be greatly affected. To address this issue, frequency control strategies such as the frequency-tracking approach can be applied. In order to simplify the CPT system design, priority can be given to compensation circuits where the operating conditions are coupling-independent.

4.2.2 Sensitivity to Compensation Parameters

At the primary side, L_p serves as the main designed parameter determined by the operating condition listed in Tables 2.4 and 4.1. Taking S/S, LCL/S and S/LCL circuits with LIV output as examples, when L_p fluctuates to αL_p, the sensitivity of the S/S compensated circuit against L_p can be expressed as

$$S_v(L_\mathrm{p})_{\mathrm{S/S}} = \frac{\omega C_\mathrm{m} C_\mathrm{r} R_\mathrm{L}}{|jC_\mathrm{r} + ((\alpha-1)C_\mathrm{m} - \alpha C_\mathrm{r})(-\omega C_\mathrm{m} R_\mathrm{L} + j)|}. \tag{4.16}$$

Similarly, the sensitivity expressions of LCL/S and S/LCL compensated circuits against L_p are given by

$$S_v(L_\mathrm{p})_{\mathrm{LCL/S}} = 0 \tag{4.17}$$

$$S_v(L_\mathrm{p})_{\mathrm{S/LCL}} = \frac{\omega C_\mathrm{m} C_\mathrm{r} C_2 R_\mathrm{L}}{\left|j(\alpha-1){C_\mathrm{m}}^2 + \omega C_\mathrm{r} {C_2}^2 R_\mathrm{L}\right|}. \tag{4.18}$$

It can be readily observed from the calculation results that the compensated inductor L_p at the primary side theoretically has no effect on the voltage gain of the LCL/S circuit when LIV output is required. Likewise, the theoretical expressions of the sensitivity of other compensation circuits analyzed in Section III against L_p value can be obtained. To illustrate more clearly, simulations of the above circuits based on the T-type model presented in Section 2.1.2 are performed, using the parameters listed in Table 4.3, as shown in Figs. 4.7(c) and 4.7(d). Both theoretical and simulated results show that for the LIV output situation, the LCL/S compensated circuits demonstrate the highest tolerance to L_p fluctuation, followed by S/SP circuits, whereas the voltage gain of the other circuits drop as L_p varies. For the LIC output, the LCL/P circuits perform well when L_p changes. Other circuits show varying degrees of change with the fluctuation of L_p. Specifically, both the S/P and SP/S compensated circuits achieve a higher current output when inductance of L_p increases to a certain value, whereas the output of S/LL and S/LC compensated circuits decline rapidly as L_p value changes.

At the secondary side, the effects of the main compensated parameter L_s on system output can be assessed in a likewise fashion, based on the definition of sensitivity in (4.12) and transfer expressions (2.20) and (2.21). Analytical results are shown graphically in Figs. 4.7(e) and 4.7(f). From Fig. 4.7(e), the results reveal that by extending the S/S compensated circuit at the load side to higher order S/SP and S/LCL compensated circuits, the LIC output can be converted to an LIV output, and this conversion maintains the high tolerance to L_s fluctuation. Likewise, it can be observed from Fig. 4.7(f) that by adding a capacitor or an inductor in series at the output side, the conversion of LIV to LIC as well as the preservation of high tolerance to L_s fluctuation of the S/P compensated circuit can be achieved.

4.3 General Design Strategies for CPT Compensation Circuits

Based on the afore-described extensions at the input and output sides, as well as the discussion on the exhibited transfer characteristics, the basic second-order and higher order compensation schemes of CPT converters can be systematically connected. In the design of CPT converters, a higher-order compensation usually allows a higher degree of freedom of parameter choice because of the extended components in the circuit. In addition, the expected transfer properties can be achieved when appropriate topologies and corresponding parameters are matched. Detailed descriptions are summarized as follows:

1. The S/S, S/P, P/S and P/P compensation circuits are the four basic types of second-order compensated CPT circuits, of which S/S and S/P circuits

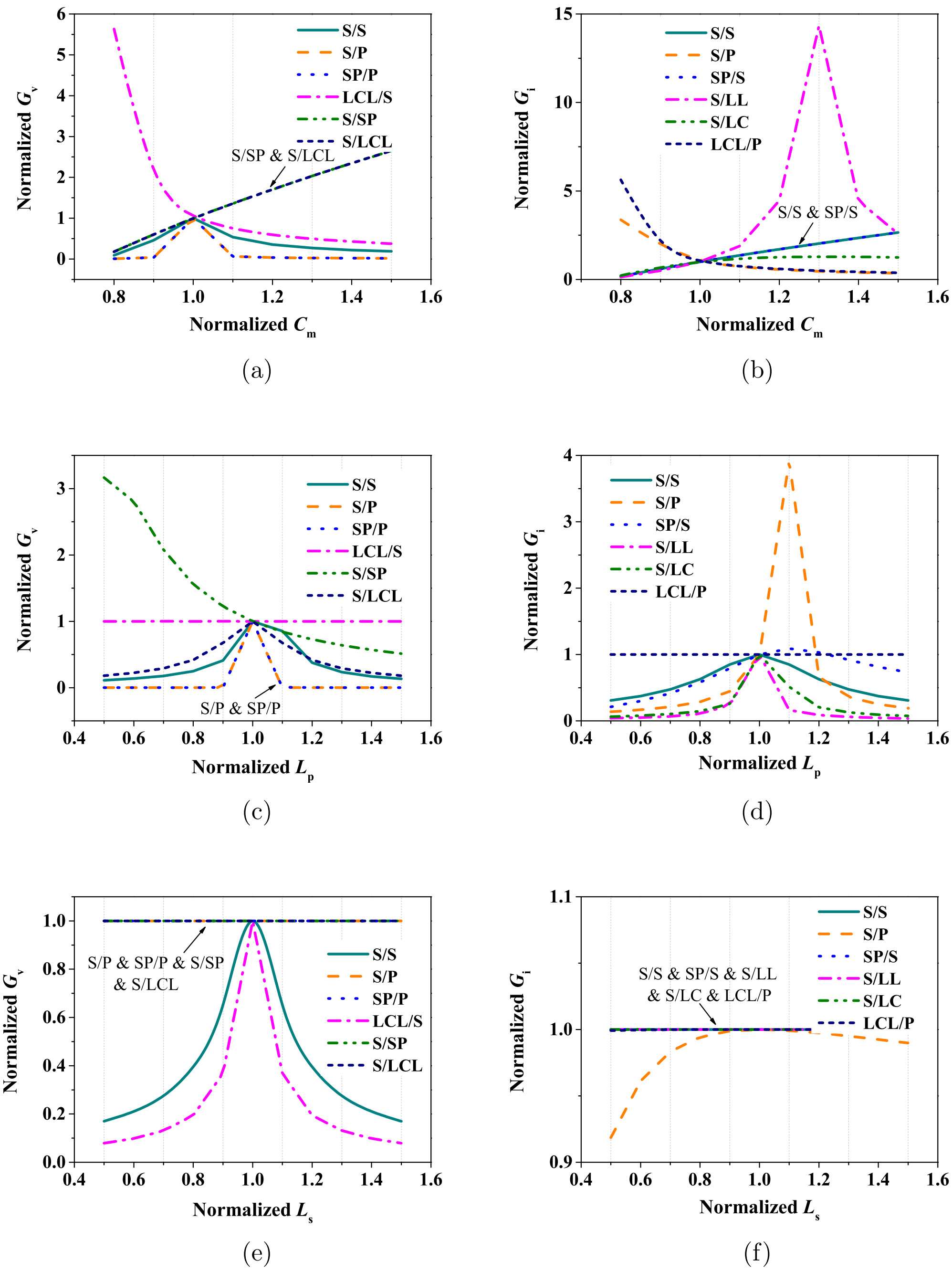

Figure 4.7: (a) Normalized voltage gain versus normalized primary inductor C_m for S/S, S/P, SP/P, S/SP, LCL/S and S/LCL compensated CPT circuits with LIV output; (b) normalized transconductance versus normalized primary inductor C_m for S/S, S/P, SP/S, S/LL, S/LC and LCL/P compensated CPT circuits with LIC output; (c) normalized voltage gain versus normalized secondary capacitor L_p for S/S, S/P, SP/P, S/SP, LCL/S and S/LCL compensated CPT circuits with LIV output; (d) normalized transconductance versus normalized secondary capacitor L_p for S/S, S/P, SP/S, S/LL, S/LC and LCL/P compensated CPT circuits with LIC output; (e) normalized voltage gain versus normalized coupling coefficient L_s for S/S, S/P, SP/P, S/SP, LCL/S and S/LCL compensated CPT circuits with LIV output; (f) normalized transconductance versus normalized coupling coefficient L_s for S/S, S/P, SP/S, S/LL, S/LC and LCL/P compensated CPT circuits with LIC output.

are terminated by input voltage source, P/S and P/P circuits are terminated by input current source. For voltage source driven circuits, which are commonly used in practical applications, S/S circuits perform much better than S/P circuits in terms of sensitivity to parameter variations in most cases.

2. The output-side LIC-LIV and LIV-LIC conversions contribute to maintaining the high tolerance to fluctuation of the compensation component L_s. Specifically, the S/S topology achieves LIC with optimized low sensitivity to L_s fluctuation. To preserve the simple advantage but serve an LIV application, one may extend the secondary side to S/SP or S/LCL to achieve LIV, which preserves the near zero sensitivity to L_s variation.

3. A near constant input current can be obtained by connecting an inductor in series with the input voltage source. The resulting schemes are SP/S and SP/P circuits, which are effectively current-fed P/S and P/P compensated CPT circuits. To reduce the system sensitivity against primary compensation component L_p's fluctuation while maintaining the constant input current, a further input-side extension can be adopted, which generates the fourth-order LCL/S and LCL/P configurations.

4. Both the input-side and output-side extensions rooted from the basic second-order compensation topologies can be systematically applied to improve the tolerance to coupling parameters. In addition to the third-order compensation topologies, higher order compensation topologies can be applied via further extension, to preserve the property of ZPA input while achieving the above desired characteristics, and hence to provide more flexibility for choosing parameter values. Specifically, the input-side further extension can achieve a higher output when the capacitor pair is loosely coupled. This means that in situations where high capacity is needed to address varying

misalignment and transfer gap, the input-side extension topologies can be considered.

5. Double-side extension with capacitors in parallel with the capacitor pair can be applied for reducing the large inductance of the compensation circuits due to small self-capacitor values.

4.4 Experimental Validation

In order to regulate the value of C_{m} conveniently and accurately during the verification process of sensitivity against coupling parameters, the value of C_{m} at various distances among the coupler pairs is measured and calculated first. Shown in Fig. 4.8 are four plates P_1 to P_4 with the same dimension of $200 \times 300 \times 1$ mm^3, adopted as the CPT coupler pairs in the experiments. The vertical distance between P_1 and P_3 (P_2 and P_4) is H, which is also noted as the gap distance between the primary side and the secondary side. D represents the horizontal distance between the two pairs.

Fig. 4.9(a) illustrates the value of coupling capacitor C_{m} changing with distance D at various gap H. Fig. 4.9(b) depicts curves of C_{m} versus H. Here the value of C_{m} at a horizontal distance of 25 mm is normalized, with the initial value of C_{m} at a gap distance of 6 mm being set to 1. The marked range of 0.8 to 1.2 is adopted in our experiments on sensitivity analysis. Figs. 4.9(a) and 4.9(b) show that C_{m} decreases with the increase in distance D, and increases with gap H. The measured results agree well with the theoretical results in Chapter 2.

To compare the characteristics of coupler plates in various materials, the coupling capacitance among four aluminium plates using the same dimensions as the copper plates are also measured. The measured results of C_{m} changes with various distance D and H are illustrated in Fig. 4.10(a) and Fig. 4.10(b) separately.

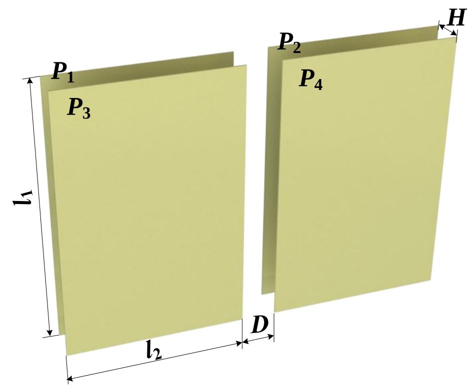

Figure 4.8: Layout illustration of capacitor plates.

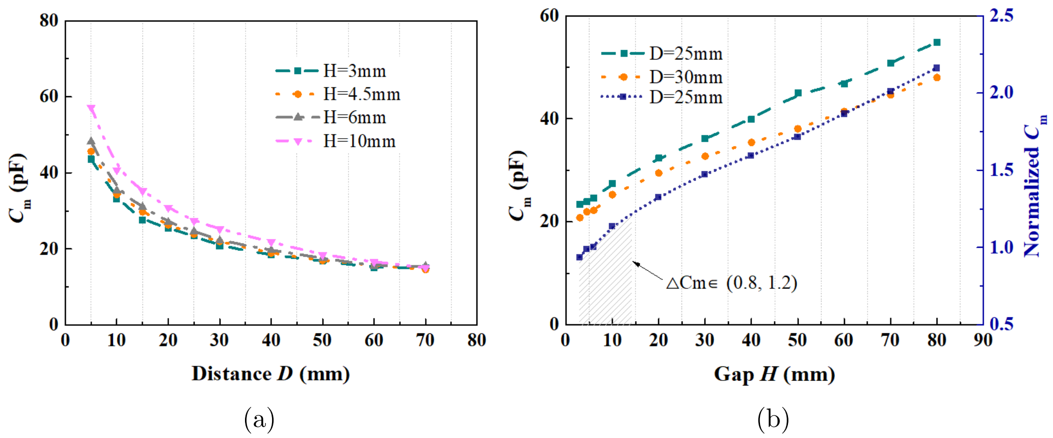

Figure 4.9: Coupling capacitance C_{m} versus (a) horizontal distance D at various gap distance and (b) gap H at various horizontal distance of copper plates.

It can be observed from Figs. 4.9 and 4.10 that compared to the copper plates, the coupling capacitance produced by aluminium plates is more susceptible to the gap distance, and varies more dramatically with the distance. In order to reduce the error that may be caused by changing distances, and hence to ensure that C_{m} changes to the desired value, the capacitor coupler composed of copper plates is adopted in the following experiments.

To verify the analysis presented above, prototypes of CPT converters with S/S and corresponding extended compensation topologies have been built, using the configuration of Fig. 5.12, a photo of which is shown in Fig. 4.12. The coupler

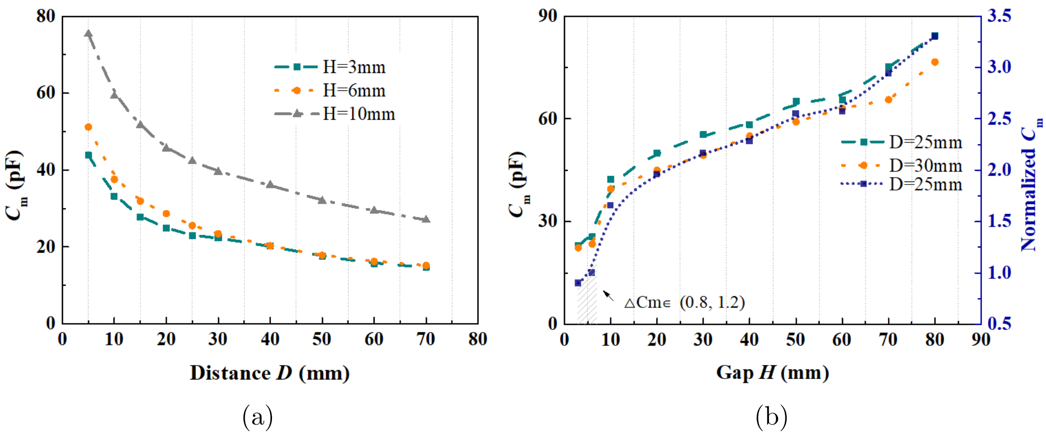

Figure 4.10: Coupling capacitance C_{m} versus (a) horizontal distance D at various gap distance and (b) gap H at various horizontal distance of aluminium plates.

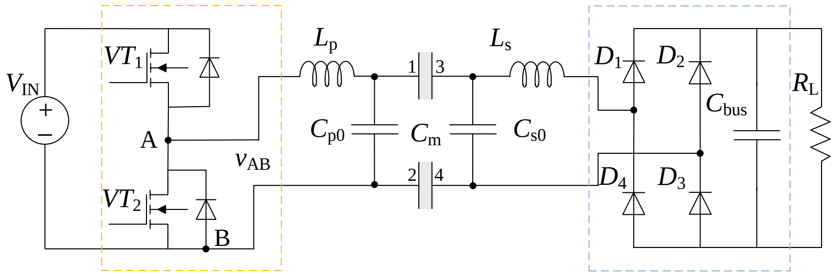

Figure 4.11: Experimental S/S compensated CPT converter.

parameters are measured and listed in Table 4.4. MOSFETS VT_1 and VT_2 are components of the half-bridge inverter, using EPC2034C. The rectifier diodes D_1 to D_4 at the secondary side are implemented by MBR20150CD, and the output filter uses C_{bus} of 100 μF. The specific parameters listed in Table 4.4 are used in our experiments.

Fig. 4.13(a) gives the transient waveforms when the equivalent resistance of load varies from 50 Ω to 8.3 Ω in the S/S compensated CPT converter. Fig. 4.13(b) shows the waveforms of the S/SP compensated converter when the load resistance is stepped from 104 Ω to 47 Ω. It can be observed that by adding a shunt capacitor at the output side with the specific value, the S/S compensation is extended to the S/SP compensation, and the desired transformation from LIC to LIV output is achieved without changing operating conditions.

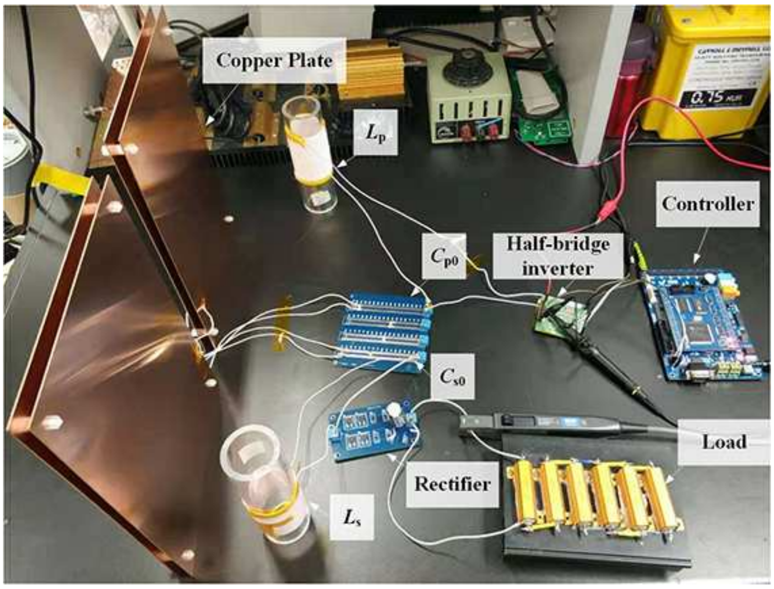

Figure 4.12: Experimental setup of the CPT converter.

Table 4.4: Parameters of CPT Circuits for Experiments

Parameter	Value	Parameter	Value
C_{12} [pF]	5.32	C_{34} [pF]	5.83
C_{13} [pF]	107.22	C_{24} [pF]	106.43
C_{14} [pF]	5.28	C_{23} [pF]	5.15
C_{p0} [pF]	470	C_{s0} [pF]	470
L_{p} [μH]	49.7	L_{S} [μH]	49.7
f [MHz]	1.2	V_{IN} [V]	20

Fig. 4.14 shows the measured results of voltage gain varies with system parameters in S/S, S/SP and LCL/S compensated converters. Here, normalization of data is adopted to compare the sensitivity among the converters with various types of compensation. Thus, with the initial values of L_{p}, L_{s} and C_{m} at the resonant point being set to 1, the ranges of variation in these parameters are normalized to 0.8∼1.2, 0.8∼1.2, and 0.8∼1.5, respectively. The corresponding output voltage is also normalized accordingly, with the initial value at the resonant point set to 1. It can be observed from Fig. 4.14(a) that when C_{m} deviates from the resonant point, the voltage gain of the S/S topology drops

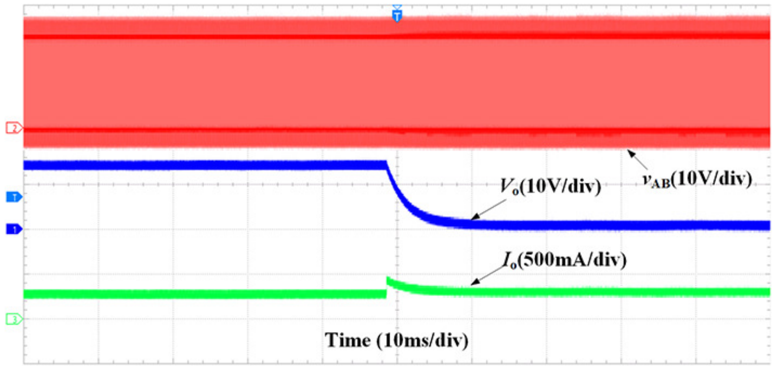

(a)

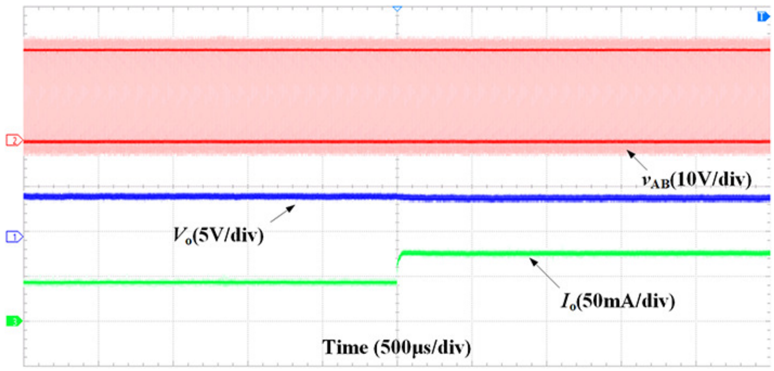

(b)

Figure 4.13: Experimental waveforms of (a) S/S compensated CPT converter when load resistance varies from 50 Ω to 8.3 Ω and (b) S/SP compensated CPT converter when load resistance varies from 104 Ω to 47 Ω.

accordingly. In addition, as C_{m} increases, the voltage gain of LCL/S and S/SP topologies show increasing and decreasing trends, respectively. Thus, input-side or output-side extensions can be adopted when a relatively high voltage gain is required. From Fig. 4.14(c), the S/SP topology is capable of maintaining a constant output voltage when L_{s} varies considerably, whereas the output voltage of S/S and LCL/S topologies drops dramatically when L_{s} fluctuates. This proves that the output-side extension helps to significantly reduces the sensitivity to the fluctuation of L_{s} at the secondary side. Likewise, Fig. 4.14(b) illustrates that the voltage gain of the S/S topology decreases rapidly with L_{p}, while the output voltage of the LCL/S topology is kept constant as L_{p} varies. The results reveal that the input-side extension serves to reduce the system sensitivity against L_{p}.

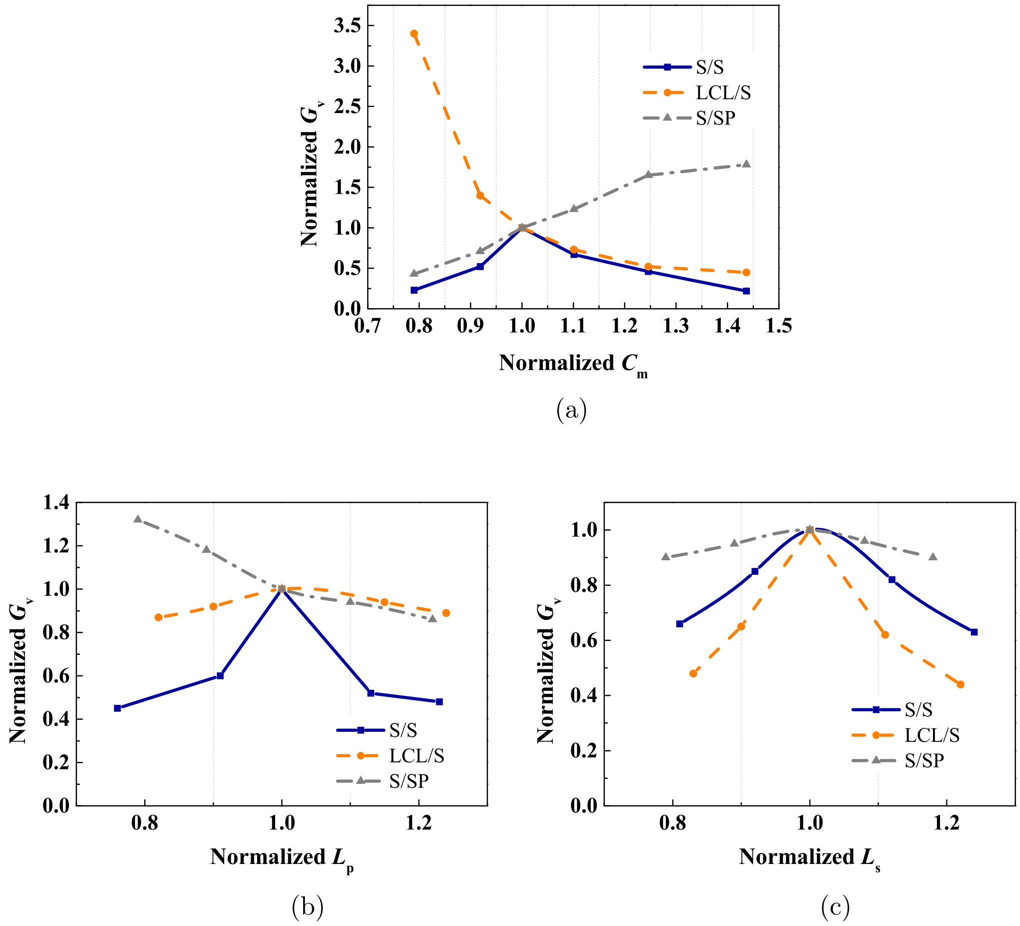

Figure 4.14: Measured normalized voltage gain versus (a) normalized C_{m}; (b) normalized L_{p}; (c) normalized L_{s} of S/S, LCL/S and S/SP compensated CPT converters.

The measured results agree with the analytical results.

4.5 Summary

In much of the reported work addressing capacitive power transfer (CPT) converters, compensation topologies were designed based on equivalent circuit models with various parameters adjusted to achieve specific operating requirements for the applications concerned. Higher order compensated CPT converters were proposed to offer a higher degree of design freedom for selecting system parameters and to alleviate the design constraints. However, connections between the basic second-order and higher order compensated CPT topologies have not been established fundamentally and systematically from the circuit viewpoint and operational viewpoints.

This chapter first presents the transfer characteristics of all possible basic second-order compensated CPT circuits, based on a T-type equivalent model. Then, a new insight into higher order compensated CPT circuits based on sensitivity analysis is proposed, and the sensitivities of various compensation schemes on CPT circuits are compared against fluctuations of the coupling and compensation parameters. The presented analysis provides a convenient connecting pathway from second-order to higher order CPT circuits, bridging each type of topological extension with the specific performance. In practice, the presented analysis provides a convenient design guideline to derive higher order compensation circuits capable of improving specific performance while maintaining the original merits of second-order compensation circuits. Specifically, the results show that adding an series inductor at the input side of a second-order CPT circuit can offer a constant primary current, and adding an inductor or capacitor in series (parallel) at the output side can converse a constant load-independent voltage (current) output to a constant load-independent current (voltage) output. In addition, the extension to fourth or higher order compensation circuits enables the CPT converter to reduce its sensitivity against parameter variations as well as to maintain the property of zero phase input. The proposed perspective of topological extension from second-order compensated CPT circuits provides a simple and effective basis for understanding the significance of specific compensation components in higher order CPT circuits and how the circuits combat parameter variations.

Chapter 5

Application: IPT Systems with Multiple Outputs

In the previous chapters, we discussed the impact of various compensation topologies on the system output and general design process of wireless power transfer converters with single input and single output (SISO). With the changing application scenarios of wireless power transfer, the development of single-input multi-output (SIMO) and multi-input multi-output (MIMO) coupling structures have gained popularity, which also come with numerous side effects on the system performance in terms of output power transfer efficiency, and so on. In this chapter, the properties of inductive power transfer (IPT) configurations constructed with various coupling structures and compensation topologies will be explained in detail. The corresponding control strategies for realizing optimum system performance will be explored. Finally, a third-order compensated IPT converter for multi-output application will be discussed to simplify the control process while retaining the merits of the original topologies.

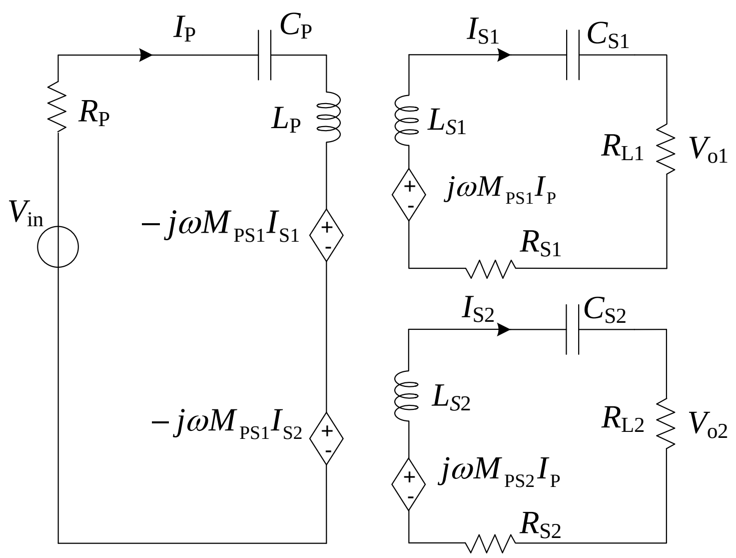

Figure 5.1: Equivalent circuit of the single-input double-output IPT circuit.

5.1 Coupling Structures

5.1.1 Single-Input Double-Output Structure

Shown in Fig. 5.1 is the equivalent circuit of a single-input double-output (SIDO) IPT converter using series-series (S/S) compensation. To facilitate the analysis, we assume that the converter is terminated by an ideal sine AC voltage source V_{in} at the input side, and two equivalent loads R_{L1} and R_{L2} at the output side. The transformer consists of a primary coil with the self-inductance L_{P} and two secondary coils with self-inductances L_{S1} and L_{S2}. Each inductor is connected with a series compensated capacitor. From Kirchhoff's voltage law (KVL), the state equation of the SIDO circuit is

$$\begin{bmatrix} \dot{V}_{\mathrm{in}} \\ 0 \\ 0 \end{bmatrix} = \begin{bmatrix} Z_{\mathrm{P}} & -j\omega M_{\mathrm{PS1}} & -j\omega M_{\mathrm{PS2}} \\ -j\omega M_{\mathrm{PS1}} & Z_{\mathrm{S1}} & j\omega M_{\mathrm{S1S2}} \\ -j\omega M_{\mathrm{PS2}} & j\omega M_{\mathrm{S1S2}} & Z_{\mathrm{S2}} \end{bmatrix} \begin{bmatrix} \dot{I}_{\mathrm{P}} \\ \dot{I}_{\mathrm{S1}} \\ \dot{I}_{\mathrm{S2}} \end{bmatrix} \tag{5.1}$$

where $M_{\mathrm{PS}i}$ ($i = 1, 2$) denotes the mutual inductance between the primary coil and the i-th secondary coil; M_{S1S2} denotes the mutual inductance between the two secondary coils; ω denotes the operating frequency; Z_{P} and $Z_{\mathrm{S}i}$ are the total impedances at the primary and the i-th secondary side, respectively; and $M_{PSi} = k\sqrt{L_{\mathrm{P}} L_{\mathrm{S}i}}$, where k is the coupling coefficient.

Assuming that both the secondary coils are placed in the same plane, the two coils are thus radially coupled. When the two coils are orthogonally positioned or are separated by a certain distance, the coupling coefficient k between the coils will be less than 0.01, i.e., $M_{\mathrm{S1S2}} \approx 0$. Then, the equivalent reflected impedance Z_r of the SIDO system can be expressed as

$$Z_r = \frac{\omega^2 M_{\mathrm{PS1}}^2}{Z_{\mathrm{S1}}} + \frac{\omega^2 M_{\mathrm{PS2}}^2}{Z_{\mathrm{S2}}} \tag{5.2}$$

Since there exist several LC-resonant networks in the SIDO system, we define the self-resonance frequency as $\omega_P = 1/\sqrt{L_{\mathrm{P}} C_{\mathrm{P}}}$, $\omega_{\mathrm{S}i} = 1/\sqrt{L_{\mathrm{S}i} C_{\mathrm{S}i}}$. Putting ω_P and $\omega_{\mathrm{S}i}$ in (5.2), the real and imaginary parts of the reflected impedance Z_{ri} can be expressed separately as

$$\begin{cases} \Re(Z_{ri}) = \dfrac{\omega L_{\mathrm{P}} {k_{\mathrm{PS}i}}^2 Q_{\mathrm{O}i}}{1 + {Q_{\mathrm{O}i}}^2 (1 - {\xi_{\mathrm{Si}}}^2)^2} \\ \Im(Z_{ri}) = -\dfrac{\omega L_{\mathrm{P}} k_{\mathrm{PS}i}^2 Q_{\mathrm{O}i}^2 (1 - {\xi_{\mathrm{S}i}}^2)}{1 + Q_{\mathrm{O}i}^2 \left(1 - {\xi_{\mathrm{S}i}}^2\right)^2} \end{cases} \tag{5.3}$$

where $\xi_{\mathrm{S}i} = \omega_{\mathrm{S}i}/\omega$, $\xi_P = \omega_P/\omega$; Q denotes the quality factor of the component; $Q_{\mathrm{L}i} = \omega L_{\mathrm{S}i}/R_{\mathrm{L}i}$; and $Q_{\mathrm{O}i} = \omega L_{\mathrm{S}i}/(R_{\mathrm{S}i} + R_{\mathrm{L}i})$, $i = 1, 2$.

Using the quality factor and the impedance expressions, the transfer efficiencies of the primary and secondary sides can be obtained as

$$\begin{cases} \eta_P &= \dfrac{\Re(Z_{r1}) + \Re(Z_{r2})}{\Re(Z_{r1}) + \Re(Z_{r2}) + R_{\mathrm{P}}} \\ \eta_S &= \eta_{\mathrm{S1}}\eta_{\mathrm{S2}} = \dfrac{Q_{\mathrm{O1}}Q_{\mathrm{O2}}}{Q_{\mathrm{L1}}Q_{\mathrm{L2}}} \end{cases} \tag{5.4}$$

Substituting (5.3) into (5.4), the transfer efficiency η of the whole SIDO system is given by

$$\eta = \eta_{\mathrm{P}}\eta_{\mathrm{S}} = \frac{Q_{\mathrm{O1}}Q_{\mathrm{O2}}}{Q_{\mathrm{L1}}Q_{\mathrm{L2}}} \left(\frac{\sum_{i=1}^{2} A_{\mathrm{S}i}}{1 + \sum_{i=1}^{2} A_{\mathrm{S}i}} \right) \tag{5.5}$$

where

$$A_{\mathrm{S}i} = \frac{{k_{\mathrm{PS}i}}^2 Q_{\mathrm{P}} Q_{\mathrm{O}i}}{1 + Q_{\mathrm{O}i}^2 (1 - \xi_{\mathrm{S}i}^2)^2}.$$

When operating at the resonance frequency, i.e., $\xi_P = \xi_{\mathrm{S}i} = 1$, the transfer efficiency can be simplified as

$$\eta = \frac{Q_{\mathrm{P}} Q_{\mathrm{O1}} Q_{\mathrm{O2}} {Q_{\mathrm{L1}}}^{-1} {Q_{\mathrm{L2}}}^{-1}}{1 + \left({k_{\mathrm{PS1}}}^2 Q_{\mathrm{O1}} + {k_{\mathrm{PS2}}}^2 Q_{\mathrm{O2}} \right)^{-1}} \tag{5.6}$$

Combining (5.1), (5.3) and (5.6), the output power of the SIDO IPT system operating at the resonance frequency is given by

$$\begin{aligned} P_{\mathrm{o}} &= \frac{{V_{\mathrm{in}}}^2 \eta}{\sqrt{\left(R_{\mathrm{P}} + \sum_{i=1}^{2} \Re(Z_r) \right)^2 + \Im(Z_r)^2}} \\ &= \frac{{V_{\mathrm{in}}}^2 \frac{Q_{\mathrm{O1}}Q_{\mathrm{O2}}}{Q_{\mathrm{L1}}Q_{\mathrm{L2}}} \sum_{i=1}^{2} {k_{\mathrm{PS}i}}^2 Q_{\mathrm{P}} Q_{\mathrm{O}i}}{R_{\mathrm{P}} \left(1 + \sum_{i=1}^{2} {k_{\mathrm{PS}i}}^2 Q_{\mathrm{P}} Q_{\mathrm{O}i} \right)^2} \end{aligned} \tag{5.7}$$

5.1.2 Double-Input Double-Output Structure

The transfer characteristics of a double-input double-output (DIDO) IPT converter can be extended from the above analysis. As shown in Fig. 5.2, the two primary coils (equivalent to inductors L_{P1} and L_{P1}) of the DIDO converter are terminated by two independent sine AC voltage sources at the input side. The

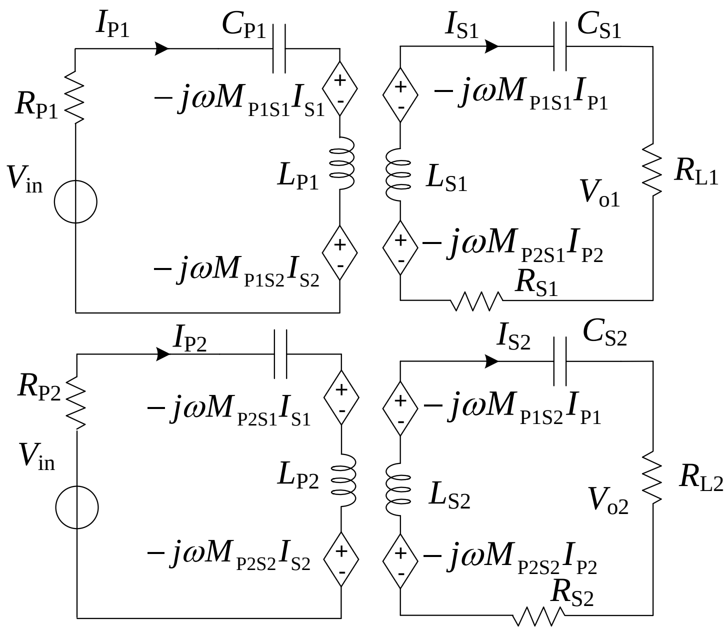

Figure 5.2: Equivalent model of the double-input double-output IPT circuit.

mutual inductance M_{P1P2} can be neglected when the two primary coils are orthogonally positioned or are separated by a certain distance. Thus, the transfer efficiency of the DIDO system is given by

$$\begin{cases} \eta = \prod_{j=1}^{2} \prod_{i=1}^{2} \eta_{\mathrm{P}j} \eta_{\mathrm{S}i} \\ \eta_{\mathrm{P}j} = \dfrac{\sum_{i=1}^{2} \Re(Z_{rji})}{\sum_{i=1}^{2} \Re(Z_{rji}) + R_{\mathrm{P}j}} \\ \eta_{\mathrm{S}i} = \dfrac{Q_{\mathrm{O}i}}{Q_{\mathrm{L}i}} \end{cases} \tag{5.8}$$

The real and imaginary parts of the reflected impedance Z_{rji} of the i-th secondary side to the j-th primary side in (5.8) are

$$\begin{cases} \Re(Z_{rji}) = \dfrac{\omega L_{\mathrm{P}j} {k_{ji}}^2 Q_{\mathrm{O}i}}{1 + {Q_{\mathrm{O}i}}^2 (1 - {\xi_{\mathrm{S}i}}^2)^2} = R_{\mathrm{P}j} A_{ji} \\ \Im(Z_{rji}) = -\dfrac{\omega L_{\mathrm{P}j} {k_{ji}}^2 {Q_{\mathrm{O}i}}^2 (1 - {\xi_{\mathrm{S}i}}^2)^2}{1 + {Q_{\mathrm{O}i}}^2 (1 - {\xi_{\mathrm{S}i}}^2)^2} = -R_{\mathrm{P}j} B_{ji} \end{cases} \tag{5.9}$$

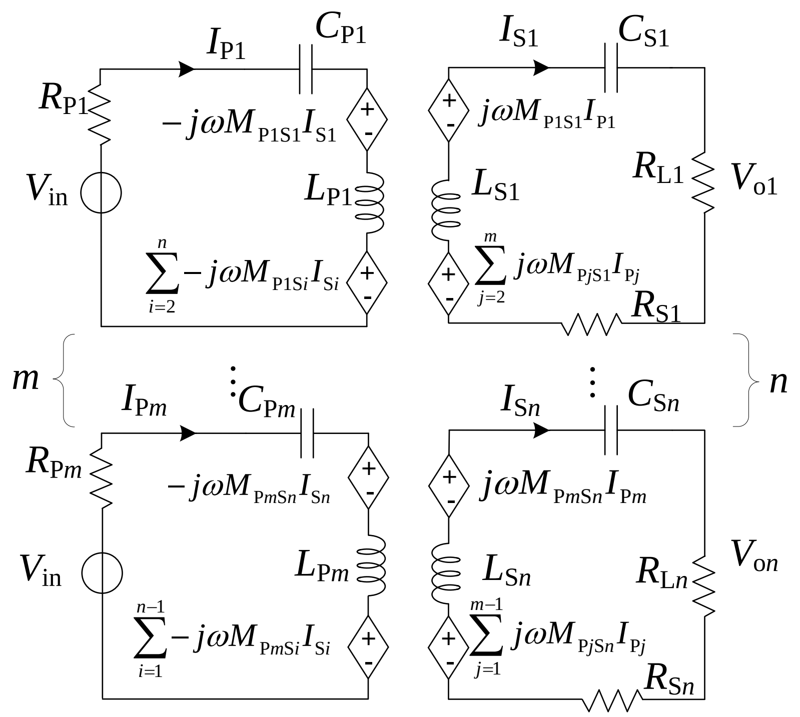

Figure 5.3: Equivalent model of the multi-input multi-output IPT circuit.

where

$$\begin{aligned} A_{ji} &= \frac{{k_{ji}}^2 Q_{\mathrm{P}j} Q_{\mathrm{O}i}}{1+{Q_{\mathrm{O}i}}^2(1-{\xi_{\mathrm{S}i}}^2)^2}, \\ B_{ji} &= \frac{{k_{ji}}^2 Q_{\mathrm{P}j} {Q_{\mathrm{O}i}}^2(1-{\xi_{\mathrm{S}i}}^2)^2}{1+{Q_{\mathrm{O}i}}^2(1-{\xi_{\mathrm{S}i}}^2)^2} \end{aligned}$$

for $i, j = 1, 2$. Then, substituting (5.9) into (5.8) gives a simplified representation of efficiency, which leads to an expression for output power P_o of the DIDO IPT system as

$$\begin{aligned} P_\mathrm{o} &= P_\mathrm{in} \cdot \eta \\ &= \prod_{j=1}^{2}\prod_{t=1}^{2} \frac{Q_{\mathrm{O}t}}{Q_{\mathrm{L}t}} \frac{\sum_{i=1}^{2} A_{ji}}{1+\sum_{i=1}^{2} A_{ji}} \\ &\times \sum_{j=1}^{2} \frac{{V_\mathrm{in}}^2}{R_{\mathrm{P}j}\sqrt{\left(1+\sum_{i=1}^{2} A_{ji}\right)^2 + \sum_{i=1}^{2} {B_{ji}}^2}} \end{aligned} \tag{5.10}$$

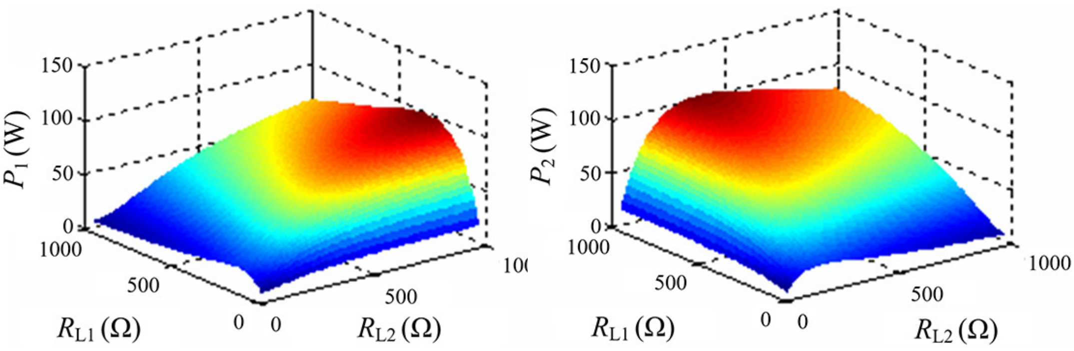

(a) (b)

Figure 5.4: (a) Simulated output power on R_{L1} versus value of R_{L2}; and (b) output power on R_{L2} versus value of R_{L1}.

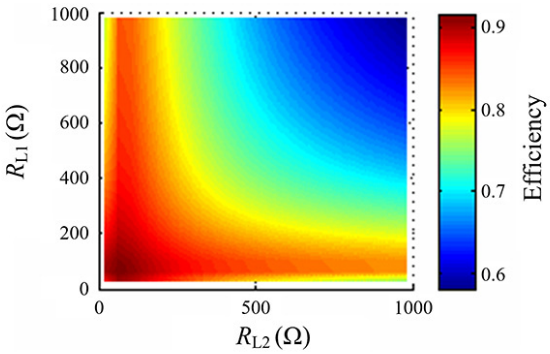

Figure 5.5: Simulated transfer efficiency versus load impedance.

5.1.3 General Multi-Input Multi-Output Structure

Based on the above analysis, a logical extension from the DIDO IPT converter to a MIMO IPT converter is possible, as shown in Fig. 5.3. The corresponding transfer efficiency and output power can be readily obtained as follows:

$$\eta = \prod_{j=1}^{m} \prod_{t=1}^{n} \frac{Q_{\text{O}t}}{Q_{\text{L}t}} \frac{\sum_{i=1}^{n} A_{ji}}{1 + \sum_{i=1}^{n} A_{ji}} \tag{5.11}$$

$$\begin{aligned} P_{\text{o}} &= P_{\text{in}} \cdot \eta \\ &= \prod_{j=1}^{m} \prod_{t=1}^{n} \frac{Q_{\text{O}t}}{Q_{\text{L}t}} \cdot \frac{\sum_{i=1}^{n} A_{ji}}{1 + \sum_{i=1}^{n} A_{ji}} \\ &\times \sum_{j=1}^{m} \frac{{V_{\text{in}}}^2}{R_{\text{P}j} \sqrt{(1 + \sum_{i=1}^{n} A_{ji})^2 + \sum_{i=1}^{n} {B_{ji}}^2}} \end{aligned} \tag{5.12}$$

where $Q_{\mathrm{O}t} = \omega L_{\mathrm{S}t}/(R_{\mathrm{S}t}+R_{\mathrm{L}t})$ and $Q_{\mathrm{L}t} = \omega L_{\mathrm{S}t}/R_{\mathrm{L}t}$, for $t = 1, ..., n$. Thus, we can obtain the transfer characteristics of any S/S compensated MIMO IPT converter under various operating conditions using the calculation results above. Here, with the requirement of load-independent output, the simple constant current (CC) output conditions are adopted. Both primary and secondary sides of the converter operate at the self-resonance frequency, i.e., $\omega_P = \omega_S = \omega$ and $\xi_P = \xi_S = 1$. Substituting these operating conditions into (5.9), it can be readily obtained that the factor $B_{ji} = 0$, and the simplified impedance Z_{rji} is given by

$$Z_{rji} = {k_{ji}}^2 R_{\mathrm{P}j} Q_{Pj} Q_{\mathrm{O}i}. \tag{5.13}$$

Then, the total transfer efficiency of an MIMO IPT converter with S/S compensation can be further simplified as

$$\eta = \prod_{j=1}^{m}\prod_{t=1}^{n} \frac{Q_{\mathrm{O}t}}{Q_{\mathrm{L}t}} \frac{\sum_{i=1}^{n} k_{ji}^2 Q_{\mathrm{O}i}}{1+\sum_{i=1}^{n} k_{ji}^2 Q_{\mathrm{O}i}} \tag{5.14}$$

Similarly, the total output power of the MIMO IPT converter is simplified as

$$P_{\mathrm{o}} = \prod_{j=1}^{m}\prod_{t=1}^{n} \frac{Q_{\mathrm{O}t}}{Q_{\mathrm{L}t}} \frac{\sum_{i=1}^{n} {k_{ji}}^2 Q_{\mathrm{O}i}}{1+\sum_{i=1}^{n} {k_{ji}}^2 Q_{\mathrm{O}i}} \sum_{j=1}^{m} \frac{{V_{\mathrm{in}}}^2}{R_{\mathrm{P}j}(1+\sum_{i=1}^{n} {k_{ji}}^2 Q_{\mathrm{O}i})} \tag{5.15}$$

Assume that the system parameters of each input or output branch are consistent with the MIMO IPT converter. The total output power given in (5.15) becomes

$$P_{\mathrm{o}} = \frac{m{V_{\mathrm{in}}}^2 {Q_{\mathrm{O}}}^n (nk^2 Q_{\mathrm{P}} Q_{\mathrm{O}})^m}{R_{\mathrm{P}} {Q_{\mathrm{L}}}^n (1+nk^2 Q_{\mathrm{P}} Q_{\mathrm{O}})^{m+1}} \tag{5.16}$$

In order to achieve maximum power output, we differentiate (5.16) with respect to R_{L}, giving the optimal load value as

$$R_{\mathrm{L},P_m} = \frac{1}{2m}\left[R_{\mathrm{S}}(n-m) + \frac{\omega^2 M^2 n}{R_{\mathrm{P}}}\right.$$

$$+ \frac{1}{R_\mathrm{P}} \Big(\big(R_\mathrm{S} R_\mathrm{P} (n-m) - \omega^2 M^2 n \big)^2 \\ + 4mnR_\mathrm{S} (\omega^2 M^2 n + R_\mathrm{S} R_\mathrm{P}) \Big)^{\frac{1}{2}} \Big] \tag{5.17}$$

Thus, by transitioning from SIDO IPT circuits to DIDO IPT circuits, and finally extending to a generic MIMO IPT circuit, we can obtain theoretical results for the transfer features of any MIMO IPT circuit with S/S compensation based on the above formulas. Accordingly, the optimal operating point for maximum power output or maximum efficiency transfer can be calculated. In this paper, normal operation of each load is mainly concerned. Then, the priority of maximum power output is considered as higher than maximum efficiency transfer. Therefore, the unified design will be centered on power distribution and regulation. The above formulas will also be used later in our proposed unified design procedure.

5.1.4 Illustrations by Simulations

In order to reveal the load characteristics of multi-output IPT systems, we present simulations based on the equivalent model shown in Fig. 5.1. The parameter values listed in Table 5.1 are used. From Fig. 5.4(a), it can be readily observed that with a certain value of R_L1, the power delivered to R_L1 increases as R_L2 increases, and the growth gradually slows down. Similar results can be observed from Fig. 5.4(b). In addition, the maximum power transfer points to R_L1 and R_L2 can be identified. Likewise, Fig. 5.5 illustrates the trend of the transfer efficiency as the values of R_L1 and R_L2 increase. With one load fixed, the optimal efficiency point of the other load can be readily identified.

In short, from the foregoing illustration, the output power of each load in a multi-load IPT system is affected by the change of resistance in either load of the system. Thus, when the number of output terminals changes, regulation of the

Table 5.1: Simulation Parameters of Single-input Double-output IPT Circuits

Parameter	Value
Primary inductor L_{P}	300 μH
Secondary inductor L_{S1}, L_{S2}	80 μH
Coupling coefficient k_{PS1}, k_{PS2}	0.15
Operating frequency f	100 kHz
ESR R_{P}	0.4 Ω
ESR R_{S1}, R_{S2}	0.2 Ω
Input voltage V_{in} (rms)	50 V

ESR: Equivalent series resistance.

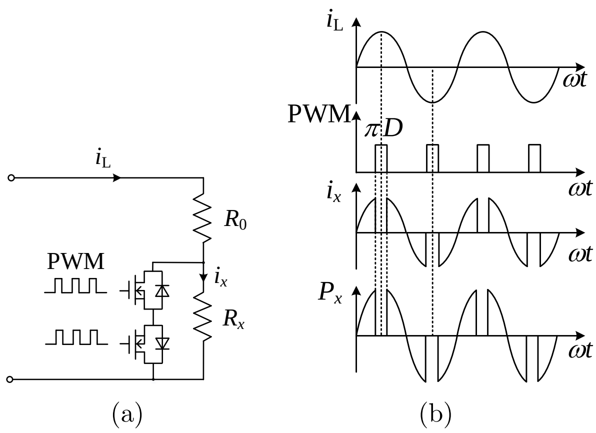

Figure 5.6: (a) Equivalent circuit and (b) corresponding theoretical waveforms of a tunable resistor R_{L}. ($R_{\mathrm{L}} = R_0 + R_x$)

output power or equivalent load value is necessary to achieve maximum power transfer.

5.2 Control Strategies

5.2.1 Load Control

As mentioned in Section 5.1, the primary and secondary sides of the MIMO IPT system with S/S compensation operate at the same resonance frequency ω. In this case, A_{ji} and B_{ji} in the Z_{ji} expression (5.9) are

$$\begin{cases} A_{ji} = {k_{ji}}^2 Q_{\mathrm{O}i} \\ B_{ji} = 0, \end{cases} \tag{5.18}$$

implying that the input impedance Z_{ji} is purely resistive, i.e., zero phase angle (ZPA) input is achieved. Since the output current of the system is independent of the load, using the standard transfer ratio expression of S/S compensated IPT circuit with LIC output [86], we get the output current $I_{\mathrm{o}i}$ of the i-th secondary side as

$$I_{\mathrm{o}i} = \sum_{j=1}^{m} \frac{V_{\mathrm{in}}}{\omega M_{\mathrm{P}j\mathrm{S}i}} \tag{5.19}$$

As discussed in Section 5.1.4, in order to fulfill the power required for normal operation of the load and the maximum power output condition when the number of input and output terminals varies, it is necessary to regulate the load resistance R_{L} without changing the coupling parameters of the IPT system.

In the following, a control strategy is presented to conveniently set the load resistance to the desired value. Assume that the equivalent resistance of each load is the same, and the coupling distance between each primary coil and the i-th secondary coil does not vary a lot. Then, each output terminal of the IPT system is expected to deliver the same current value.

Shown in Fig. 5.6(a) is the equivalent circuit of a tunable resistor R_{L}, consisting of an initial resistor R_0 and a variable resistor R_x, i.e.,

$$R_{\mathrm{L}} = R_0 + R_x. \tag{5.20}$$

By adjusting the duty cycle D of the anti-parallel MOSFETs connected in parallel with resistor R_x, the value of R_{L} can be controlled. The corresponding waveforms of current i_L, the PWM wave, current i_x flowing through R_x, and the output power delivered to R_x are illustrated in Fig. 5.6(b). The conduction angle can be adjusted by controlling duty cycle D, thus regulating the equivalent output power P_x. Specifically, the alignment position of the PWM signal is πD in a current cycle. By detecting the zero-crossing current and delaying the angle by $(\pi/2 - \pi D/2)$, precise control of the load resistance can be achieved. Thus, the equivalent load value R_x with initial resistance of R_{x0} can be expressed in terms of duty cycle D as

$$\frac{R_x}{R_{x0}} = \frac{I_{x0}^2}{I_x^2} = 1 - D - \frac{1}{\pi}\sin(\pi D). \tag{5.21}$$

5.2.2 Power Tracking Control

The aforementioned control method enables the IPT system to achieve the maximum power output by regulating the load value, and can be utilized in specific applications such as heating and energy storage. However, this control strategy of load regulation is no longer applicable when the load impedance is fixed. In this case, DC-DC converters can be employed between the rectifier and the load to regulate the equivalent resistance of DC load. Three most commonly used DC-DC converters of buck, boost, and buck-boost converters, as shown in Fig. 5.7, are analyzed in detail here for various applicable scenarios in terms of the number of input and output terminals.

From Fig. 5.7(a), when current i_{L} flowing through inductor L maintains a positive value throughout the switching period T, the converter operates in continuous conduction mode (CCM); If the value of inductor L is too small or the period is too long, then inductor current i_{L} could fall to zero during OFF time of the period. In this case, an idling interval is introduced where $i_{\mathrm{L}} = 0$, and the converter operates in discontinuous conduction mode (DCM). Then, the relationship between the input voltage and output voltage of the buck converter in

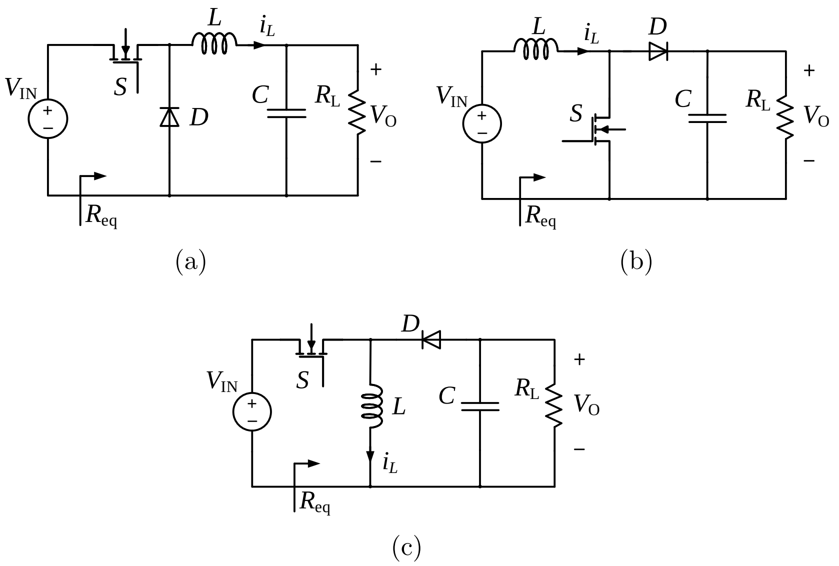

Figure 5.7: Three typical DC-DC converters of (a) buck converter, (b) boost converter and (c) buck-boost converter.

CCM and DCM can be obtained as follows:

$$\begin{cases} V_{\mathrm{O}} = DV_{\mathrm{IN}} & \text{for CCM} \\ V_{\mathrm{O}} = \dfrac{2V_{\mathrm{IN}}}{1+\sqrt{1+\frac{8L_1}{R_{\mathrm{L}}TD^2}}} & \text{for DCM} \end{cases} \tag{5.22}$$

where D is the duty cycle of the converter.

According to the rule of volt-second balance, we can get the expression of equivalent input resistance R_{eq} of the buck converter as

$$\begin{cases} R_{\mathrm{eq}} = \dfrac{R_{\mathrm{L}}}{D^2} & \text{for CCM} \\ R_{\mathrm{eq}} = \dfrac{R_{\mathrm{L}}}{4}\left(1+\sqrt{1+\dfrac{8L}{R_{\mathrm{L}}TD^2}}\right)^2 & \text{for DCM} \end{cases} \tag{5.23}$$

Similarly, the output voltage and the equivalent resistance in CCM and DCM of the boost converter, as illustrated in Fig. 5.7(b), can be found as

$$\begin{cases} V_{\mathrm{o}} = \dfrac{V_{\mathrm{IN}}}{(1-D)}, \\ \\ R_{\mathrm{eq}} = (1-D)^2 R_{\mathrm{L}}, \end{cases} \quad \text{for CCM.} \tag{5.24}$$

$$\begin{cases} V_{\mathrm{o}} = \dfrac{V_{\mathrm{IN}}}{2}\left(1+\sqrt{1+\dfrac{2R_{\mathrm{L}}TD^2}{L}}\right), \\ \\ R_{\mathrm{eq}} = R_{\mathrm{L}}\left(1+\sqrt{1+\dfrac{2R_{\mathrm{L}}TD^2}{L}}\right)^{-2}, \end{cases} \quad \text{for DCM.} \tag{5.25}$$

For the buck-boost converter shown in Fig. 5.7(c), we have

$$\begin{cases} V_{\mathrm{o}} = \dfrac{-DV_{\mathrm{IN}}}{(1-D)}, \\ \\ R_{\mathrm{eq}} = (D^{-1}-1)^2 R_{\mathrm{L}}, \end{cases} \quad \text{for CCM.} \tag{5.26}$$

$$\begin{cases} V_{\mathrm{o}} = -DV_{\mathrm{IN}}\sqrt{\dfrac{R_{\mathrm{L}}T}{2L}}, \\ \\ R_{\mathrm{eq}} = \dfrac{TL}{D^2}, \end{cases} \quad \text{for DCM.} \tag{5.27}$$

Thus, by controlling duty cycle D of the converters, the desired value of equivalent resistor R_{eq} can be obtained.

According to equation (5.17) in Section 5.1.3, the optimal load value should increase as the number of outputs, and decrease as the number of inputs, to ensure the tracking of output power. Since the buck converter is a step-down converter, the output voltage is lower than the input voltage. In this case, the equivalent resistance of R_{eq} is larger than R_{L}. Therefore, the buck converter can be adopted in multi-output scenarios, not applicable to multi-input scenarios.

Table 5.2: Simulation Parameters of Buck, Boost and Buck-boost Converters

Parameter	Buck	Boost	Buck-boost
Inductor L in CCM	230 μH	30 μH	230 μH
Inductor L in DCM	20 μH	2 μH	2 μH
Load resistor R_L	50 Ω	50 Ω	50 Ω
Operating frequency f	100 kHz	100 kHz	100 kHz

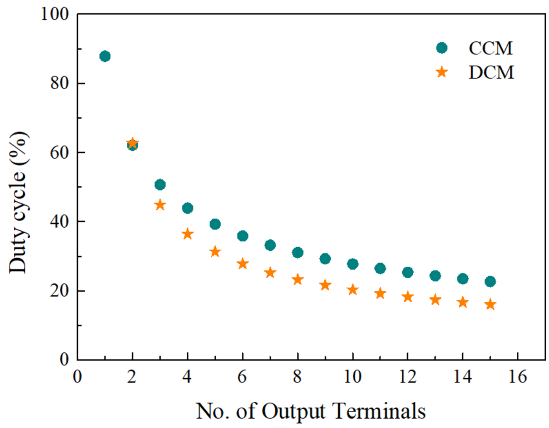

Figure 5.8: Duty cycle of the buck converter versus number of output terminals.

Compared to the buck converter, the boost converter contributes to step up the output voltage, and R_{eq} is smaller than R_L. In this case, the boost converter is suitable for IPT systems with multiple inputs and single output. For buck-boost converters, since both step-up and step-down of the voltage can be achieved, the resistance of R_{eq} can be adjusted to larger or smaller than load resistance R_L by virtue of regulation in duty cycle. Thus, the buck-boost converter is applicable to IPT systems with multiple inputs and multiple outputs.

Numerical simulations of theses three converters are conducted to evaluate the range of regulation in duty cycle D, using the parameters listed in Table 5.2. Curves in Figs. 5.8, 5.9 and 5.10 explicate the relationship between the duty cycle with the number of input or output terminals of in CCM and DCM of various converters. The simulations results agree well with the theoretical results.

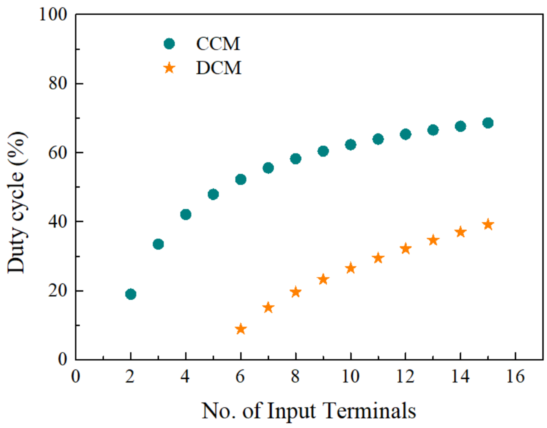

Figure 5.9: Duty cycle of the boost converter versus number of input terminals.

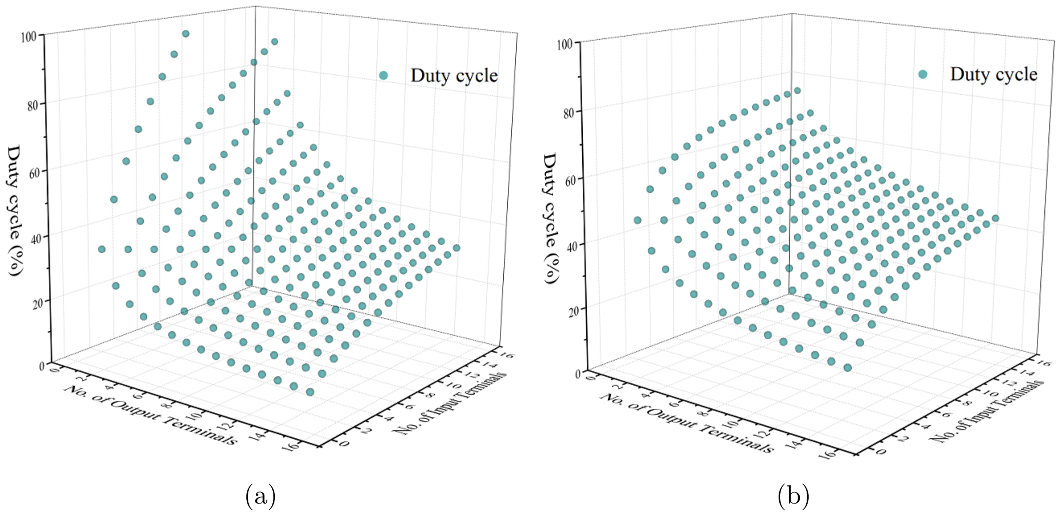

Figure 5.10: Duty cycle of the buck-boost converter versus number of input output terminals in (a) discontinuous conduction mode (DCM) and (b) continuous conduction mode (CCM).

5.3 Design Principle

In this section, a design process for MIMO IPT systems with optimal power output is presented. Let P_E represent the total rated power of the loads, and P_o denote the output power capacity of the system. The design procedure starts with a single-input structure, and the series of steps are:

1. Obtain the load information, e.g., number of outputs n, rated output P_E, and operating conditions.

2. Determine if a single-output or multi-output structure is required.

3. Obtain theoretical results of output power $P_{\rm o}$ and the equivalent reflected impedance Z_r using the procedure given in Section 5.1.

4. If $P_{\rm o}$ exceeds P_E, retain the single-input structure and calculate the desired optimal load value for each load using equation (5.17) in Section 5.1, or calculate the value of load under normal operating conditions using Ohm's Law. Otherwise, choose the multi-input structure and go back to Step 2.

5. Apply the load or the voltage control to regulate the load value(s) to the optimal point(s), based on the control strategies presented in Section 5.2.

As the equivalent load of each output is set to the optimal value, maximum power output can be achieved.

5.4 Experimental Validation

In order to verify the analysis presented above, a laboratory prototype is constructed based on the SIDO IPT system shown in Fig. 5.1. In order to simplify the design of the load side, the same structure of the secondary coil is used with a different value of load resistance. Moreover, to estimate the mutual inductance between the two secondary coils, a large primary coil is adopted in this experiment, and the two secondary coils are symmetrically arranged with respect to the primary coil (i.e., diagonally positioned), as illustrated in Fig. 5.11, thus ensuring the same mutual inductance between the receiver and the transmitter, i.e., $M_{\rm PS1} = M_{\rm PS2}$.

As shown in Fig. 5.12, the designed configuration consists of a DC power supply, a high-frequency inverter, a transformer composed by a primary coil (transmitter) and two secondary coils (receiver), compensation circuits and the

Figure 5.11: Layout of coupling structure used in experimental single-input double-output IPT system.

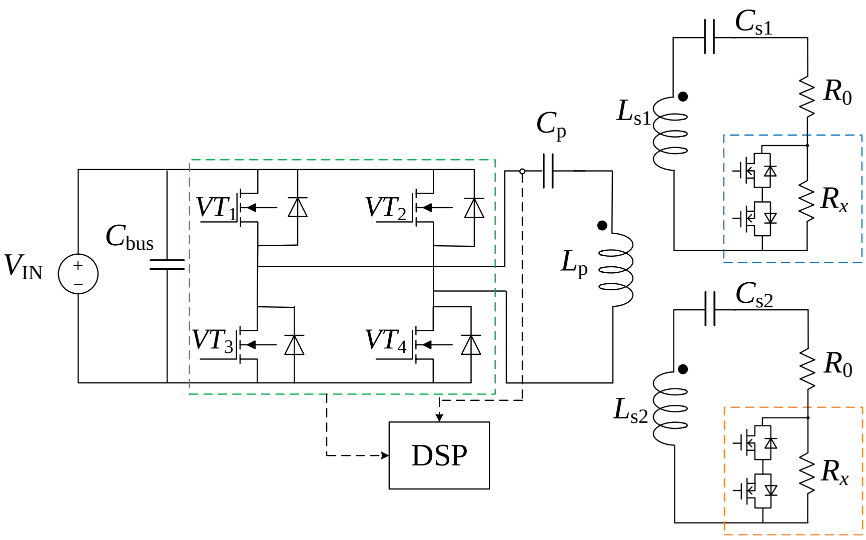

Figure 5.12: Configuration of experimental single-input double-output IPT system.

corresponding controller. The bus DC voltage source is supplied to the H-bridge inverter made up of SiC power components (C2M0080120), which have low conduction and switching losses. Current detection and protection circuits for the inverter are included to ensure the stability of the switching devices. The threshold of the detection and protection current is set to 7 A. For the compensation components, NP0 ceramic capacitors are utilized as the compensation capacitors for both primary and secondary sides to minimize the effect of temperature on the capacitances, thus ensuring the stability of resonance parameters. The values

Table 5.3: Parameters of Experimental Single-Input Double-Output IPT Circuit

Parameter	Value
Primary inductor L_P	228.45 μH
Secondary inductor L_S1	99.58 μH
Secondary inductor L_S2	98.23 μH
Primary capacitor C_P	11.2 nF
Secondary capacitor C_S1	25.8 nF
Secondary capacitor C_S2	26.2 nF
Transformer size (primary)	475×475 mm^2
Transformer size (secondary)	327×245 mm^2
Coupling coefficient k_PS1, k_PS2	0.19
Operating frequency f	100 kHz
Input voltage V_in	50 V

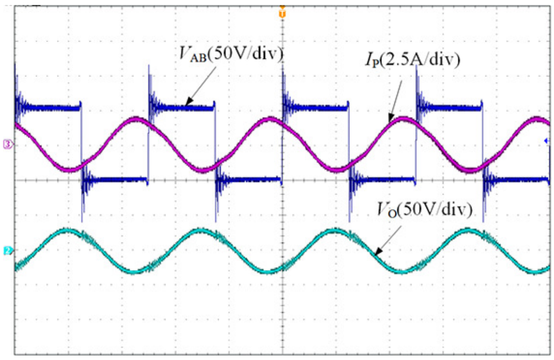

Figure 5.13: Measured waveforms of single-input single-output IPT system with $R_L = 10\ \Omega$.

of the components used in the experiment are shown in Table 5.3.

To compare the performance of IPT systems with various output terminals at various load resistance, only one output terminal of the system in Fig. 5.12 is adopted first, which changes the SIDO system to a SISO system with same parameters. Then, the SIDO system is evaluated with the same load value as in the SISO system. Fig. 5.13 shows the measured waveforms of the SISO IPT configuration when the load resistance is regulated to the optimal point of 10 Ω, with the maximum output power of 31.2 W.

Fig. 5.14 shows the measured waveforms of the SIDO IPT configuration when the two secondary coils are connected to loads with the same equivalent resistance

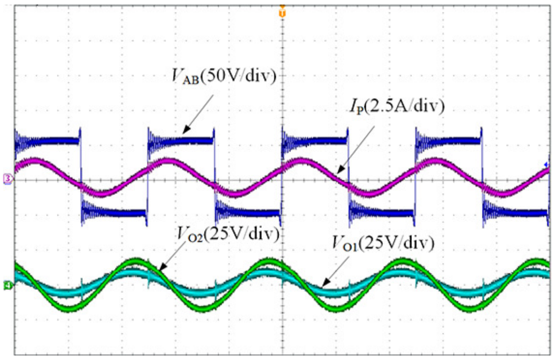

Figure 5.14: Measured waveforms of single-input double-output IPT system with $R_{L1} = R_{L2} = 10\ \Omega$.

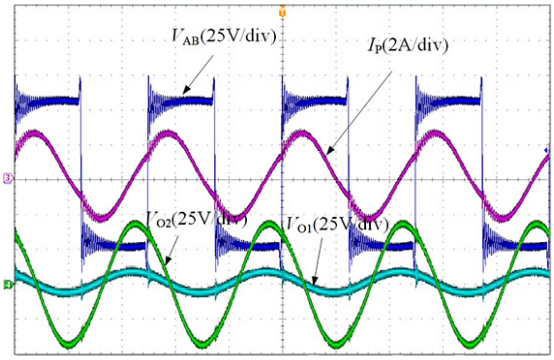

Figure 5.15: Measured waveforms of single-input double-output IPT system with $R_{L1} = 10\ \Omega$, $R_{L2} = 30.5\ \Omega$.

of 10 Ω. The measured waveforms indicate that the output power of each load is approximately 20.2 W, which is unable to maintain normal operation of the load, and the load value is also not the optimal point.

Fig. 5.15 shows the measured waveforms of the SIDO IPT configuration when the control is applied to regulate the resistance of load R_{L2} to the optimal point of 30.5 Ω, while keeping R_{L1} unchanged. It can be observed that the output power of load R_{L2} increases to 33.7 W. Both the measured and theoretical results reveal that by adjusting the load value, it is possible to achieve a variety of power output combinations for different loads, as well as to better meet the output requirements of different load characteristics. Furthermore, by regulating the equivalent resistance of the load to the optimal point, maximum power output can be preserved despite variation in the output terminals.

5.5 Optimal design with LC/S compensation

The previous section introduces load control and output voltage control strategies to achieve expected output power based on the S/S compensation in multi-load applications. In practical operations, the output current on each branch is affected by changes in the number of outputs, resulting in the requirement to constantly adjust the control parameters to achieve stable power tracking. According to the analysis on transfer performance of various compensation topologies in Chapters 2 and 3, higher order compensation with an inductor connected in series with the voltage source can provide a constant primary current. This property can be adopted here to address the issue of unstable output power and optimize the design.

To facilitate the topology design for multi-load applications, the series compensation at the secondary side is retained, and LC compensation is adopted at the primary side. The system satisfies operating conditions of $\omega = \frac{1}{\sqrt{L_{\mathrm{P}}C_{\mathrm{P}}}} = \frac{1}{\sqrt{L_{\mathrm{S}}C_{\mathrm{S}}}}$, and $L_1 = L_{\mathrm{P}}$. Assuming that the mutual inductance is fixed, based on the analysis in Chapters 3, primary current I_{P} is constant. This constant I_{P} ensures a constant induced voltage source at the secondary side, i.e., jMI_{P} is constant. According to the properties of LC/S compensation circuits listed in Table 3.1, the output voltage of the i-th output terminal can be expressed as

$$V_{\mathrm{o}i} = \frac{M_{\mathrm{PS}i}V_{\mathrm{in}}}{L_1} \tag{5.28}$$

which is constant and load-independent. Then, the output power of the i-th output terminal is given by

$$P_{\mathrm{o}i} = \frac{{M_{\mathrm{PS}i}}^2{V_{\mathrm{in}}}^2}{{L_1}^2R_{\mathrm{L}}} \tag{5.29}$$

Similarly, For the LC/S compensated MIMO IPT system with m inputs and n outputs shown in Fig. 5.16, the output voltage and output power of the i-th

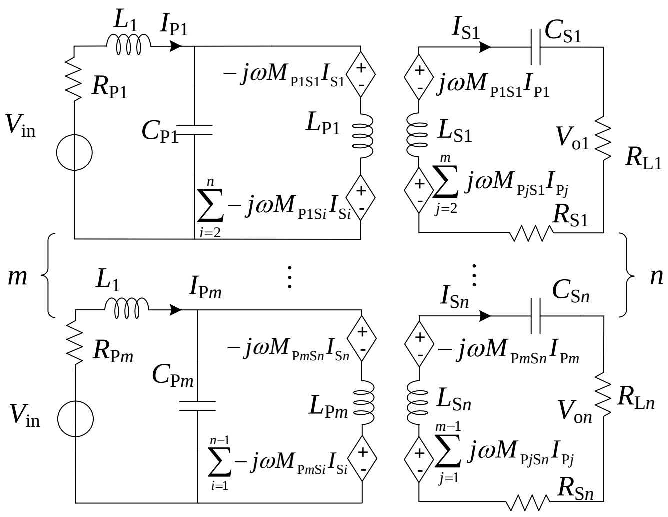

Figure 5.16: Equivalent circuit of the LC/S compensated multi-input multi-output IPT circuit.

output terminal can be found as

$$V_{\mathrm{o}i} = \frac{\sum_{j=1}^{m} M_{\mathrm{P}j\mathrm{S}i} V_{\mathrm{in}}}{L_1} \tag{5.30}$$

$$P_{\mathrm{o}i} = \frac{\sum_{j=1}^{m} {M_{\mathrm{P}j\mathrm{S}i}}^2 {V_{\mathrm{in}}}^2}{{L_1}^2 R_{\mathrm{L}}} \tag{5.31}$$

Thus, by simply optimizing the design of the compensation topology at the primary side, the output performance of IPT systems with various input and output terminations is improved. Specifically, this optimization is better applied to multi-load scenarios since the secondary-side structures remain the same. In addition to the LC/S compensated topologies, higher order ones such as LCL/S and LCC/S topologies can also be adopted for high-power requirements.

5.6 Summary

In this chapter, we have further explained the effect of compensation topology on the application of multi-output inductive power transfer (IPT) systems, and attempted to provide general design guidelines for IPT systems for multi-load applications. Transfer characteristics and the respective suitable applications of various coupling structures with series-series (S/S) compensations have been discussed in detail via circuit analysis. A set of design procedures of IPT systems has been proposed to meet various operating conditions, power requirements and the number of loads. Furthermore, phase-shift control and PWM control strategies at the load side are presented to permit an optimal power output with various load impedance. Moreover, a third-order LC/S compensated IPT converter with multiple outputs has been developed to enhance the constant output at various output terminals and facilitate the control design.

Chapter 6

Conclusions and Suggestions for Future Work

In this chapter, we summarize the main contributions which have been achieved in this project. Also, some suggestions and potential areas of investigation will be given for future research extension.

6.1 Contributions of the Thesis

Inductive power transfer (IPT) and capacitive power transfer (CPT) are two common approaches of wireless power transfer (WPT) in a variety of applications such as battery charging for consumer electronics, electric vehicles, implantable medical devices, and so on. For the design of compensation topologies in IPT and CPT systems, it is generally accepted that higher order circuits offer better flexibility and a higher degree of design freedom by expanding the parameter space. Unlike the previous studies that focus on topological properties and performance enhancement for specific applications, this project aims to provide general design pathways from basic second-order to higher order compensation by establishing systematic connections among various compensation topologies. In particular, since studies on compensation design for CPT converters are still at a preliminary stage, basic second-order and higher order compensation topologies are systematically analyzed. The analysis presented in this thesis offers a quick design guideline for deriving IPT and CPT systems with various compensation circuits ranging from second order to higher order. Specifically, the main contributions can be summarized as follows:

1. A unified circuit model of IPT and CPT converters for simplifying the analysis on transfer properties has been explored.

First, transfer properties of basic second-order compensated IPT circuits have been studied based on a T-type two-port network model. Then, various existing models of CPT couplers have been introduced. On this basis, we have presented an equivalent T-type model which is coupling-independent for CPT converters. Comparison and evaluation of the presented model with a most commonly used model have been conducted, to highlight the advantage of the T-type model with regard to simplicity and accuracy in the analysis of compensation topologies. Finally, a unified equivalent model for IPT and CPT converters have been developed with a standard set of system parameters.

2. Characteristics of compensation topologies in CPT converters have been systematically investigated.

Based on the proposed equivalent circuit model, all possible CPT topologies with basic second-order compensation terminated by a voltage source or a current source have been investigated in detail. The transfer properties in terms of constant load-independent output and corresponding operating conditions, zero phase input and corresponding operating conditions have been developed. Unified conditions satisfying various desired characteristics have been derived to offer a theoretical basis for investigating the transfer properties in extended higher order compensated IPT and CPT converters.

3. General design pathways to higher order compensation of IPT and CPT

converters have been studied in detail.

A new physical perspective of higher order compensation circuits has been presented, connecting basic second-order and higher order compensation topologies through current and voltage interchange at the input side, and conversion between constant current and voltage at the output side, for IPT and CPT converters separately. Then, the sensitivities of various topologies with the second-order and higher order compensation in terms of coupling parameter and compensation parameter changes have been compared and assessed in detail. Numerical simulations and experimental prototypes constructed by IPT and CPT configurations with various compensation topologies have been conducted to verify the theoretical analysis. Both theoretical and experimental results suggest that adding an inductor or capacitor at the input side and output side of a second-order circuit in specific fashions can effectively reduce the sensitivity of the system to parameter variation, provided the added inductor or capacitor exceeds a certain value. In addition, for IPT converters, with higher order compensation at the output side, the system can achieve a higher voltage gain. For CPT converters, the extension to fourth or higher order compensation circuits enables the CPT converter to reduce its sensitivity against parameter variations as well as to maintain the property of zero phase input. Moreover, double side extensions comprised by external shunt capacitors contribute to enhance the self-capacitance of capacitor pairs.

4. Application of IPT configurations with multiple outputs has been developed.

To highlight the function of various compensation topologies in WPT systems, configurations of IPT converters constructed by various number of input and output terminals with second and third order compensation topologies have been studied in depth. First, the transfer characteristics and the respective suitable applications of various coupling structures with series-series (S/S) compensations have been discussed in detail via circuit analysis. Then, a set of design procedures of IPT systems has been proposed to meet various operating conditions, power requirements and the number of loads. Furthermore, phase-shift control and PWM control strategies at the load side haven been presented to achieve an optimal power output with various load impedance. Finally, enhancement of a third order compensated IPT converter with corresponding parameter design has been presented. By adding an external compensated component and changing operating conditions, the topology and control design has been significantly simplified.

6.2 Suggestions for Future Work

The work conducted in this thesis has focused on the characteristics of IPT and CPT converters. Various theoretical analyses, system and component level simulations, and experimental verifications have been undertaken to achieve the research objectives. Useful results have been presented for practical design and applications. To conclude this thesis, several topics are suggested here for future research.

6.2.1 Design of System Control Strategy

In Chapters 3 and 4, we have analyzed the properties of IPT and CPT converters with second and higher order compensation topologies, and compared the sensitivity of system gain to various system parameters' fluctuations. In practical operation, the main purpose of analysis on parameter fluctuation is to obtain the pre-control range of the system, that is, to achieve strong robustness against specific parameter fluctuations. Thus, the capabilities including passive fault tolerance achieved by designing the compensation topologies, and active fault tolerance realized by controlling the values of system parameters can be integrated to improve the system's stability.

By designing a compensation topology with enhanced robustness, the passive fault tolerance of the system can be improved. Moreover, for gain fluctuation caused by parameter variations, the capability of control modules in combating parameter constraints can be improved to make the system more stable.

The sensitivity of the system gain in the case of single parameter fluctuation has been analyzed in this thesis. However, in some specific applications, the system is usually affected by simultaneous multi-dimensional parameter variations. Thus, it is necessary to conduct a more complete analysis and evaluation of the sensitivity against multi-dimensional parameters, thereby improving the controllability and the stability of the system in the case of simultaneous multiple parameter perturbations.

6.2.2 Optimization of System Efficiency

In Chapters 2 to 4, compensation topologies with various operating conditions are studied. Following the connections among these topologies based on sensitivity analysis, the impact of compensated converters of various order on system efficiency can be analyzed in depth. Theoretically, with the same operating conditions, the transfer efficiency of higher order compensated systems would be lower than that of basic second order compensated systems due to the addition of passive components in higher order compensation topologies. In this case, optimal design of higher order compensated IPT or CPT systems can be explored in terms of changing resonance conditions and parameter values in specific topologies to improve the transfer efficiency. In addition, on the basis of the system's stability mentioned in the previous section, the effects of multi-dimensional parameter fluctuations on the transfer efficiency can be further investigated to develop useful design methods for achieving optimal efficiency of IPT or CPT systems with various compensation topologies under single or multiple parameter fluctuations.

6.2.3 Study on Various Coupling Structures

In Chapter 5, applications for IPT systems with multiple inputs and outputs have been investigated in terms of the basic second-order and improved third-order compensation circuits. From the perspective of IPT or CPT, with the diversification of application scenarios, the future wireless charging mode will gradually change from the traditional one-to-one to the many-to-many mode, thus further reducing the dependence of the system on the position of WPT, as well as improving the spatial adaptability and energy availability. In particular, the diversity of coupling structures is worthy of further study for large-range and low-power sensor networks and consumer electronics. For follow-up work, on the basis of sensitivity analysis of single-input single-output converters, the impact of various coupling structures (various input and output terminations) on the system stability and transfer efficiency is worthy of further analysis. Meanwhile, as the number of input and output terminals increases, the order of the system increases exponentially, resulting in the design of system parameters becoming much more complicated. Thus, the design of simplifying the topology together with combating parameter constraints applied for various coupling structures is also a topic worthy of discussion.

6.2.4 Design Pathways for Hybrid Inductive and Capacitive Power Transfer Converters

For IPT converters, additional capacitors are required as components of the topology to compensate equivalent self inductance of the transformer, thereby reducing the reactive power transfer and enhancing the power transfer capability. In CPT converters, which can be viewed as a dual version of the IPT converters, inductors are the necessary compensating components. In order to make full use of the components in the compensation topologies, hybrid IPT and CPT converters are employed in recent research. The mixed technique of IPT and CPT combines the advantages of the IPT system in terms of high-power and long-distance power transfer with those of the CPT system in terms of high tolerance to metal objects and low heat generation, while compensating for the high voltage produced by capacitor plates and wide range of electric-field radiation, hence improving the safety and reliability of the system. Despite the individual reports focusing on the use of selected hybrid compensation topologies for specific desired performance, general design methods for combined IPT and CPT compensation with various orders in combating parameter variation remain open for further research. In addition, with the enhancement of power transfer performance due to the use of higher order compensation, the external passive components may have higher voltage and current stresses, especially in the case of CPT. Therefore, in the design process of hybrid converters, the capability in reducing voltage and current stresses of various topologies can be considered for optimization of the parameter design of hybrid IPT and CPT circuits, and for improving the reliability of the overall system.

Bibliography

[1] F. H. Sumi, L. Dutta, and F. Sarker, “Future with wireless power transfer technology,” *J. Electr. & Electron. Syst.*, vol. 7, no. 4, 2018.

[2] L. Xie, Y. Shi, Y. T. Hou, and A. Lou, “Wireless power transfer and applications to sensor networks,” *IEEE Wireless Commun.*, vol. 20, no. 4, pp. 140–145, Aug. 2013.

[3] A. M. Jawad, R. Nordin, S. K. Gharghan, H. M. Jawad, and M. Ismail, “Opportunities and challenges for near-field wireless power transfer: A review,” *Energies*, vol. 10, no. 7, p. 1022, Jul. 2017.

[4] B. H. Waters, J. T. Reed, K. R. Kagi, A. P. Sample, P. Bonde, and J. R. Smith, “A portable transmitter for wirelessly powering a ventricular assist device using the free-range resonant electrical energy delivery (FREE-D) system,” in *Wirelessly Powered Sensor Networks and Computational RFID*. USA: Springer Science & Business Media, 2013, pp. 235–247.

[5] K. Afridi, “Wireless charging of electric vehicles,” in *Frontiers of Engineering: Reports on Leading-Edge Engineering from the 2017 Symposium.* USA: National Academies Press, 2018, pp. 37–46.

[6] S. Li and C. Mi, “Wireless power transfer for electric vehicle applications,” *IEEE J. Emer. Select. Topics Power Electron.*, vol. 3, no. 1, pp. 4–17, Apr. 2014.

[7] S. Li, Z. Liu, H. Zhao, L. Zhu, C. Shuai, and Z. Chen, “Wireless power transfer by electric field resonance and its application in dynamic charging,” *IEEE Trans. Ind. Electron.*, vol. 63, no. 10, pp. 6602–6612, Oct. 2016.

[8] F. Lu, H. Zhang, and C. Mi, “A two-plate capacitive wireless power transfer system for electric vehicle charging applications,” *IEEE Trans. Power Electron.*, vol. 33, no. 2, pp. 964–969, Aug. 2017.

[9] H. Zhang, F. Lu, H. Hofmann, W. Liu, and C. Mi, “A four-plate compact capacitive coupler design and LCL-compensated topology for capacitive power transfer in electric vehicle charging application,” *IEEE Trans. Power Electron.*, vol. 31, no. 12, pp. 8541–8551, Dec. 2016.

[10] F. Lu, H. Zhang, H. Hofmann, and C. Mi, “A double-sided LCLC-compensated capacitive power transfer system for electric vehicle charging,” *IEEE Trans. Power Electron.*, vol. 30, no. 11, pp. 6011–6014, Jun. 2015.

[11] C. T. Rim and C. Mi, *Wireless Power Transfer for Electric Vehicles and Mobile Devices.* New York: Wiley-IEEE Press, 2018.

[12] K. V. T. Piipponen, R. Sepponen, and P. Eskelinen, “A biosignal instrumentation system using capacitive coupling for power and signal isolation,” *IEEE. Trans. Biomed. Eng.*, vol. 54, no. 10, pp. 1822–1828, Oct. 2007.

[13] H.-J. Kim, H. Hirayama, S. Kim, K. J. Han, R. Zhang, and J.-W. Choi, “Review of near-field wireless power and communication for biomedical applications,” *IEEE Access*, vol. 5, pp. 21 264–21 285, 2017.

[14] A. M. Sodagar and P. Amiri, “Capacitive coupling for power and data telemetry to implantable biomedical microsystems,” in *Proc. IEEE Int. IEEE/EMBS Conf. Neural Eng.*, 2009, pp. 411–414.

[15] T. Orekan, P. Zhang, and C. Shih, "Analysis, design, and maximum power-efficiency tracking for undersea wireless power transfer," *IEEE J. Emer. Select. Topics Power Electron.*, vol. 6, no. 2, pp. 843–854, Feb. 2017.

[16] C. Cai, S. Wu, Z. Zhang, L. Jiang, and S. Yang, "Development of a fit-to-surface and lightweight magnetic coupler for autonomous underwater vehicle wireless charging systems," *IEEE Trans. Power Electron.*, Early Access 2021.

[17] T. Kan, Y. Zhang, Z. Yan, P. P. Mercier, and C. Mi, "A rotation-resilient wireless charging system for lightweight autonomous underwater vehicles," *IEEE Trans. Veh. Technol.*, vol. 67, no. 8, pp. 6935–6942, Aug. 2018.

[18] Z. Yan, Y. Zhang, K. Zhang, B. Song, and C. Mi, "Underwater wireless power transfer system with a curly coil structure for AUVs," *IET Power Electron.*, vol. 12, no. 10, pp. 2559–2565, Oct. 2019.

[19] S. R. Hui and W. W. Ho, "A new generation of universal contactless battery charging platform for portable consumer electronic equipment," *IEEE Trans. Power Electron.*, vol. 20, no. 3, pp. 620–627, May 2005.

[20] M. Su, Z. Liu, Q. Zhu, and A. P. Hu, "Study of maximum power delivery to movable device in omnidirectional wireless power transfer system," *IEEE Access*, vol. 6, pp. 76 153–76 164, Nov. 2018.

[21] H. Hoang, S. Lee, Y. Kim, Y. Choi, and F. Bien, "An adaptive technique to improve wireless power transfer for consumer electronics," *IEEE Trans. Consum. Electron.*, vol. 58, no. 2, pp. 327–332, Jul. 2012.

[22] C. Liu, A. P. Hu, B. Wang, and N.-K. C. Nair, "A capacitively coupled contactless matrix charging platform with soft switched transformer control," *IEEE Trans. Ind. Electron.*, vol. 60, no. 1, pp. 249–260, Oct. 2011.

[23] N. Tesla, “Apparatus for transmitting electrical energy,” U.S. Patent 1 119 732, Dec. 1, 1914.

[24] A. Marincic, “Nikola tesla and the wireless transmission of energy,” *IEEE Trans. Power Appar. Syst.*, vol. PAS-101, no. 10, pp. 4064–4068, Oct. 1982.

[25] N. Tesla, *My Inventions: The Autobiography of Nikola Tesla.* USA: Wildside Press, 2005.

[26] A. Kurs, A. Karalis, R. Moffatt, J. D. Joannopoulos, P. Fisher, and M. Soljačić, “Wireless power transfer via strongly coupled magnetic resonances,” *Science*, vol. 317, no. 5834, pp. 83–86, 2007.

[27] C.-S. Wang, G. A. Covic, and O. H. Stielau, “Power transfer capability and bifurcation phenomena of loosely coupled inductive power transfer systems,” *IEEE Trans. Ind. Electron.*, vol. 51, no. 1, pp. 148–157, Jan. 2004.

[28] C.-S. Wang, O. H. Stielau, and G. A. Covic, “Design considerations for a contactless electric vehicle battery charger,” *IEEE Trans. Ind. Electron.*, vol. 52, no. 5, pp. 1308–1314, May 2005.

[29] S.-T. Khang, D.-J. Lee, I.-J. Hwang, T.-D. Yeo, and J.-W. Yu, “Microwave power transfer with optimal number of rectenna arrays for midrange applications,” *IEEE Antennas Wirel. Propag. Lett.*, vol. 17, no. 1, pp. 155–159, Nov. 2017.

[30] H. Matsumoto, “Numerical estimation of SPS microwave impact on ionospheric environment,” *Acta Astronaut.*, vol. 9, no. 8, pp. 493–497, Aug. 1982.

[31] W. C. Brown, “The history of power transmission by radio waves,” *IEEE Trans. Microw. Theory Tech.*, vol. 32, no. 9, pp. 1230–1242, Sep. 1984.

[32] W. C. Brown and E. E. Eves, "Beamed microwave power transmission and its application to space," *IEEE Trans. Microw. Theory Tech.*, vol. 40, no. 6, pp. 1239–1250, Jun. 1992.

[33] W. G. Hurley and W. H. Wölfle, *Transformers and Inductors for Power Electronics: Theory, Design and Applications.* UK: John Wiley & Sons, 2013.

[34] I. Mayordomo, T. Dräger, P. Spies, J. Bernhard, and A. Pflaum, "An overview of technical challenges and advances of inductive wireless power transmission," *Proc. IEEE*, vol. 101, no. 6, pp. 1302–1311, Jun. 2013.

[35] G. A. Covic and J. T. Boys, "Inductive power transfer," *Proc. IEEE*, vol. 101, no. 6, pp. 1276–1289, Jun. 2013.

[36] M. Budhia, J. T. Boys, G. A. Covic, and C. Huang, "Development of a single-sided flux magnetic coupler for electric vehicle IPT charging systems," *IEEE Trans. Ind. Electron.*, vol. 60, no. 1, pp. 318–328, Jan. 2013.

[37] A. Zaheer, G. A. Covic, and D. Kacprzak, "A bipolar pad in a 10-kHz 300 W distributed IPT system for AGV applications," *IEEE Trans. Ind. Electron.*, vol. 61, no. 7, pp. 3288–3301, Jul. 2014.

[38] S. Li, W. Li, and C. Mi, "A double-sided LCC compensation network and its tuning method for wireless power transfer," *IEEE Trans. Power Electron.*, vol. 64, no. 6, pp. 2261–2273, Jun. 2015.

[39] W. Zhang, S. C. Wong, C. K. Tse, and Q. Chen, "Load-independent duality of current and voltage outputs of a series or parallel compensated inductive power transfer converter with optimized efficiency," *IEEE J. Emer. Select. Topics Power Electron.*, vol. 3, no. 1, pp. 137–146, Mar. 2015.

[40] B. Esteban, M. Sid-Ahmed, and N. C. Kar, "A comparative study of power supply architectures in wireless EV charging systems," *IEEE Trans. Power Electron.*, vol. 30, no. 11, pp. 6408–6417, Nov. 2015.

[41] M. Kiani and M. Ghovanloo, "The circuit theory behind coupled-mode magnetic resonance-based wireless power transmission," *IEEE Trans. Circuits Syst. I: Reg. Papers*, vol. 59, no. 9, pp. 2065–2074, Sep. 2012.

[42] S. Cheon, Y.-H. Kim, S.-Y. Kang, M. L. Lee, J.-M. Lee, and T. Zyung, "Circuit-model-based analysis of a wireless energy-transfer system via coupled magnetic resonances," *IEEE Trans. Ind. Electron.*, vol. 58, no. 7, pp. 2906–2914, Sep. 2010.

[43] F. Mastri, M. Mongiardo, G. Monti, M. Dionigi, and L. Tarricone, "Gain expressions for resonant inductive wireless power transfer links with one relay element," *Wireless Power Transfer*, vol. 5, no. 1, p. 27, 2018.

[44] B. Minnaert and N. Stevens, "Single variable expressions for the efficiency of a reciprocal power transfer system," *Int. J. Circuit Theory Appl.*, vol. 45, no. 10, pp. 1418–1430, Oct. 2017.

[45] X. Qu, Y. Jing, H. Han, S. C. Wong, and C. K. Tse, "Higher order compensation for inductive-power-transfer converters with constant voltage or constant-current output combating transformer parameter constraints," *IEEE Trans. Power Electron.*, vol. 32, no. 1, pp. 394–405, Jan. 2017.

[46] K. A. Kalwar, M. Aamir, and S. Mekhilef, "Inductively coupled power transfer (ICPT) for electric vehicle charging–a review," *Renew. and Sustain. Energy Rev.*, vol. 47, pp. 462–475, 2015.

[47] C. Liu, A. P. Hu, G. A. Covic, and N.-K. C. Nair, "Comparative study of ccpt systems with two different inductor tuning positions," *IEEE Trans. Power Electron.*, vol. 27, no. 1, pp. 294–306, Jan. 2011.

[48] M. P. Theodoridis, "Effective capacitive power transfer," *IEEE Trans. Power Electron.*, vol. 27, no. 12, pp. 4906–4913, Dec. 2012.

[49] Z. Zhang, H. Pang, A. Georgiadis, and C. Cecati, "Wireless power transfer—an overview," *IEEE Trans. Ind. Electron.*, vol. 66, no. 2, pp. 1044–1058, Feb. 2018.

[50] A. Di Gioia, I. P. Brown, Y. Nie, R. Knippel, D. C. Ludois, J. Dai, S. Hagen, and C. Alteheld, "Design and demonstration of a wound field synchronous machine for electric vehicle traction with brushless capacitive field excitation," *IEEE Trans. Ind. Appl.*, vol. 54, no. 2, pp. 1390–1403, Feb. 2017.

[51] W. Zhou, Y.-G. Su, L. Huang, X.-D. Qing, and A. P. Hu, "Wireless power transfer across a metal barrier by combined capacitive and inductive coupling," *IEEE Trans. Ind. Electron.*, vol. 66, no. 5, pp. 4031–4041, May 2018.

[52] L. Huang, A. P. Hu, A. K. Swain, and Y. Su, "Z-impedance compensation for wireless power transfer based on electric field," *IEEE Trans. Power Electron.*, vol. 31, no. 11, pp. 7556–7563, Nov. 2016.

[53] L. J. Zou, Q. Zhu, C. W. Van Neste, and A. P. Hu, "Modeling single-wire capacitive power transfer system with strong coupling to ground," *IEEE J. Emer. Select. Topics Power Electron.*, vol. 9, no. 2, pp. 2295–2302, Sep. 2019.

[54] L. Huang and A. P. Hu, "Defining the mutual coupling of capacitive power transfer for wireless power transfer," *Electron. Lett.*, vol. 51, no. 22, pp. 1806–1807, Oct. 2015.

[55] S. Wang, J. Liang, and M. Fu, “Analysis and design of capacitive power transfer systems based on induced voltage source model,” *IEEE Trans. Power Electron.*, vol. 35, no. 10, pp. 10 532–10 541, Mar. 2020.

[56] A. Hussein and I. Batarseh, “A review of charging algorithms for nickel and lithium battery chargers,” *IEEE Trans. Veh. Technol.*, vol. 60, no. 3, pp. 830–838, Mar. 2011.

[57] F. Musavi and W. Eberle, “Overview of wireless power transfer technologies for electric vehicle battery charging,” *IET Power Electron.*, vol. 7, no. 7, pp. 60–66, Jul. 2014.

[58] X. Qu, H. Han, S. C. Wong, and C. K. Tse, “Hybrid IPT topologies with constant-current or constant-voltage output for battery charging applications,” *IEEE Trans. Power Electron.*, vol. 30, no. 11, pp. 6129–6337, Nov. 2015.

[59] S. Y. R. Hui, W. Zhong, and C. K. Lee, “A critical review of recent progress in mid-range wireless power transfer,” *IEEE Trans. Power Electron.*, vol. 29, no. 9, pp. 4500–4511, Sep. 2013.

[60] D. J. Thrimawithana and U. K. Madawala, “A contactless bi-directional power interface for plug-in hybrid vehicles,” in *Proc. IEEE Veh. Power Propulsion Conf. (VPPC)*, 2009, pp. 396–401.

[61] W. Zhang and C. Mi, “Compensation topologies of high-power wireless power transfer systems,” *IEEE Trans. Veh. Technol.*, vol. 65, no. 6, pp. 4768–4778, Jun. 2016.

[62] C. Cheng, W. Li, Z. Zhou, Z. Deng, and C. Mi, “A load-independent wireless power transfer system with multiple constant voltage outputs,” *IEEE Trans. Power Electron.*, vol. 35, no. 4, pp. 3328–3331, Sep. 2019.

[63] W. Zhang and C. Mi, "Compensation topologies of high-power wireless power transfer systems," *IEEE Trans. Veh. Technol.*, vol. 65, no. 6, pp. 4768–4778, Jul. 2015.

[64] S. Wang, J. Chen, Z. Hu, C. Rong, and M. Liu, "Optimization design for series–series dynamic WPT system maintaining stable transfer power," *IET Power Electron.*, vol. 10, no. 9, pp. 987–995, Sep. 2017.

[65] Q. Zhu, L. Wang, C. Liao, and F. Li, "Improving the misalignment tolerance of wireless charging system by optimizing the compensate-capacitor," *IEEE Trans. Ind. Electron.*, vol. 62, no. 8, pp. 4832–4836, Aug. 2015.

[66] J. Hou, Q. Chen, S. C. Wong, C. K. Tse, and X. Ruan, "Analysis and control of series/series-parallel compensated resonant converters for contactless power transfer," *IEEE J. Emer. Select. Topics Power Electron.*, vol. 3, no. 1, pp. 124–136, Jan. 2015.

[67] H. Hao, G. A. Covic, and J. T. Boys, "A parallel topology for inductive power transfer power supplies," *IEEE Trans. Power Electron.*, vol. 29, no. 3, pp. 1140–1151, Mar. 2013.

[68] S. Samanta and A. K. Rathore, "Small-signal modeling and closed-loop control of a parallel–series/series resonant converter for wireless inductive power transfer," *IEEE Trans. Ind. Electron.*, vol. 66, no. 1, pp. 172–182, Jan. 2018.

[69] M. L. G. Kissin, C. Y. Huang, G. A.Covic, and J. T. Boys, "Detection of the tuned point of a fixed-frequency lcl resonant power supply," *IEEE Trans. Power Electron.*, vol. 24, no. 4, pp. 1140–1143, Apr. 2009.

[70] U. K. Madawala and D. J. Thrimawithana, "Current sourced bi-directional inductive power transfer system," *IET Power Electron.*, vol. 4, no. 4, pp. 471–480, Apr. 2011.

[71] J. T. Boys and G. A. Covic, "The inductive power transfer story at the university of auckland," *IEEE Circ. Syst. Mag.*, vol. 15, no. 2, pp. 6–27, Jun. 2015.

[72] C. Liu, S. Ge, Y. Guo, H. Li, and G. Cai, "Double-LCL resonant compensation network for electric vehicles wireless power transfer: experimental study and analysis," *IET Power Electron.*, vol. 9, no. 11, pp. 2262–2270, Nov. 2016.

[73] S. Varikkottil and J. Febin Daya, "High-gain LCL architecture based IPT system for wireless charging of EV," *IET Power Electron.*, vol. 12, no. 2, pp. 195–203, Feb. 2019.

[74] A. Ramezani, S. Farhangi, H. Iman-Eini, B. Farhangi, R. Rahimi, and G. R. Moradi, "Optimized LCC-series compensated resonant network for stationary wireless EV chargers," *IEEE Trans. Ind. Electron.*, vol. 66, no. 4, pp. 2756–2765, Apr. 2019.

[75] X. Qu, H. Chu, S. C. Wong, and C. K. Tse, "An IPT battery charger with near unity power factor and load-independent constant output combating design constraints of input voltage and transformer parameters," *IEEE Trans. Power Electron.*, vol. 34, no. 8, pp. 7719–7727, Aug. 2019.

[76] J. Lu, G. Zhu, H. Wang, F. Lu, J. Jiang, and C. Mi, "Sensitivity analysis of inductive power transfer systems with voltage-fed compensation topologies," *IEEE Trans. Veh. Technol.*, vol. 68, no. 5, pp. 4502–4513, May 2019.

[77] Y. Liu, C. K. Tse, C. Zhu, and S. C. Wong, "Comparison of second-order and third-order compensation of inductive power transfer converters based on sensitivity analysis," in *Proc. IEEE Int. Symp. Circuits Syst. (ISCAS)*, Oct. 2020, pp. 1–5.

[78] M. Kline, I. Izyumin, B. Boser, and S. Sanders, "Capacitive power transfer for contactless charging," in *Proc. IEEE Appl. Power Electron. Conf. and Expo. (APEC)*, 2011, pp. 1398–1404.

[79] H. Zhang, F. Lu, H. Hofmann, and C. Mi, "A loosely coupled capacitive power transfer system with LC compensation circuit topology," in *Proc. IEEE Energy Conv. Cong. Expo. (ECCE)*, 2016, pp. 1–5.

[80] F. Lu, H. Zhang, H. Hofmann, and C. Mi, "A double-sided LC-compensation circuit for loosely coupled capacitive power transfer," *IEEE Trans. Power Electron.*, vol. 33, no. 2, pp. 1633–1643, Feb. 2017.

[81] R. Mai, B. Luo, Y. Chen, and Z. He, "Double-sided CL compensation topology based component voltage stress optimisation method for capacitive power transfer charging system," *IET Power Electron.*, vol. 11, no. 7, pp. 1153–1160, Apr. 2018.

[82] M. P. Theodoridis, "Effective capacitive power transfer," *IEEE Trans. Power Electron.*, vol. 27, no. 12, pp. 4906–4913, Apr. 2012.

[83] T. C. Beh, M. Kato, T. Imura, S. Oh, and Y. Hori, "Automated impedance matching system for robust wireless power transfer via magnetic resonance coupling," *IEEE Trans. Ind. Electron.*, vol. 60, no. 9, pp. 3689–3698, Sep. 2013.

[84] S. Sinha, A. Kumar, B. Regensburger, and K. K. Afridi, "A new design approach to mitigating the effect of parasitics in capacitive wireless power transfer systems for electric vehicle charging," *IEEE Trans. Transp. Electrification*, vol. 5, no. 4, pp. 1040–1059, Dec. 2019.

[85] L. Li, Z. Wang, F. Gao, S. Wang, and J. Deng, "A family of compensation topologies for capacitive power transfer converters for wireless electric vehicle charger," *Appl. Energy*, vol. 260, pp. 114–156, Feb. 2020.

[86] Y. C. Liu, J. Zhang, C. K. Tse, C. Zhu, and S. C. Wong, "General pathways to higher order compensation circuits for IPT converters via sensitivity analysis," *IEEE Trans. Power Electron.*, vol. 36, pp. 9897–9906, Sep. 2021.

[87] G. L. Matthaei, L. Young, and E. M. T. Jones, *Microwave Filters, Impedance-Matching Networks, and Coupling Structures.* USA: Artech House, 1980.

[88] S. Ghosh, *Network Theory: Analysis and Synthesis.* IN: Prentice-Hall, 2005.

[89] X. Qu, H. Chu, S. C. Wong, and C. K. Tse, "An IPT battery charger with near unity power factor and load-independent constant output combating design constraints of input voltage and transformer parameters," *IEEE Trans. Power Electron.*, vol. 34, no. 8, pp. 7719–7727, Aug. 2019.

[90] W. Zhang, S. C. Wong, C. K. Tse, and Q. Chen, "Load-independent duality of current and voltage outputs of a series-or parallel-compensated inductive power transfer converter with optimized efficiency," *IEEE J. Emer. Select. Topics Power Electron.*, vol. 3, no. 1, pp. 137–146, Jan. 2015.

[91] C. G. Montgomery, R. H. Dicke, E. M. Purcell, and E. M. Purcell, *Principles of Microwave Circuits.* UK: Peter Peregrinus, 1987.

[92] D. C. Ludois, M. J. Erickson, and J. K. Reed, "Aerodynamic fluid bearings for translational and rotating capacitors in noncontact capacitive power transfer systems," *IEEE Trans. Ind. Appl.*, vol. 50, no. 2, pp. 1025–1033, Feb. 2013.